Aus der Klinik und Poliklinik für Kinder- und Jugendmedizin

Direktor: Herr Prof. Dr. med. R. Berner

Role of ALADIN for Oxidative Stress Response and Microsomal Steroidogenesis in Human Adrenocortical Cells

Dissertationsschrift

zur Erlangung des akademischen Grades

Doctor of Philosophy (Ph.D.)

vorgelegt

der Medizinischen Fakultät Carl Gustav Carus

der Technischen Universität Dresden

von

Ramona Jühlen, M.Sc.

aus Bonn Bad-Godesberg

Dresden 2015

1. Gutachter:
2. Gutachter:

Tag der mündlichen Prüfung:

gez.:

Vorsitzender der Promotionskommission

Contents

List of Figures

List of Tables

List of Abbreviations

17OHP	17-hydroxyprogesterone
AAAS	Achalasia-adrenal insufficiency-alacrima syndrome
ACTB	ß-actin
ACTH	Adrenocorticotropic hormone
ALADIN	Alacrima-achalasia-adrenal insufficiency neurologic disorder
ALD	X-linked adrenoleukodystrophy
APTX	Aprataxin
BSO	L-buthionine-(S,R)-sulfoximine
CAC	Citric acid cycle
Co-IP	Co-immunoprecipitation
Compound S	11-deoxycortisol
COX	Cytochrome oxidase protein
CREB	cAMP-response-element-binding-protein
CRH	Corticotropin-releasing hormone
CYP450	Cytochrome P450 enzyme
CYP17A1	17α-hydroxylase/17,20lyase
CYP21A2	21-hydroxylase
$CYPb_5$	$NADH$-$CYPb_5$ reductase
DHCR24	24-dehydrocholesterol reductase
DOC	Deoxycorticosterone
ECL	Enhanced chemiluminescence
ERMES	ER-mitochondrion encounter structure
FAD	Flavin adenine dinucleotide
FDXR1	Ferredoxin reductase
FGD	Familial glucocorticoid deficiency
FMN	Flavin mononucleotide
FTH1	Ferritin heavy chain 1

GAPDH	Glyceraldehyde 3-phosphate dehydrogenase
GPX	Glutathione peroxidase
GR	Glucocorticoid receptor
GSH	Glutathione (reduced state)
GSR	Glutathione reductase
$GSSG$	Glutathione (oxidised state)
HNRNP	Heterogeneous nuclear ribonucleoprotein
HO	Heme oxygenase
IBSN	Infantile bilateral striatal necrosis
ITS-G	Insulin-transferrin-selenium
LC/MS-MS	Liquid chromatography/tandem mass spectrometry
LCAH	Lipoid congenital adrenal hyperplasia
LDS	Lithium dodecyl sulphate
LIG1	DNA ligase 1
MAPR	Membrane-associated progesterone receptors
MCM4	Minichromosome maintenance complex component 4
MC2R	Melanocortin 2 receptor
MDM	Mitochondrial distribution and morphology
MIA	Mitochondrial intermembrane space assembly machinery
MLR	Mitochondrially localised mRNA
Mmm1	Maintenance of mitochondrial morphology 1
MnSOD	Manganese-dependent superoxide dismutase
MRAP	Melanocortin receptor accessory protein
mRNP	Messenger ribonucleoprotein
NAC	Nascent polypeptide-associated complex
NNT	Nicotinamide nucleotide transhydrogenase
NPC	Nuclear pore complex
NUP	Nucleoporin
OXA	Oxidase assembly machinery

PAGE	Polyacrylamide gel electrophoresis
PGRMC1	Progesterone receptor membrane compartment 1
POR	Cytochrome P450 oxidoreductase
PORD	Cytochrome P450 oxidoreductase deficiency
PRDX	Peroxiredoxin
PUF	Pumilio family
ROI	Region of interest
ROS	Reactive oxygen species
SAM	Sorting and assembly machinery
SDS	Sodium dodecyl sulphate
shRNA	Short hairpin RNA
SIPS	Stress-induced premature senescence
siRNA	Small interfering RNA
SOD	Superoxide dismutase
SRP	Signal recognition particle
SSR1	Signal sequence receptor 1
StAR	Steroidogenic acute regulatory protein
TIM	Translocase of the inner mitochondrial membrane
TOM	Translocase of the outer mitochondrial membrane
TRAP	Translocon-associated protein
TXN2	Thioredoxin 2
TXNRD	Thioredoxin reductase
VLCFA	Very long chain fatty acids

1 Introduction

1.1 The triple A syndrome and the adrenal gland function

The triple A syndrome (MIM #231550) is an autosomal recessive disease manifesting with the triad of adrenocorticotropic hormone (ACTH)-resistant adrenal insufficiency, achalasia of the stomach cardia and impaired tear production (alacrima) in combination with progressive neurological impairment of the central, peripheral and autonomic nervous systems (Allgrove et al., 1978; Grant et al., 1992). Patients suffer from heterogeneous neurological symptoms featuring neurodegeneration, cerebellar ataxia, peripheral neuropathy with consecutive weakness of preferably distal muscles and mild mental retardation (Tullio-Pelet et al., 2000; Handschug et al., 2001). Adrenal insufficiency may appear later in life than achalasia and alacrima and may develop gradually (Milenkovic et al., 2010).

The adrenal gland consists of two endocrine distinct tissues: the steroid hormone-producing adrenal cortex and the medulla where chromaffin cells synthesise catecholamines. However, it is known that this view is too simplified and the distribution of the different cell types is not as distinct as firstly thought (Ehrhart-Bornstein et al., 1998). The two tissues originate from different embryonal lineages. During embryogenesis the adrenal primordium consists of mesoderm-derived cells which develop into adrenocortical cells.

The mammalian adrenal cortex consists of three distinct zones depending on morphology and type of steroid synthesis. Cells of the zona glomerulosa synthesise the unique mineralocorticoid aldosterone, zona fasciculata is the production site for glucocorticoids and cells of the zona reticularis produce androgens (sex steroids) (Figure 1) (Ehrhart-Bornstein et al., 1998). The enzymes, responsible for the steroid synthesis in all three zones, reside either in mitochondria (type I) or in the ER (type II). These enzymes are cytochrome P450 enzymes (CYP P450s) (nomenclature for these enzymes: CYP followed by a number for the gene family, a capital letter for the gene sub-family and a second number for the specific gene, e.g. CYP17A1). These enzymes produce steroids with the help of a heme prosthetic group in a redox reaction involving $NADPH$ and molecular oxygen (Pandey and Fluck, 2013; Nelson, 2009). The chemical reaction steps are explained in detail in subsection 1.3 Oxidative stress.

Chromaffin cells in the adrenal medulla originate form ectodermal precursor cells which immigrate in the adrenal “Anlagen” where they develop into medullary cells under the influence of the adrenocortex (Pohorecky and Wurtman, 1971; Axelrod and Reisine, 1984). In these chromaffin cells catecholamines (in particular epinephrine and nor-epinephrine), transmitters, neuropeptides and other proteins are produced (Winkler et al., 1986). In my thesis the work is focussed on the adrenal cortex.

Ehrhart-Bornstein et al. discussed the possible interaction between adrenal cortex and medulla in detail and it is shown that the different cells in the adrenal communicate with each other in a cortical-medullary fashion (Ehrhart-Bornstein et al., 1998). Moreover, the adrenocortical function is regulated by a variety of external and internal stimuli: the internal cortical-medullary communication, external vascular supply and neural innervation, the immune system, internal and external produced growth factors, the renin-angiotensin II and corticotropin-releasing hormone (CRH)-ACTH systems.

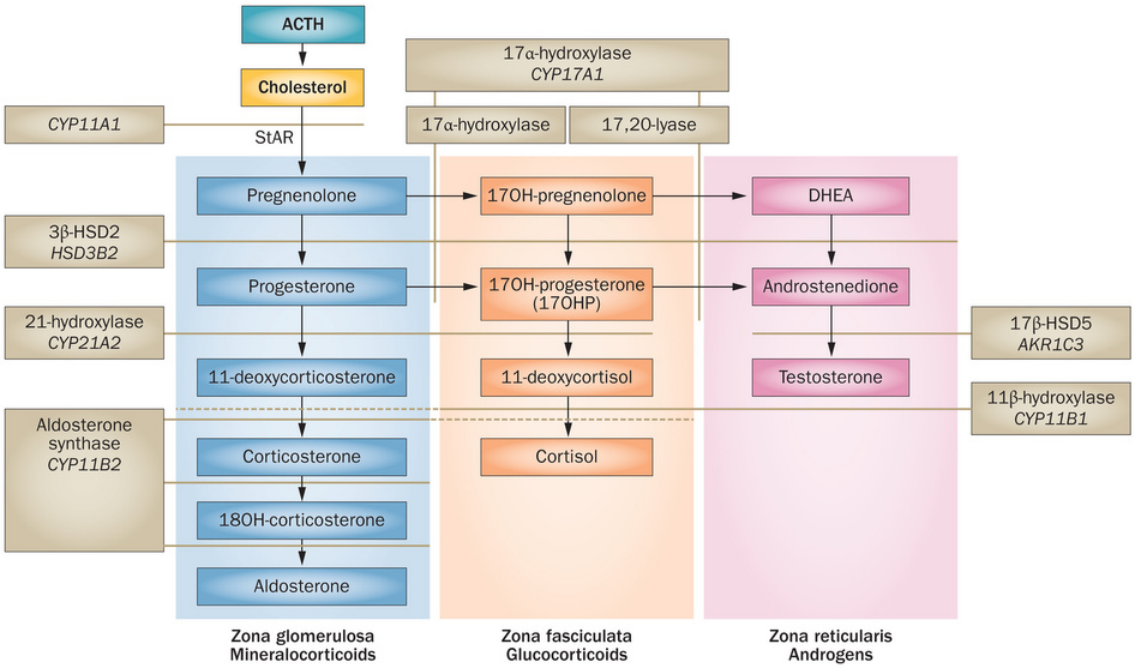

Figure 1 – Overview of adrenal steroidogenesis.
The genes coding for enzymes are written in italic typeface (olive). All enzymes are microsomal enzymes, despite the mitochondrial CYP11A1, CYP11B1 and CYP11B2. CYP17A1 has hydroxylase and lyase activity. The zona glomerulosa mainly produces mineralocorticoids (blue), zona fasciculata is responsible for production of glucocorticoids (orange) and androgens are made in zona reticularis (pink). Stimulation by adrenocorticotropic hormone (ACTH) leads to the initiation of steroidogenesis by facilitating the import of cholesterol from the liver into the mitochondria of adrenocortical cells with the help of steroidogenic acute regulatory protein (StAR) in the outer mitochondrial membrane (Han et al., 2014).

The release of glucocorticoids in the adrenal zona fasciculata is primarily regulated by the hypothalamus-pituitary-adrenal axis by its secretagogues CRH, ACTH and adiuretin and a negative cortisol-related feedback loop. Briefly, stimulation of the seven transmembrane G-protein-coupled ACTH receptor (melanocortin 2 receptor (MC2R)) by stress-induced high ACTH levels leads to cAMP increase by adenylate cyclase and protein kinase A activation resulting in genomic (e.g. through the transcription factor SF1) and non-genomic (e.g. phosphorylation) responses (Figure 2). Since ACTH can partly stimulate mineralocorticoid synthesis, production of glucocorticoids leads to the inhibition of aldosterone production in a negative feedback through corticosterone (Clark and Weber, 1998).

The secretion of aldosterone in the adrenal zona glomerulosa is primarily dependent on the plasma renin-angiotensin II system. Glomerulosa cells express high amounts of G-protein-coupled angiotensin 1 receptor compared to the other two zonae. Thus, innervation by angiotensin II is highly cell type-specific. Shortly, the pathway is regulated by the inositol triphosphate/ diacylglycerole pathway leading to calcium release from the ER and activation of protein kinase C which in turn activates expression of genes responsible for aldosterone synthesis.

Triple A syndrome patients suffer from ACTH-resistant adrenal insufficiency. Glucocorticoid and androgen production is most frequently affected in these patients and about 15-25 % of triple A patients show a deficiency in mineralocorticoid production (Clark and Weber, 1998; Tsigos, 1999; Lanes et al., 1980) (unpublished data). This may be explained by the cellular degeneration seen in histological sections of adrenal glands of triple A syndrome patients: in both, zona fasciculata and zona reticularis hormonal active cells are displaced by nondescript

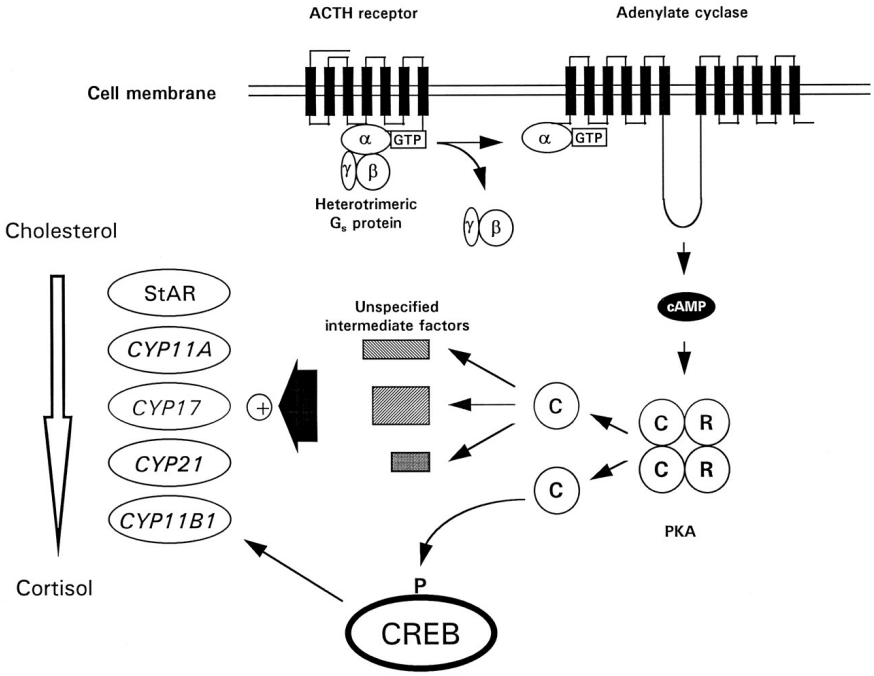

Figure 2 – Second messenger pathways after adrenocorticotropic hormone stimulation in adrenal fasciculata cells.

Adrenocorticotropic hormone (ACTH) binds to its seven-transmembrane G-protein-coupled receptor which leads to the activation of the $G_s\alpha$-subunit by GTP and separation of the βγ-subunits. The $G_s\alpha$-subunit activates the membrane-associated adenylate cyclase and cAMP is produced. cAMP activates PKA and its catalytic subunits (C) consecutively phosphorylate a row of substrates including cAMP-response-element-binding-protein (CREB) and SF1 (not shown here). This activation leads to initiation of glucocorticoid synthesis through steroidogenic acute regulatory protein (StAR) (Clark and Weber, 1998).

cells. In contrast, zona glomerulosa is almost normally developed and seems to escape cell degeneration (Figure 3) (Allgrove et al., 1978; Clark and Weber, 1998).

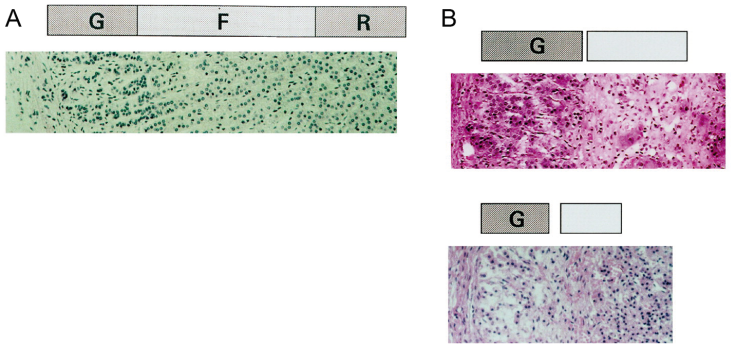

Figure 3 – Histology of the adrenal cortex of a child who died from non-endocrine manifestations (A) and two children who died from triple A syndrome (B).

Zona glomerulosa (marked with the grey box G) is preserved in all patients but zona fasciculata (F) and reticularis (R) are displaced by atypical nondescript cells (Clark and Weber, 1998, modified).

Mutations in the *AAAS* (achalasia-adrenal insufficiency-alacrima syndrome) gene cause triple A syndrome. *AAAS* encodes the protein ALADIN (alacrima-achalasia-adrenal insufficiency neurologic disorder) (Tullio-Pelet et al., 2000; Handschug et al., 2001; Huebner et al., 2002). ALADIN is ubiquitously expressed but shows enhanced levels in neuroendocrine and gastrointestinal structures; tissues which are most affected in triple A patients implying a cell type-specific function of ALADIN (Handschug et al., 2001). In order to develop an animal model for human triple A syndrome, mice lacking a functional *AAAS* gene were developed.

Knock-out mice showed a mild phenotype with normal hormone measurements and normal adrenal histology. Surprisingly, no such adrenal phenotype seen in triple A patients has been so far described in *AAAS* knock-out mice; probably, because mice predominantly have a zona glomerulosa (Huebner et al., 2006). This underlines the assumption that ALADIN supports a species-specific role in human cellular biology.

1.2 The nuclear pore complex

1.2.1 Structure and architecture

In 2002 ALADIN was identified as a component of the nuclear pore complex (NPC) (Cronshaw et al., 2002). Eukaryotic NPCs are large protein complexes residing in the nuclear envelope composed of ~30 different proteins, known as nucleoporins (NUPs), which mediate the transport of macromolecules between the cytoplasm and the nucleus. The bi-directional transport facilitates trafficking of proteins and RNA across the nuclear envelope (Fahrenkrog, 2014).

NPC structures and actions are highly specific and tightly regulated in eukaryotic cells. NUPs assemble in repetitive sub-complexes to build NPCs (Lim et al., 2008; Maimon et al., 2012; Bui et al., 2013; D'Angelo and Hetzer, 2008). It was analysed by scanning electron microscopy and proteomic analyses that one NPC is actually formed of 500-1000 individual proteins making up a total molecular weight of 110 MDa in vertebrates (Bui et al., 2013; Alber et al., 2007). Most information about highly evolutionary conserved NPC structures has been determined from isolated *Xenopus laevis* oocyte nuclei but also from yeast, amoebozoa, plants and humans (Maimon et al., 2012; Bui et al., 2013; Frenkiel-Krispin et al., 2010; Kiseleva et al., 2004; Fiserova et al., 2009; Beck et al., 2004; Capelson et al., 2010; Stoffler et al., 2003).

Briefly summarised, NPCs are built of a central framework (spoke-ring complex) aligned with eight cytoplasmic filaments and a nuclear basket which is formed of eight filaments which join in a distal ring (Figure 4). The central framework consists of eight spokes which form the ~40-45 nm central pore/channel (at the nuclear envelope mid plane) (Maimon et al., 2012; Bui et al., 2013; Frenkiel-Krispin et al., 2010; Beck et al., 2004; Stoffler et al., 2003; Beck et al., 2007; Pante and Kann, 2002). The channel facilitates the nucleo-cytoplasmic exchange of molecules of maximal ~39 nm in a signal-, receptor- and energy-dependent fashion whereas small molecules of about 9 nm can diffuse freely between the two cell compartments (Pante and Kann, 2002; Enss et al., 2003; Mohr et al., 2009).

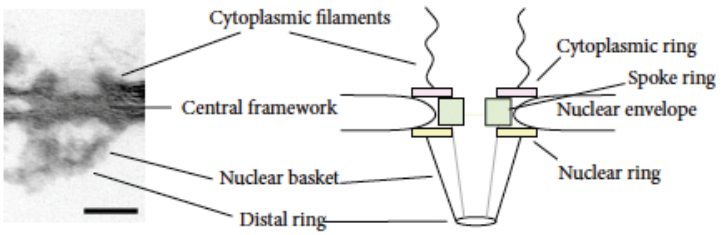

Figure 4 – Nuclear pore complex architecture.
Nuclear pore complex side view of Xenopus laevis oocyte nuclei visualised by transmission electron microscopy (left) and schematic presentation of main structural components of the nuclear pore complex (right) (Fahrenkrog, 2014).

The 30 different NUPs building the NPC structure are grouped in sub-complexes according to their amino acid sequence and their predicted structural motifs (Figure 5) (Schwartz, 2005; Devos et al., 2006). Transmembrane NUPs reside in the nuclear envelope and sit at the section between central framework and pore membrane (e.g. NDC1). Scaffold NUPs are distinct in their structural motifs as all contain α-helical solenoid and β-propeller fold motifs (e.g. NUP107-160). The last group of NUPs can further sub-divided in NUPs of the cytoplasmic filaments (e.g. NUP358), of the central channel (e.g. NUP62) and of the nuclear basket (e.g. NUP153). All proteins of the last group contain characteristic phenylalanine-glycine (FG) rich repeats interspersed with hydrophobic linkers and/or coiled-coil motifs (Fahrenkrog, 2014). FG repeats have been shown to be essential for trafficking due to their affinity for transport receptors like importin β (Suntharalingam and Wente, 2003).

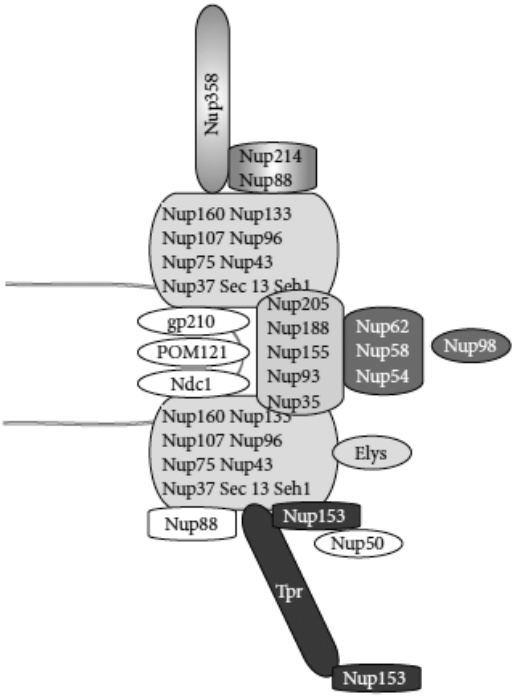

Figure 5 – Grouping and localisation within the nuclear pore complex.
Depending on their amino acid sequence, structural motifs and localisation, nucleoporins (NUPs) can be divided into different groups: transmembrane proteins (white), scaffold NUPs (light grey), NUPs of the cytoplasmic filaments (gradient), central channel NUPs (middle grey) and nuclear basket NUPs (dark grey) (Fahrenkrog, 2014).

1.2.2 ALADIN as a scaffold nucleoporin

Cronshaw et al. identified ALADIN as a protein of the NPC in a proteomic approach of the mammalian NPC (Cronshaw et al., 2002). ALADIN is anchored within the NPC by the transmembrane NUP NDC1 (Kind et al., 2009; Yamazumi et al., 2009). Together with NUP93 and NUP214 it belongs to the group of barely exchangeable NUPs based on their dissociation rates and residence times at the NPC and therefore seems to build the structural scaffold backbone of the complex. ALADIN does not seem to be important for integrity of NPCs because nuclei lacking the protein do not show structural impairments in these complexes (Cronshaw and Matunis, 2003). Rabut et al. classified several tryptophan-aspartic acid (WD) repeats-containing NUPs in the group of proteins which form the stable NPC backbone. Their WD repeats can initiate

a number of protein-protein interactions (Rabut et al., 2004). ALADIN belongs to this group (Tullio-Pelet et al., 2000).

Most of the known *AAAS* mutations result in mislocalisation of the altered ALADIN protein mainly to the cytoplasm (Cronshaw and Matunis, 2003; Krumbholz et al., 2006; Koehler et al., 2008). It is suspected that ALADIN facilitates cell type-specific nucleo-cytoplasmic transport and is therefore of great importance for the maintenance of distinct tissues involved in the pathogenesis in triple A syndrome (Cronshaw and Matunis, 2003).

1.3 Oxidative stress

1.3.1 Introduction and role of the adrenal

Cellular reactive oxygen species (ROS) originate from molecular oxygen and comprise the following molecules which all have different reaction properties: superoxide anion radical $O_2^{\bullet -}$, hydrogen peroxide H_2O_2 and hydroxyl radical $HO^{\bullet}$. Biotransformation reactions involving oxidations, reductions, hydrolyses (all phase I) and conjugation reactions (phase II) are the most common causes of ROS production. In the following I will focus on phase I reactions and conjugation reaction involving glutathione.

An imbalance in cellular ROS levels can have deleterious effects on the cell in several ways. DNA can be damaged by hydrogen radicals attacking purines (8-guanine), bases and sugars can be oxidised, single-stranded and double-stranded DNA breaks can occur and proteins can be cross-linked. Amino acids like cysteine and methionine are very likely to be affected by ROS. In addition, free amino acid side chains can be oxidised, and proteins can be cross-linked and fragmented. Unsaturated and saturated fatty acids involved in lipid metabolism and sterols can easily be attacked by hydrogen radicals forming lipid peroxide radicals which have similar effects as ROS. Moreover ROS can (dis-)regulate genes resulting in apoptosis, stress, tumour development, fibrosis and chemokine production. Besides ROS there also exist reactive nitrogen species which are generated of decomposed nitrogen dioxide by photons. Molecular oxygen can also be used as photo-initiator resulting in the production of ozone. These types of radicals will attack other cellular compartments in more aggressive ways (Dekant, 2009).

Adrenocortical cells have a huge number of mitochondria which are responsible for steroid production and oxidative respiration. The increased turnover of lipids and uncoupling of the respiratory chain leads to an increased risk of ROS leakage. In addition, several other bio-reaction systems can lead to leakage of ROS when being dysregulated; among these are xanthine/xanthine oxidase, nitric oxide synthases, $NADPH$-dependent oxidases and most strikingly the adrenal cortex CYP P450s (Prasad et al., 2014b).

All CYP P450s are hemoproteins with an iron-protoporphyrin IX prosthetic group whereby the iron undergoes cyclic oxidation Fe^{3+} and reduction Fe^{2+}. Iron has six binding sites of which five are occupied. The sixth can bind to an α-OH of the hemoprotein or water. The reaction consists of a mixed-function oxidase system in which the CYP P450 exploits the key position and different flavoproteins interact with the reducing agent $NAD(P)H$ (Dekant, 2009). Flavoproteins contain a prosthetic group flavin adenine dinucleotide (FAD) and/or flavin mononucleotide (FMN) and are electron transfer-proteins facilitating the redox reaction of all CYP P450s with $NAD(P)H$ and molecular oxygen. Type I CYP P450s rely on the flavoenzyme ferredoxin re-

ductase (FDXR1) and type II on the microsomal flavoprotein cytochrome P450 oxidoreductase (POR) (and $NADH$-$CYPb_5$ reductase ($CYPb_5$)). FDXR1 accepts two electrons from $NADPH$ by FAD and transfers them firstly to ferrodoxin before passing them on to mitochondrial CYP P450 (Pandey and Fluck, 2013; Prasad et al., 2014b). POR receives two electrons from $NADPH$ by FAD, passes them onto FMN and finally transfers them directly or via $CYPb_5$ to several microsomal CYP P450s (exemplified for CYP17A1 in Figure 6). $CYPb_5$ can act in a similar fashion like POR (Pandey and Fluck, 2013). The role of POR will be described in detail in subsection 1.5 Involvement of the endoplasmic reticulum in steroidogenesis. During the CYP P450 redox reaction the substrate SH first binds to Fe^{3+}-CYP P450. $NAD(P)H$ gives off two electrons which are passed on to CYP P450 by the previously mentioned flavoenzymes. Oxygen is incorporated into Fe^{2+}-CYP P450 and activated to superoxide anion. The substrate is hydroxylated to SOH, water and Fe^{3+}-CYP P450 are split off. The reaction steps can be summarised in the following equation:

$$SH + O_2 + NAD(P)H + H^+ \rightarrow SOH + H_2O + NAD(P)^+.$$

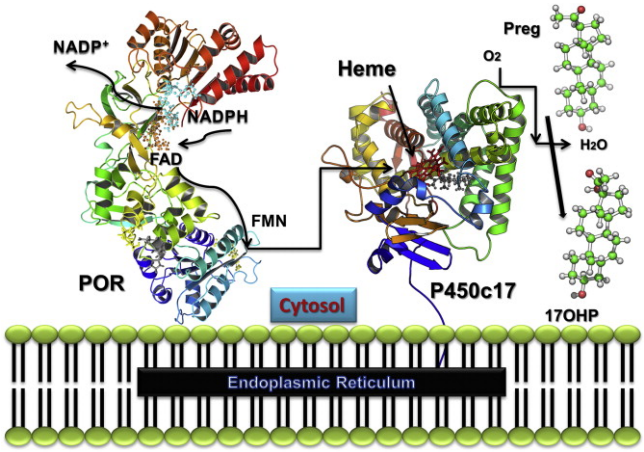

Figure 6 – Electron flow to CYP17A1 is facilitated by cytochrome P450 oxidoreductase.
Cytochrome P450 oxidoreductase (POR) is an integral endoplasmic reticulum protein and binds $NADPH$. Two electrons are received by flavin adenine dinucleotide (FAD) inducing a conformational change. FAD and flavin mononucleotide (FMN) are moved closer and the electrons are passed to FMN and further to the catalytic prosthetic heme group of CYP17A1 (P450c17) (Pandey and Fluck, 2013).

Mitochondrial steroidogenesis significantly adds to ROS formation in the cell because uncoupling of the CYP P450 redox reaction can occur in different steps of the reaction: during the incorporation of molecular oxygen and during its activation. Under these circumstances superoxide anions and hydrogen peroxide can leak and escape from the reaction (Dekant, 2009). During the last step of cortisol synthesis, the production of cortisol from 11-deoxycortisol by CYP11B1, approximately 40 % of total electron flow is passed into ROS formation (Rapoport et al., 1995). During the reaction of cholesterol to pregnenolone by CYP11A1 approximately 15 % of electrons are transferred into ROS formation (Rapoport et al., 1995).

1.3.2 Anti-oxidant defence in the adrenal

In contrast to other organs with a high metabolic rate like brain and liver, the adrenal gland has a high level of enzymatic and non-enzymatic anti-oxidants. Imbalances in ROS production

result in cellular oxidative stress and have been implicated in several different diseases including cancer, neurological manifestations and diabetes mellitus. Therefore, an equilibrated level of anti-oxidative mechanisms is of high importance, especially in the adrenal cortex.

Among the non-enzymatic anti-oxidants are ascorbic acid (vitamin C), α-tocopherol (vitamin E) and coenzyme Q10.

Enzymatic anti-oxidants are superoxide dismutase (SOD), catalase and glutathione peroxidase (GPX). Superoxide anion radicals are detoxified by SOD to hydrogen peroxide and molecular oxygen. Hydrogen peroxide is further inactivated to water by peroxisomal catalase. Cytosolic GPX (predominantly GPX1), with the help of glutathione (GSH), and peroxiredoxin (predominantly PRDX3), which depends on the electron donor thioredoxin 2 (TXN2), are also able to neutralise hydrogen peroxide. Both latter systems depend on the reducing agent $NADPH$ which is synthesised by nicotinamide nucleotide transhydrogenase (NNT). Regenerated $NADPH$ is used to produce GSH from its oxidised form $GSSG$ by glutathione reductase (GSR) and by the TXN2 system to produce reduced PRDX. GPX belong to the group of selenoproteins and use a selenocysteine residue as redox reactive prosthetic group. The selenium content of the adrenal is actually shown to be high (Prasad et al., 2014b). During inactivation of hydrogen peroxide a PRDX dimer is oxidised to a disulphide dimer and reduced again by TXN2. GPX catalyses the reaction more efficiently than the thioredoxin system (Figure 7) (Prasad et al., 2014b).

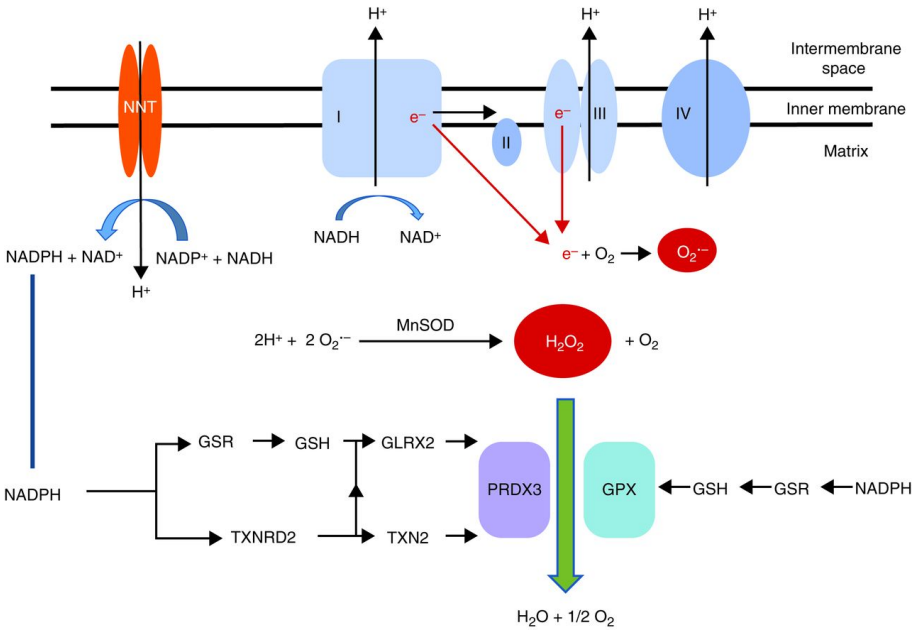

Figure 7 – Detoxification pathways after leakage of electrons of the mitochondrial respiratory chain. Superoxide anions $O_2^{\bullet -}$ can be protonated by manganese-dependent superoxide dismutase (MnSOD) to form hydrogen peroxide H_2O_2 which is in turn neutralised to result water by thioredoxin 2 (TXN2) and glutathione (GSH) systems. This antioxidants are dependent on high levels of $NADPH$ provided by nicotinamide nucleotide transhydrogenase (NNT) (Prasad et al., 2014b).

1.3.3 Nucleoporins and mitochondrial energy metabolism

It is suspected that a dysfunction of ALADIN may play a role in cellular accumulation of ROS causing species-specific impairments in cells which are hypersensitive to oxidative stress. There is increasing evidence that ALADIN-deficient cells are more susceptible to oxidative stress (Kind

et al., 2010; Prasad et al., 2013; Jühlen et al., 2015). In fibroblast cell cultures of different triple A syndrome patients all mean enzyme expression levels of the ROS detoxifying enzymes SOD1, SOD2, catalase and GSR were altered. The expression of *SOD1* increased significantly, the expression of catalase decreased 0.7 fold. Furthermore it was shown that the mitochondrial network in patient cells is more pronounced than in control fibroblasts. The maximal ATP synthesis was the same in patient cells as in controls, but synthesis was decreased per mitochondrion. In addition, the rate of cell division was decreased in patient cells. It was concluded that fibroblasts of triple A patients have a higher basal ROS level and an increased response to artificially induced oxidative stress (Figure 8) (Kind et al., 2010).

In addition, studying differential gene expression in ALADIN-deficient or -mutated cells under oxidative stress, it was previously seen that cells of triple A patients show an altered induction or down-regulation of genes associated with oxidative stress and anti-oxidant defence (Koehler et al., 2013).

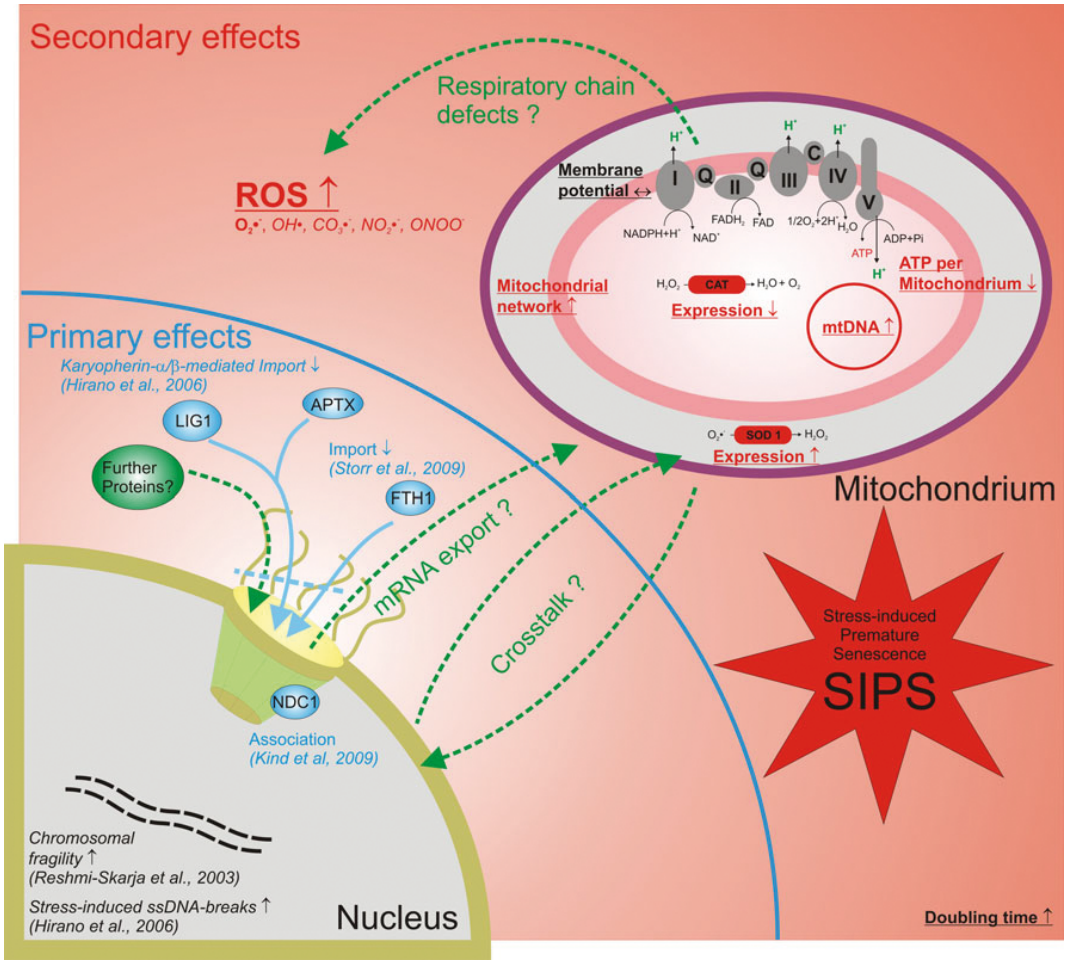

Figure 8 – Model of the suspected pathogenesis in triple A syndrome.
ALADIN-deficient cells are more sensitive to oxidative stress due to several mechanisms in the cell leading to stress-induced premature senescence (SIPS). It is hypothesised that there is an ALADIN-dependent cross-talk between the nucleus and mitochondria and mRNA export (Kind et al., 2010).

Ferritin heavy chain protein (FTH1) was identified as an interaction partner of ALADIN in a bacterial two-hybrid screen of cDNA libraries (Storr et al., 2009). In addition to its well-known iron storage role, FTH1 has been shown to protect the nucleus from oxidative damage. It was hypothesised that mutant ALADIN impairs the nuclear import of FTH1 in triple A syndrome. A

deficiency of nuclear FTH1 results in an enhanced susceptibility of cells to ROS and cellular damage (Storr et al., 2009). Furthermore it was shown that cells of triple A patients have a higher degree of chromosomal fragility (Reshmi-Skarja et al., 2003). Concomitantly, Hirano et al. observed a reduced nuclear import of DNA ligase 1 (LIG1) and aprataxin (APTX) in a patient fibroblast cell line which both have functions in DNA single strand break repair. It was concluded that these cells have an increased sensitivity to oxidative stress (Hirano et al., 2006).

So far one other NPC component, the cytoplasmic filament RANBP2/NUP358, has been identified to localise to the mitochondria via nuclear-encoded cytochrome oxidase assembly protein 11 (COX11) and hexokinase type I *in vitro* and *in vivo* and to exploit a distinct mechanism in glucose metabolism and energy homeostasis selectively in the central nervous system in mice (Aslanukov et al., 2006; Cho et al., 2007). In humans heterozygous mutations in *RANBP2* cause a neurological disorder called acute necrotising encephalopathy (MIM #608033) (Neilson et al., 2009).

Another pathology affecting the central nervous system was found due to mutations in the central channel nucleoporin *NUP62* (autosomal recessive infantile bilateral striatal necrosis (IBSN) (MIM #271930)) (Basel-Vanagaite et al., 2006). Many clinical features of IBSN overlap with Leigh syndrome (subacute infantile necrotising encephalopathy) (MIM #256000) which is caused by mutations in nuclear- and mitochondrial-encoded genes regulating energy metabolism (Finsterer, 2008).

The detailed pathogeneses in the described nucleoporinopathies caused by *RANBP2* and *NUP62* are unclear, but it has been shown that adaptor proteins like RANBP2 mediate the transport of a broad range of different cargoes and are mediators of mitochondrial function and energy maintenance (Cho et al., 2007; Neilson et al., 2009). Up to now functions of ALADIN in animal and human cell physiology remain in parts elusive. Animal and human disease states share some of their pathophysiological pathways leading specifically to neurological manifestations. The increased sensitivity to oxidative stress may be one major reason for the neurodegeneration causing the various symptoms in triple A syndrome (Kind et al., 2010).

1.4 Adrenocortical disorders and redox imbalances

As discussed earlier the adrenal cortex has a great capacity of buffering ROS which are especially produced during lipid metabolism and steroidogenesis in the mitochondria. Impairment in mitochondrial redox homeostasis by liberating ROS can therefore lead to uncoupling of steroidogenic pathways. Several disorders causing adrenocortical deficiency have been recently associated with an adrenal redox imbalance. These disorders will be summarised in the following.

1.4.1 Familial glucocorticoid deficiency

Familial glucocorticoid deficiency (FGD) is a rare life-threatening autosomal recessive disorder characterised by glucocorticoid deficiency and ACTH unresponsiveness. Forty-five percent of the cases are caused by impaired ACTH signalling due to mutations in key components of the signalling cascade: mutations in *MC2R* (MIM #202200) account to 25 % of FGD patients and mutations in the adrenal specific melanocortin receptor accessory protein (*MRAP*) (MIM

#607398) for further 20 % of all cases (Weber and Clark, 1994; Metherell et al., 2005; Clark et al., 2009; Metherell et al., 2009).

The role of MRAP is trafficking of the MC2R from the ER to the surface of the cell (Webb and Clark, 2010). Most mutations in *MRAP* cause retention of the MC2R at the ER, some mutations cause reduced signalling of the receptor. These patients show a milder phenotype with later onset than those with loss-of function in MRAP (Hughes et al., 2010).

Notably, more than 40 mutations in steroidogenic acute regulatory protein (*StAR*) have been identified to cause lipoid congenital adrenal hyperplasia (LCAH) (MIM #201701), and some of these patients were shown to develop the phenotype of a severe form of FGD (Metherell et al., 2009; Miller and Bose, 2011). StAR initiates the first step in steroidogenesis by importing cholesterol across the mitochondrial membrane. Most mutations in *StAR* causing LCAH are loss-of function mutations. These results in excessive accumulation of cholesterol and destruction of adrenocortical cells, characteristics seen in the phenotype of LCAH (Meimaridou et al., 2013).

In about FGD patients without mutations in *MC2R* and *MRAP*, two new genes causing FGD have been identified. Recently, mutations in minichromosome maintenance complex component 4 (*MCM4*) (MIM #609981) in an Irish Traveller community are shown to cause FGD (O'Riordan et al., 2008; Hughes et al., 2012; Gineau et al., 2012). In addition, mutations in *NNT* (MIM #614736) lead to FGD (Meimaridou et al., 2012). Novoselova et al. also described a *NNT* pseudogene activation as the cause for FGD (Novoselova et al., 2014).

MCM4 codes for a DNA replicase leading to increased genomic instability, DNA breakage during DNA replication in mitosis and natural killer cell deficiency when being mutated (O'Riordan et al., 2008; Hughes et al., 2012; Gineau et al., 2012). *NNT* is a highly conserved gene encoding an integral proton pump of the inner mitochondrial membrane catalysing the conversion of $NADP^+$ to $NADPH$ by using $NADH$ produced in the citric acid cycle (CAC) (Meimaridou et al., 2012). Detoxification of mitochondrial ROS by GPX and PRDX3 depends on the regeneration of $NADPH$ (Prasad et al., 2014b). Importantly, another member of the TXN2 system, thioredoxin reductase 2 (TXNRD2) (Figure 7), has lately been associated with FGD (Prasad et al., 2014a).

The exact mechanisms why mutations in these genes affect the hormone production in the adrenal cortex is not known. Both proteins, NNT and MCM4, seem to have specific functions in adrenal cells causing the FGD phenotype (Meimaridou et al., 2013). NNT shows high protein expression levels in the adrenal gland affecting sensitive organelles in these cells – the mitochondria (Meimaridou et al., 2012). Increased ROS levels will lead to cell damage including increased DNA strand breakage and genomic instability which resembles pathogenic features of patients carrying *MCM4* mutations. It seems that not only mitochondria, but also cell divisions are sensitive processes in adrenocortical cells leading to impaired steroidogenesis; a clinical hallmark in triple A syndrome patients (Hirano et al., 2006).

1.4.2 X-linked adrenoleukodystrophy

X-linked adrenoleukodystrophy (ALD) (MIM #300100) mainly affecting males (females are mostly symptomatic carriers) is caused by mutations in *ABCD1* coding for the peroxisomal ATP-

binding cassette, subfamily D, member 1 protein. ALD and triple A syndrome have in common that both the nervous system and the adrenal gland are involved. The clinical manifestations in ALD presented at any age can vary even within families. Symptoms are heterogeneous, mainly affecting the adrenal cortex, the myelin of the central nervous system and the Leydig cells of the testes. Adrenal insufficiency may precede neurological symptoms and can also occur solely (Prasad et al., 2014b; Moser et al., 2000; Moser et al., 2005). Moser et al. described the existence of seven different phenotypes affected with ALD (Moser et al., 2000).

ABCD1 is involved in peroxisomal β-oxidation of fatty acids in peripheral tissues. Mutations lead to accumulation of saturated very long chain fatty acids (VLCFA) (24-30 carbons) in plasma and body tissues due to an ineffective import into the peroxisome for degradation. Lipid metabolism is a prerequisite for functional steroid production. Accumulation of VLCFA is mainly seen in zonae fasciculata and reticularis of the adrenal cortex, myelin sheath and testes; according to the affected areas of the disease (Forss-Petter et al., 1997). Therefore, the disease is classified as a lipid-storage disease. VLCFA may interfere with adrenal steroidogenesis and myelin production in the central nervous system. It is thought that adrenal impairment is caused by excessive VLCFA, which (a) cannot be used for re-synthesis and steroid production, (b) disturb balances in fatty acid precursors for cholesterol esters and that (c) can impair MC2R signalling (Moser, 1997).

Interestingly, an involvement of oxidative stress has been seen in histology of specimens from ALD patients and from the mouse model involving altered enzyme activities for hemoxygenase 1 and manganese-dependent SOD and lipid peroxidation (Powers et al., 2005). In addition depletion of glutathione and increased levels of ROS have been determined in patient skin fibroblasts (Fourcade et al., 2008). Decreased levels of $NADPH$ and ATP have been seen in *ABCD1* knock-out mice suggesting an impaired energy balance (Galino et al., 2011). It is still unclear how accumulation of VLCFA leads to the induction of oxidative stress, but there have been proposed several hypotheses. Peroxisomes are in near communication with mitochondria and are additionally important for lipid metabolism in the cell; therefore disturbances in peroxisomes would ultimately lead to mitochondrial redox imbalances (Ivashchenko et al., 2011). In the mouse model accumulation of VLCFA is seen in mitochondria, probably directly affecting the function of the organelle (Forss-Petter et al., 1997).

However, *ABCD1* knock-out mice do not develop a phenotype as seen in ALD patients before 16-20 weeks when locomotion alterations occur. Importantly, no ALD adrenal phenotype could be determined in mice so far – neither under basal condition nor under stress induction (Forss-Petter et al., 1997). This observation is consistent with the *AAAS* knock-out mice where no adrenal phenotype could be analysed (Huebner et al., 2006). Presumably, both proteins ABCD1 and ALADIN undertake a species-specific role in adrenal steroidogenesis leading to adrenal insufficiency in both diseases.

1.5 Involvement of the endoplasmic reticulum in steroidogenesis

As already outlined, triple A patients suffer from high levels of oxidative stress and impaired anti-oxidant defence (Kind et al., 2010; Prasad et al., 2013; Jühlen et al., 2015). Mitochondria of these patients show impaired function and are altered in their energy homeostasis (Kind et

al., 2010). In this subsection it will be discussed how mitochondria interact with the ER and how this interaction can be of importance in understanding the pathogeneses of triple A syndrome.

1.5.1 Mitochondrial tethering

The translocase of the outer membrane (TOM) complex is the main entry site for all mitochondrial proteins which are nuclear-encoded (~99 %). It is composed of distinct subunits: the core complex consisting of a protein-conducting channel TOM40, the central receptor TOM22 and three smaller proteins TOM5-7. Two further receptors, TOM70 and TOM20, are associated with the core complex (general import pore complex) (Wiedemann et al., 2009).

Mitochondrial precursor proteins contain specific target signals which guide them to different compartments of the mitochondria. There are at least five different mitochondrial sorting pathways described which are conducted each by different sorting and assembly machineries within the mitochondria (Figure 9) (Wiedemann et al., 2009; Chacinska et al., 2009; Schmidt et al., 2010; Becker et al., 2012). Subunits of the respiratory chain mediating cellular oxidative homeostasis are both mitochondrial-encoded (the three core subunits COX1-3) and nuclear-encoded (the remaining subunits). Nuclear-encoded proteins, like COX5, are translated on cytosolic ribosomes and are transported into the mitochondria through TOM (Mick et al., 2011). The identification of unidentified nuclear-encoded regulators for the assembly of the respiratory complex and its stability shall shed light on this specific pathway. As already mentioned earlier, COX11 co-localises with RANBP2/NUP358 *in vitro* and *in vivo* (Aslanukov et al., 2006; Cho et al., 2007).

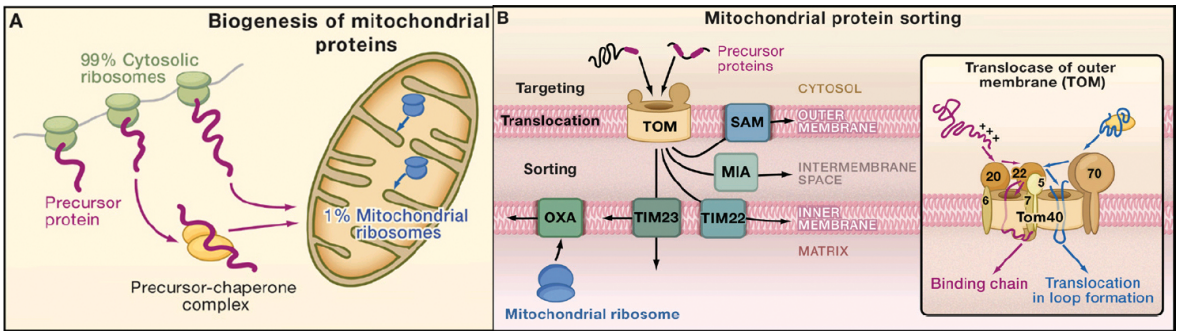

Figure 9 – Biogenesis of mitochondrial proteins (A) and protein sorting through the import machinery translocase of the outer membrane (B).
The translocase of the outer membrane (TOM) complex mediates the main entry for all nuclear-encoded proteins and shuttles them to their final mitochondrial destination by five different pathways outlined in (B). SAM, sorting and assembly machinery. MIA, mitochondrial intermembrane space assembly machinery. TIM22, translocase of the inner mitochondrial membrane 22. TIM23, translocase of the inner mitochondrial membrane 23. OXA, oxidase assembly machinery (Chacinska et al., 2009).

It is known that the TOM complex interacts through TOM7 with the junctions between ER and mitochondria which are formed by the mitochondrial distribution and morphology (MDM) complex. The MDM complex consists of maintenance of mitochondrial morphology 1 (Mmm1), cytosolic Mdm12 and Mdm34 and Mdm10 of the outer mitochondrial membrane (Figure 10) (Schmidt et al., 2010; Becker et al., 2012). Mmm1 is embedded in the ER membrane and shown to be glycosylated (Kornmann et al., 2009). The MDM complex connects the outer ER membrane with parts of the outer mitochondrial membrane and is therefore termed the ER-mitochondrion encounter structure (ERMES).

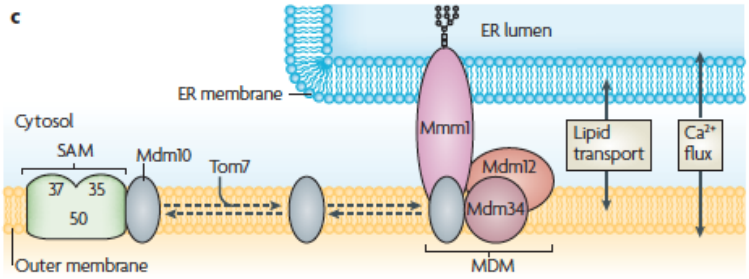

Figure 10 – Endoplasmic reticulum-mitochondrion junction.
The ER-mitochondrion encounter structure (ERMES) is formed by the mitochondrial distribution and morphology (MDM) complex consisting of maintenance of mitochondrial morphology 1 (Mmm1), Mdm12, Mdm34 and Mdm10. The translocase of the outer membrane (TOM) complex interacts through TOM7 with the junctions between ER and mitochondria. ERMES associates with the sorting and assemble machinery (SAM) which is responsible for shuttling of β-barrel proteins of the outer mitochondrial membrane (Schmidt et al., 2010).

These structures are thought to shuttle the transport of different molecules between the two organelles such as lipids and calcium ions. It is highlighted that mitochondrial morphological alterations result from defect ER-mitochondrial junctions, but the detailed molecular function of the MDM complex is yet unknown (Schmidt et al., 2010). Recently, in yeast it has been shown that ERMES is responsible for transfer of phosphatidylserines between the two organelles. Phosphatidylserines are necessary for the synthesis of phosphatidylethanolamine which is an important compound of cellular membranes and necessary for lipid metabolism (Lahiri et al., 2014). Two dynamin-like GTPases mitofusin 1 and 2 have been shown to be essential for ER-mitochondrion junctions and in addition, for mitochondrial steroidogenesis as shown by Duarte and co-workers (de Brito and Scorrano, 2008; Duarte et al., 2014; Duarte et al., 2012).

1.5.2 Cytochrome P450 oxidoreductase

POR is a flavoprotein residing at the cytoplasmic site of the ER and acting as a co-factor facilitating the redox reaction between all microsomal CYP P450 enzymes and the reducing agent $NADPH$ (Figure 6) (Arlt et al., 2004; Fluck et al., 2007). POR is involved in a variety of biochemical pathways within the steroid and drug metabolism, iron homeostasis or sterol synthesis. The flavoprotein supplies electrons to heme oxygenases, fatty acid desaturases and elongases, squalene monooxygenase, $CYPb_5$ and sterol reductases (Figure 11) (Pandey and Fluck, 2013; Fluck et al., 2007; Fluck and Pandey, 2011; Riddick et al., 2013). $CYPb_5$ has been reported to be an allosteric co-factor for some interactions between POR and CYP P450s. Since all microsomal P450s depend on POR for their catalytic reaction, the specific biochemical steroid output can be altered even if the involved CYP P450 enzyme activity is otherwise normal (Fluck and Pandey, 2011).

Initially, patients with *POR* mutations were diagnosed with Antley-Bixler syndrome. A rare variant of congenital adrenal hyperplasia showing combined CYP17A1 and CYP21A2 deficiencies has been reported since 1985 and has been shown to be the cause of mutant *POR* in 2004 (Arlt et al., 2004; Peterson et al., 1985; Fluck et al., 2004; Miller et al., 2004). POR deficiency (PORD) has then be separately called disordered steroidogenesis due to cytochrome P450 oxidoreductase deficiency (MIM #613571) and Antley-Bixler syndrome with genital anomalies and disordered steroidogenesis (MIM #201750).

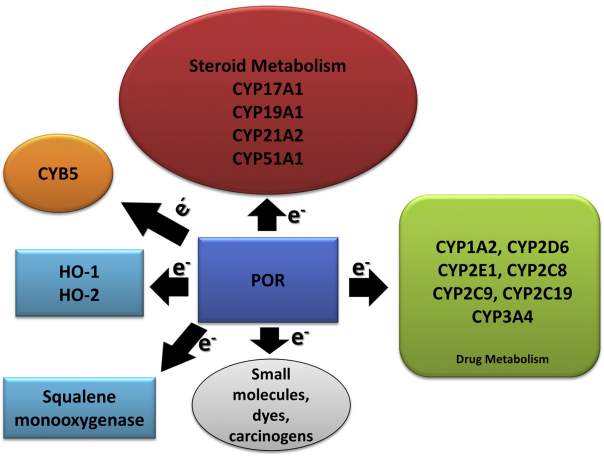

Figure 11 – Role of cytochrome P450 oxidoreductase in several biochemical pathways.
Cytochrome P450 oxidoreductase (POR) regulates steroid and drug metabolism through several CYP P450 enzymes (CYP17A1, CYP1A2, etc.). Cytochrome b5 ($CYPb_5$) is an allosteric co-factor donating a second electron through POR to some CYP P450s. Many small molecules can be directly de- or inactivated by POR. Furthermore, POR donates electrons to heme oxygenases (HO) in iron metabolism and squalene monooxygenase for sterol synthesis (Pandey and Fluck, 2013).

Since then, many different mutations in *POR* have been described and associated with disturbed steroidogenesis. Many of the described mutations can be found in co-factor-binding sites and there seems to exist specific founder mutations in distinct populations (Fluck et al., 2007; Miller et al., 2011; Pandey and Sproll, 2014). Many patients with skeletal deformations, ambiguous genitalia and impaired steroidogenesis have been linked to PORD. It was shown that PORD affects steroidogenesis in adrenal and gonads; thus leading to impaired sexual development and genital ambiguity at birth in males and females (Pandey and Sproll, 2014; Huang et al., 2005; Pandey et al., 2004). *POR* knock-out is embryonic lethal in mice whereas the liver-specific knock-out leads to decreased cellular metabolism and lipid accumulation (Shen et al., 2002; Gu et al., 2003).

1.6 Aims of the Study

Overall, the scaffold NUP ALADIN stabilising the structural backbone of the NPC seems to facilitate a cell-type specific nucleo-cytoplasmic transport and to cause a cell-type specific damage in its absence. There exists a wide spectrum of diseases sharing clinical and cellular pathologies with triple A syndrome. It has to be assumed that impaired function of ALADIN predominantly affects specialised cells; neurotransmitter-releasing cells of the central and peripheral nervous system (e.g. neurons) and secretory cells of the adrenal cortex. Regulation of adrenocortical steroidogenesis is complex and there is increasing evidence that oxidative stress due to ROS accumulation and mitochondria are significantly involved. Furthermore, there may be an important cross-talk between functional organelles comprising nucleus, ER and mitochondria which presumably involves lipid metabolism.

It is hypothesised that oxidative stress in triple A syndrome patient fibroblasts leads to degeneration and to stress-induced premature senescence (Kind et al., 2010). Therefore, it can be assumed that patient adrenocortical cells are likewise affected by increased levels of oxidative stress resulting in impaired steroidogenesis and degeneration of these cells. To elucidate these assumptions, the cellular role of ALADIN was investigated in this study by creating two experimental models using the adrenocortical tumour cell line NCI-H295R1, a sub-strain showing characteristics of the glucocorticoid-producing zona fasciculata of the adrenal cortex (Wang et al., 2012). Cells were engineered to either over-express or down-regulate *AAAS* by inducible stable transfection. Subsequently, alterations in steroidogenic gene expression were determined and functional consequences were assessed by steroid quantification from cell supernatants employing a liquid chromatography/tandem mass spectrometry (LC/MS-MS) method for simultaneous quantification of 13 key steroids of the adrenal steroidogenic pathway. In addition, the role of ALADIN on cell viability, oxidative stress response and nuclear import of APTX, LIG1 and FTH1 was examined in these models.

In an approach to identify new interaction partners of ALADIN co-immunoprecipitation (co-IP) followed by proteome analyses using mass spectrometry was conducted in an exogenous ALADIN over-expression model using NCI-H295R. These results were verified in endogenous co-IP using NCI-H295R wild-type cells. The goal of this work was to elucidate the function of ALADIN for adrenocortical steroidogenesis and its consequences for the cellular oxidative stress response.

2 Materials

Table 1 – Antibodies.

PRODUCT	COMPANY
ALADIN antibody (B-11): sc-374073	Santa Cruz Biotechnology, Inc., Heidelberg, Germany
Alexa fluor 488 goat anti-rabbit IgG	Molecular Probes, Life Technologies, Darmstadt, Germany
Alexa fluor 555 goat anti-mouse IgG	Molecular Probes, Life Technologies, Darmstadt, Germany
Anti-PGRMC2	Sigma-Aldrich, Munich, Germany
Cytochrome P450 reductase antibody (ab13513)	Abcam plc, Cambridge, UK
Goat anti-mouse IgG conjugated to horseradish peroxidase	Invitrogen, Life Technologies, Darmstadt, Germany
Goat anti-rabbit IgG conjugated to horseradish peroxidase	Cell Signalling Technology Europe B.V., Leiden, Netherlands
Monoclonal ß-actin antibody produced in mouse, clone AC-74	Sigma-Aldrich, Munich, Germany
Normal mouse IgG and normal rabbit IgG	Invitrogen, Life Technologies, Darmstadt, Germany

Table 2 – Buffer solutions and reagents.

PRODUCT	COMPANY
Agarose for DNA electrophoresis	SERVA Electrophoresis GmbH, Heidelberg, Germany
Amersham enhanced chemiluminescence (ECL) prime western blotting detection system	GE Healthcare GmbH, Little Chalfont, United Kingdom
Ampicillin	AppliChem GmbH, Darmstadt, Germany
Antibiotic-antimycotic solution	PAA, GE Healthcare GmbH, Little Chalfont, United Kingdom
Blasticidin S	InvivoGen, Toulouse, France
Bovine serum albumin	Sigma-Aldrich, Munich, Germany
Carestream Kodak autoradiography GPX replenisher/fixer	Kodak, Laborversand A. Hartenstein, Würzburg, Germany
COmplete protease and PhosSTOP phosphatase inhibitor cocktail tablets	Roche Diagnostics Corporation, Indianapolis, IN, United States
Difco LB agar and broth, Miller	BD Biosciences, Heidelberg, Germany
DMEM/F12 medium	Lonza, Cologne, Germany
DNA annealing solution	Invitrogen, Life Technologies, Darmstadt, Germany
Doxycyline hydrochloride	MP Biomedicals, Eschwege, Germany
Formaldehyde	SAV LP, Flinsbach, Germany
GelRed DNA stain	Biotium, Inc., Hayward, CA, United States
Glycerol	Carl Roth GmbH & Co KG, Karlsruhe, Germany
Hi-Di formamide	Applied Biosystems, Life Technologies, Darmstadt, Germany

PRODUCT	COMPANY
Insulin-tranferrin-selenium (ITS-G)	Gibco, Life Technologies, Darmstadt, Germany
L-glutamine	Lonza, Cologne, Germany
Methyl tertiary butyl ether	Sigma-Aldrich, Munich, Germany
Methyl viologen dichloride (paraquat)	Sigma-Aldrich, Munich, Germany
Milk powder	Sigma-Aldrich, Munich, Germany
Nu-Serum	BD Biosciences, Heidelberg, Germany
Paraformaledhyde	Sigma-Aldrich, Munich, Germany
Phosphate buffered saline	Sigma-Aldrich, Munich, Germany
Trypsin	Invitrogen, Life Technologies, Darmstadt, Germany
VECTASHIELD mounting medium for fluorescence with and without DAPI	Vector Laboratories, Burlingame, CA, USA
X-tremeGENE HP DNA transfection reagent	Roche Diagnostics, Mannheim, Germany
Zeocin	InvivoGen, Toulouse, France

Table 3 – Cells and enzymes.

PRODUCT	COMPANY
Antarctic phosphatase	New England Biolabs, Inc., Ipswich, MA, United States
Benzonase nuclease	Novagen, Merck Millipore, Darmstadt, Germany
Mix & Go competent cells – strain Zymo 5α	Zymo Research, Irvine, CA, United States
NCI-H295R	ATCC, Manassas, United States
NCI-H295R GFP-AAAS and NCI-H295R GFP	Katrin Köhler
NCI-H295R1-TR	Enzo Lalli
NCI-H295R1-TR AAAS knock-down	Ramona Jühlen
NCI-H295R1-TR AAAS over-expression	Ramona Jühlen
NCI-H295R1-TR pcDNA4/TO empty	Ramona Jühlen
NCI-H295R1-TR scrambled shRNA	Ramona Jühlen
Platinum Pfx DNA polymerase	Invitrogen, Life Technologies, Darmstadt, Germany
Restriction enzymes (BglII, HindIII, XhoI and PvuI)	New England Biolabs, Inc., Ipswich, MA, United States
T4 ligase	Invitrogen, Life Technologies, Darmstadt, Germany
T4 polynucleotide kinase	New England Biolabs, Inc., Ipswich, MA, United States

Table 4 – Equipment.

PRODUCT	COMPANY
20 G cannula	BD Biosciences, Heidelberg, Germany
24-well culture dish	Corning Costar, Kaiserslautern, Germany
30 G cannula	B. Braun Melsungen AG, Melsungen, Germany
3x1 inch microscope slides	Engelbrecht, Edermünde, Germany
6-well culture dish	Corning Costar, Kaiserslautern, Germany
70 µm ultra clear pressure sensitive sealing film	Axygen Scientific, Corning Costar, Kaiserslautern, Germany
96-well culture dish	Corning Costar, Kaiserslautern, Germany
96-well garbage plate	Qiagen GmbH, Hilden, Germany
96-well microplate	Corning Costar, Kaiserslautern, Germany
96-well PCR plate	Axygen Scientific, Corning Costar, Kaiserslautern, Germany
96-well silicone rubber septa mat	Corning Costar, Kaiserslautern, Germany
ABI 7300 fast real-time PCR system	Applied Biosystems, Life Technologies, Darmstadt, Germany
ABI prism genetic analyzer 3130xl	Applied Biosystems, Life Technologies, Darmstadt, Germany
AcroPrep 96-well filter plate	Pall GmbH, Dreieich, Germany
Amersham hybond-enhanced chemiluminescence (ECL) nitrocellulose membrane (0.45 µm)	GE Healthcare GmbH, Little Chalfont, United Kingdom
Avanti J-30I ultra centrifuge with a JA-10 and a JA-30.50 Ti rotor	Beckman Coulter GmbH, Krefeld, Germany
Axiovert 200 M with Axiocam MRm	Carl Zeiss, Jena, Germany
BBD6220 Incubator	Heraeus Holding GmbH, Hanau, Germany
Biofuge prime R	Heraeus Holding GmbH, Hanau, Germany
Biofuge primo R	Heraeus Holding GmbH, Hanau, Germany
Borosilicate glass tube	Fisherbrand, Schwerte, Germany
CASY TT- cell counter and analyzer system	OLS OMNI Life Science GmbH & Co KG, Bremen, Germany
Centrifuge 5417C	Eppendorf AG, Hamburg, Germany
Fresco 17 centrifuge	Thermo Scientific, Fischer Scientific, Schwerte, Germany
GFP-Trap_A agarose beads	ChromoTek GmbH, Planegg-Martinsried, Germany
Glass cover slip	Carl Zeiss, Jena, Germany
IDL TRM 50 rolling platform	IDL GmbH & Co KG, Nidderau, Germany
Illustra Sephadex G-50 DNA grade, fine	GE Healthcare GmbH, Little Chalfont, United Kingdom

PRODUCT	COMPANY
Incubator Type B12	Heraeus Holding GmbH, Hanau, Germany
Infinite 200 PRO multimode microplate reader	Tecan Group AG, Männedorf, Switzerland
Innova 4430 incubator shaker	New Brunswick, Eppendorf, Enfield, CT, United States
Laser scanning spectral confocal microscope TCS SP2	Leica Microsystems, Mannheim, Germany
Mithras LB940 luminometer	Berthold Technologies, Bad Wildbad, Germany
Multifuge 3 S-R	Heraeus Holding GmbH, Hanau, Germany
MultiScreen centrifuge alignment frame	Pall GmbH, Dreieich, Germany
MultiScreen column loader and scraper	Merck Millipore, Merck Chemicals GmbH, Schwalbach, Germany
Nanodrop spectrophotometer (ND-1000)	NanoDrop Technologies, Wilmington, DE, USA
Nitrogen evaporator	Gebrüder Liebisch Labortechnik GmbH, Bielefeld, Germany
Novex sharp pre-stained protein standard	Invitrogen, Life Technologies, Darmstadt, Germany
OV3 rotation chamber	Biometra GmbH, Göttingen, Germany
Petri dish	Greiner Bio-One GmbH, Frickenhausen, Germany
Protein G ultraLink resin sepharose beads	Pierce, Thermo Scientific, Fischer Scientific, Schwerte, Germany
PYREX 6x8 mm cloning cylinder	Sigma-Aldrich, Munich, Germany
Thermomixer comfort	Eppendorf AG, Hamburg, Germany
WT16 rocking platform	Biometra GmbH, Göttingen, Germany

Table 5 – Kits and assays.

PRODUCT	COMPANY
Amplex red hydrogen peroxide/peroxidase assay	Invitrogen, Life Technologies, Darmstadt, Germany
BigDye terminator v1.1 and v3.1 cycle sequencing	Applied Biosystems, Life Technologies, Darmstadt, Germany
CellTiter-Blue cell viability assay	Promega, Mannheim, Germany
DC protein assay	BioRad Laboratories, München, Germany
EasyPrep pro plasmid miniprep	Biozym Scientific GmbH, Hessisch Oldendorf, Germany
GoScript reverse transcription system	Promega, Mannheim, Germany
GoTaq probe qPCR master mix	Promega, Mannheim, Germany
GoTaq qPCR master mix	Promega, Mannheim, Germany
GSH/GSSG-Glo assay	Promega, Mannheim, Germany

PRODUCT	COMPANY
NucleoSpin RNA	Macherey-Nagel, Düren, Germany
NUPAGE bis-Tris mini gel 4-12 %, LDS sample buffer and reducing agent	Invitrogen, Life Technologies, Darmstadt, Germany
PureLink HiPure plasmid filter maxiprep	Invitrogen, Life Technologies, Darmstadt, Germany

Table 6 – Vectors and plasmids.

CONSTRUCT	PRODUCER
pcDNA4/TO	Invitrogen, Life Technologies, Darmstadt, Germany
pcDNA4/TO-*AAAS* cDNA	Ramona Jühlen
pCRII TOPO-*AAAS* cDNA	Barbara Kind
pTER	Enzo Lalli
pTER-*AAAS*1 and pTER-*AAAS*2 shRNA	Ramona Jühlen
pYFP C1-*LIG1*, *APTX*-N3 and *FTH1*-N3	Barbara Kind

Table 7 – siRNA oligonucleotides for cloning.

SIRNA TARGET	SEQUENCE
AAAS (region 1)	
siRNA-forward	GATCCATGAAATTGCAAACTCAGATTCAAGAGATCTGAGTTTGCAATTTCATTTTTTTGGAAA
siRNA-reverse	AGCTTTTCCAAAAAAATGAAATTGCAAACTCAGATCTCTTGAATCTGAGTTTGCAATTTCATG
AAAS (region 2)	
siRNA-forward	GATCCGATCTGATCGCTGAATTTGTTCAAGAGACAAATTCAGCGATCAGATCTTTTTTGGAAA
siRNA-reverse	AGCTTTTCCAAAAAAGATCTGATCGCTGAATTTGTCTCTTGAACAAATTCAGCGATCAGATCG
Scrambled	
siRNA-forward	GATCCAGTACTGCTTACGATACGGTTCAAGAGACCGTATCGTAAGCAGTACTTTTTTGGAAA
siRNA-reverse	AGCTTTTCCAAAAAAGTACTGCTTACGATACGGTCTCTTGAACCGTATCGTAAGCAGTACTG

Oligonucleotides were ordered from Metabion international AG, Planegg/Steinkirchen, Germany.

Table 8 – PCR primer oligonucleotides.

PRIMER NAME	SEQUENCE
AAAS-specific *Hind*III-forward	cgccaagcttgccaccATGTGCTCTCTGGGGTTGTTCC
AAAS-specific *Xho*I-reverse	cgccctcgagTTAGAGGTGGGAATGTGGGGAG

These oligonucleotides and in the following tables were ordered from Eurofins Genomics, Ebersberg, Germany.

Table 9 – Sequencing primer oligonucleotides.

PRIMER NAME	SEQUENCE
AAAS-forward exon 11 (*AAAS*-Ex11-1104-F)	GCCGACTGCTGTTCACTGTA
AAAS-forward exon 16 (TA-WD-Exon 16/2-F)	ATGACCTGCCCCTCTTTACT
AAAS-forward exon 2 (TA-WD-cd239-F)	GATCCCCTAAAGACCCCTGG
AAAS-forward exon 6 (*AAAS*-Ex6-558-F)	GGCACCCCCACACCAACAAG
AAAS-reverse exon 2 (*AAAS*-Ex2-280-R)	GGTGATGGATGAAGGCAGTT
BGH-reverse	TAGAAGGCACAGTCGAGG
BK-PCMV-IE-forward	TGGGAGGTCTATATAAGCAGAGC
BK-SequFluo-forward 2	AGGACGACGGCAACTACAAGACC
BK-SequFluo-reverse	CAGGATGTTGCCGTCCTCCTTGA
BK-SequFluo-reverse 2	GTACAGCTCGTCCATGCCGAGA
JG 387-forward	GGATCACTCTCGGCATGG
JG 387-reverse	CCTCTACAAATGTGGTATGG

Table 10 – Real-time qPCR primer oligonucleotides.

GENE	LENGTH	NAME	SEQUENCE
AAAS	71 bp	281*AAAS*-Ex7-F	CCCTACCTCCTTGTCTACCCG
(V1: NM_015665.5)		282*AAAS*-Ex8-R	CAGGTGTATGCCCAGGGTG
		283*AAAS*-hSonde	TCTTCTGGCTGTGCCCAAGTGCTGTC
ACTB	189 bp	hs-ß-Actin-F	GCACCCAGCACAATGAAGATC
(V1: NM_001101.3)		hs-ß-Actin-R	CGCAACTAAGTCATAGTCCGC
		hs-ß-Actin-Sonde	TGCTCCTCCTGAGCGCAAGTACTCC
CYP11A1	92 bp	h*CYP11A1*-F	CGGGCTCCGGAAATTACTC
(V1: NM_0007812.2;		h*CYP11A1*-R	CTGGCGCTCCCCAAAAAT
V2: NM_0001099773.1)		h*CYP11A1*-Sonde	TTCCGCTTTGCCTTTGAGTCCATCACT
CYP11B1	81 bp	h-*CYP11B1*-F	TGAGGACCTGCACCTGGAAG
(V1: NM_000497.3;		h-*CYP11B1*-R	ATGCCTGCTCCTCCCAARTC
V2: NM_001026213.1)			
*CYP17A*1	97 bp	h*CYP17A*-F	TGCTTATTAAGAAGGGCAAGGACTT
(V1: NM_000102.3)		h*CYP17A*-R	GAGTCAGCGAAGGCGATACC
		h*CYP17A*-Sonde	TAGAGTTGCCATTTGAGGCCGCCC
*CYP21A*2	74 bp	h*CYP21A*-Ex6F	CATAGAGAAGAGGGATCACATCGT
(V1: NM_000500.7;		h*CYP21A*-Ex7R	TCCACTGGCCTGCCACG
V2: NM_001128590.3)		h*CYP21A*-Ex6/7-Sonde	CTCTCCTTGTGCTGCCTCAGCTGCAT

GENE	LENGTH	NAME	SEQUENCE
DHCR24	69 bp	*DHCR24*-F	CTGGCTGATGGCAGCTTTGT
(V1: NM_014762.3)		*DHCR24*-R	CCAGGGTACGGCATAGAACAG
		DHCR24-Sonde	CGATGCACTCCGTCCGAAAACTCAGA
GAPDH	75 bp	*GAPDH*-F	GCACCGTCAAGGCTGAGAAC
(V1: NM_002046.4;		*GAPDH*-R	AGGGATCTCGCTCCTGGAA
V2: NM_001256799.1)			
GSR	71 bp	*GSR*-F	TATGCCCTCCACCCCTCAT
(V1: NM_000637.3;		*GSR*-R	TGAAAAAATCCATCGCTGGTT
V2: NM_001195102.1;		*GSR*-Sonde	CAGATCCCCGGTGCCAGCTTAGGA
V3: NM_001195103.1;			
V4: NM_001195104.1)			
POR	92 bp	h*POR*-F	TTTGTGGAAAAGATGAAGAAAACG
(V1: NM_000941.2)		h*POR*-R	GACAGGCGGTTGGCAAACT
		h*POR*-Sonde	AACATCATCGTGTTCTACGGCTCCCAGA
STAR	98 bp	h*STAR*-F	CAGACTTCGGGAACATGCCT
(V1: NM_000349.2)		h*STAR*-R	CTTAGAGGGACTTCCAGCCAA
		h*STAR*-Sonde	ACCGTGCTCCGCCCTGATGACA

Table 11 – Software.

PRODUCT	COMPANY
3130xl v3.0 data collection	Applied Biosystems, Life Technologies, Darmstadt, Germany
7300 sequence detection v1.3.1	Applied Biosystems, Life Technologies, Darmstadt, Germany
Contig express vector NTI advance v10.3.0	Invitrogen, Life Technologies, Darmstadt, Germany
Fuji v1.48b (Fuji Is Just ImageJ)	Open-source-software
Magellan - data analysis v6.6	Tecan Group AG, Männedorf, Switzerland
MASCOT v.2.2	Matrix Science, London, United Kingdom
MikroWin 2000 v4.29	Berthold Technologies, Bad Wildbad, Germany
NanoDrop spectrophotometer ND-1000 v3.5.2	NanoDrop Technologies, Wilmington, DE, USA
OLIGO primer analysis v7.60	Molecular Biology Insights Inc., CO, United States
Primer express 3.0	Applied Biosystems, Life Technologies, Darmstadt, Germany
R i386 v2.15.0 and R Studio v0.98.1074	The R Foundation for Statistical Computing, Vienna, Austria
Web-based siRNA Target Finder	Matrix Science, London, United Kingdom

3 Methods

3.1 Plasmids and vector construction for shRNA silencing of gene expression and cDNA over-expression

For generation of the *AAAS* short hairpin (sh)RNA- and h*AAAS* cDNA-inducible NCI-H295R1 cell clones, the tetracycline-inducible T-REx system was employed. In this system the expression of a gene of interest runs under a tetracycline-inducible promoter (Figure 12). Cells were co-transfected with the repressor-expressing plasmid pcDNA6TR and the expression plasmid with the tetracycline response element. The inducible expression vector pTER for shRNA silencing was generously provided by Enzo Lalli and contained a H1 promoter specific for expression of small nuclear RNAs (van de Wetering et al., 2003). The inducible pcDNA4/TO expression vector was used for full-length h*AAAS* cDNA over-expression.

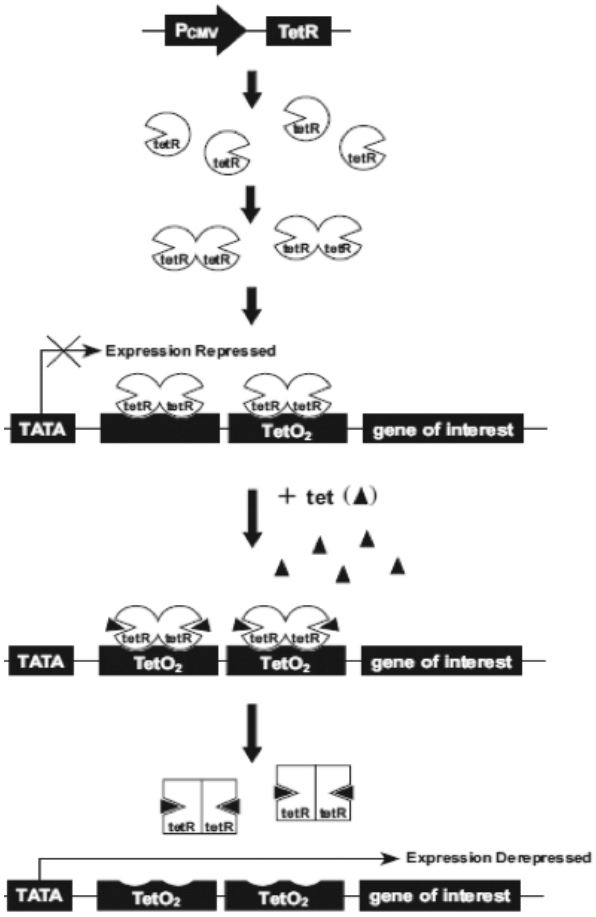

Figure 12 – Tetracycline-inducible T-REx cell-expression system.
The expression of the gene of interest (either *AAAS* shRNA in pTER or cDNA in pcDNA4/TO) was under the control of a tetracycline-inducible promoter. Cells were co-transfected with pcDNA6TR expressing a repressor tetR which binds to the operator sequence TetO2 on the expression plasmids pTER or pcDNA4/TO and repressed expression. Upon addition of doxycycline (a tetracycline analogue) the repressor is conformationally changed, falls off and the expression is de-repressed (Invitrogen, 2011, modified).

Double-stranded small interfering (si)RNA oligonucleotides were used as shRNA templates (Figure 13) and were designed using the Ambion web-based algorithm siRNA Target Finder (Invitrogen, 2015) and compared to the human genome database for no more than 16-17 contiguous base pairs of homology to other coding sequences using BLAST (U.S. National

Library of Medicine, 2015) in order to avoid incomplete complementary with other off-target genes. Six regions were selected to be the target sequence for shRNA silencing of *AAAS* (V1: NM_015665.5) and the two best regions (1: nt279-299 AAATGAAATTGCAAACTCAGA and 2: nt410-430 AAGATCTGATCGCTGAATTTG) were used for further experiments. As a negative control a region for a non-targeting scrambled shRNA (AAAGTACTGCTTACGATACGG) was used. These control experiments should give rise to all non-specific effects in mammalian cells during the stable transfection used and the shRNA silencing methodology.

To create inducible pTER expression plasmids two complementary siRNA oligonucleotides were annealed and 5'-phosphorylated by T4 polynucleotide kinase. The oligonucleotides were T4-ligated into *Bgl*II- and *Hind*III- by antarctic phosphatase 5'-dephosphorylated restriction sites of pTER. Dephosphorylation of the vector after restriction enzyme digest decreased the effect of self-religation of the vector itself and increased the yield of the desired generated plasmid. All siRNA template oligonucleotides contained a 5'-*BamH*I overhang (5'-GATC-3') which is compatible with the 3'-*Bgl*II overhang (3'-CTAG-5') of the digested pTER (Figure 13). Reaction mixtures are summarised in Tables 12-16.

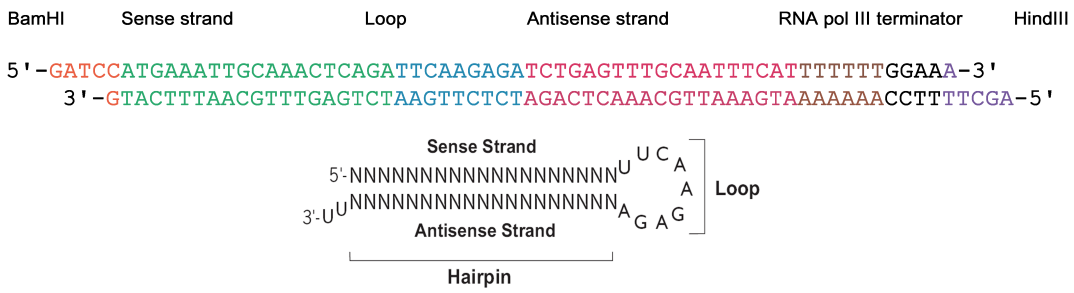

Figure 13 – Annealed complementary double-stranded small interfering RNA template and hairpin structure of the expressed short hairpin RNA.

Here as an example *AAAS* region 1 small interfering (si)RNA is shown. A short loop is introduced into the siRNA sequence. After ligation into the expression vector pTER the cell after stable transfection will express a short hairpin (sh)RNA which will be further processed into siRNA by the enzyme Dicer and other protein complexes (Bernstein et al., 2001). This system guarantees a more efficient shRNA gene silencing than transient siRNA transfection by target mRNA bypass mechanisms or degradation (Hairpin structure taken from Invitrogen, 2011).

For generation of inducible pcDNA4/TO expression plasmids the full-length h*AAAS* cDNA was used. The cDNA was previously cloned into the pCRII TOPO vector and the plasmid pCRII TOPO-h*AAAS* cDNA (200 ng/µl) was kindly provided by Barbara Kind. Restriction sites were introduced into the cDNA by PCR with *AAAS*-specific *Hind*III-forward and *Xho*I-reverse primers using the diluted plasmid pCRII TOPO-h*AAAS* cDNA (1:10^4) as template. PCR was conducted using Platinum *Pfx* DNA polymerase with proofreading and 3' to 5' exonuclease activity (Table 17). Primer sequences contained specific restriction sites in order to ligate the cDNA in the same sites in the vector after digestion of both (Table 8). The amplified h*AAAS* cDNA and the pcDNA4/TO expression vector were both digested using *Hind*III and *Xho*I. The full length cDNA was then T4-ligated between *Hind*III- and *Xho*I-sites into 5'-dephosphorylated pcDNA4/TO. The empty vector without PCR insert was used here as negative control in order to monitor all non-specific cellular effects after stable transfection.

All restriction digests were loaded on 1 % agarose gels in order to verify efficient DNA restriction enzyme digest. For gel casting 3 g of agarose for DNA electrophoresis was mixed with 300 ml Tris-borate-EDTA buffer and heated up in the microwave at 700 W for 5 minutes.

The mixture was cooled down under stirring and 15 µl of GelRed DNA stain was added. Gels were cast with 20 µl pockets. DNA digests were mixed 6:1 with a loading dye (30 % glycerol, 0.25 % bromophenol blue and 0.25 % xylene cyanol) and loaded beside GeneRuler 100 bp and 1 kb DNA Ladder on the gel. Agarose gels were run at 200 V for at least 45 minutes.

Table 12 – Annealing of siRNA template oligonucleotides.

COMPONENT	VOLUME/REACTION [µl]
Sense siRNA (1µg/µl)	2
Antisense siRNA (1µg/µl)	2
1X DNA annealing solution	46

The annealing reaction was incubated at 90 °C for 3 minutes and at 37 °C for 60 minutes.

Table 13 – Phosphorylation of siRNA 5'-hydroxyl termini using T4 polynucleotide kinase.

COMPONENT	VOLUME/REACTION [µl]
Annealed siRNA template oligonucleotides	39
5X T4 DNA ligase buffer	10
T4 polynucleotide kinase (10 U/µl)	1

Phosphorylation was done at 37 °C for 30 minutes followed by heat inactivation of the kinase at 65 °C for 20 minutes.

Table 14 – Restriction cross digest of siRNA expression vector pTER.

COMPONENT	VOLUME/REACTION
Vector (2µg/µl)	10 µg
Aqua dest.	Ad 100 µl
10X NEB2 buffer	10 µl
*Hind*III (20 U/µl)	5 µl
and afterwards	
*Bgl*II (10 U/µl)	10 µl

Restriction digest with *Hind*III and afterwards with *Bgl*II was done at 37 °C over-night and heat inactivation of *Hind*III at 65 °C for 20 minutes.

Table 15 – Dephosphorylation of pTER 5'-phosphate groups using antarctic phosphatase.

COMPONENT	VOLUME/REACTION
Digested pTER vector	10 µg
10X Antarctic phosphatase reaction buffer	10 µl
Antarctic phosphatase (5 U/µl)	2 µl

Dephosphorylation was done at 37 °C for 15 minutes and heat inactivation of the phosphatase at 65 °C for 20 minutes.

Table 16 – Ligation of siRNA inserts and pTER vector using T4 ligase.

COMPONENT	1:5 RATIO	1:10 RATIO	VECTOR CONTROL	INSERT CONTROL
Aqua dest.	Ad 20 µl	Ad 20 µl	Ad 20 µl	Ad 20 µl
5X T4 ligase buffer	4 µl	4 µl	4 µl	4 µl
Vector 4494 bp (0.1 µg/µl)	50 ng	50 ng	50 ng	-
Insert 63 bp (7 ng/µl)	3.5 ng	7 ng	-	3.5 ng
T4 ligase	1	1	1	1

Vector and inserts were ligated at 14 °C over-night. Calculation of vector and insert DNA at a ratio of free molecule ends of 1:1:

$$ng\ insert = \frac{bp\ insert * 50\ ng\ vector}{bp\ vector}$$

Table 17 – Amplification of h*AAAS* cDNA using Platinum *Pfx* DNA polymerase.

COMPONENT	VOLUME/REACTION [µl]
10X *Pfx* amplification buffer	5
dNTP mixture (10 mM)	1.5
$MgSO_4$ (50 mM)	1
Primer mix (10 µM each)	1.5
Template DNA pcRII TOPO-h*AAAS* cDNA $(1:10^4)$	1
Platinum *Pfx* DNA polymerase	0.4
Ultra pure water	Ad 50

The DNA template was denatured in an initialisation step at 94 °C for 2 minutes. Amplification was done using three-step cycling: firstly denaturation of the DNA template at 94 °C for 15 seconds, secondly annealing of the primers at 60 °C for 30 seconds and thirdly DNA extension at 68 °C for 1 minute per kb. The PCR was repeated for 35 cycles. Final hold was at 10 °C.

Investigation of nuclear import processes was done using C- or N-terminal fluorescent protein vectors (pFP C1 or pFP N3). Full length cDNA of *LIG1* (V1: NM_000234.2), *APTX* (V1: NM_175073.2; V6: NM_001195248.1; V7: NM_001195249.1) and *FTH1* (V1: NM_002032.2) were cloned to create pYFP C1-*LIG1*, *APTX*-N3 pYFP and *FTH1*-N3 pYFP plasmids. These plasmids were kindly provided by Barbara Kind.

All ligation products and provided plasmids were transformed into Mix & Go competent cells – strain Zymo 5α using the manufacturer's protocol. Ampicillin (100 µg/µl) as selection reagent for all plasmids was used in Difco LB agar and broth at a concentration of 100 µg/ml. Transformed bacteria (either 10 or 60 µl per plate) were split out on 20 ml Difco LB agar, Miller, petri dishes and grown over-night at 37 °C in an incubator Type B 12. Bacteria were picked using 10 µl pipette tips and seeded in 3 ml Difco LB broth, Miller, at 37 °C and 230 rpm over-night using an Innova 4430 incubator-shaker. Bacterial DNA was isolated using EasyPrep pro plasmid miniprep kit as described in the manufacturer's protocol. For maxi preparations 500 µl of subsequent mini preparation bacterial culture were initially mixed with 50 ml Difco LB broth, Miller, and incubated for at least 4 hours at 37 °C and 230 rpm. The subsequent culture was then mixed with 200 ml Difco LB broth, Miller, and incubated over-night at 37 °C and 230 rpm. Bacterial DNA was isolated using PureLink HiPure plasmid filter maxiprep kit as described in the protocol of the manufacturer using an Avanti J-30I ultra centrifuge with a JA-10 (17700x g) and JA-30.50 Ti (108800x g) rotor. Glycerol stocks were prepared of each bacterial maxi prep culture expressing the plasmid of interest (500 µl maxi prep culture mixed with 500 µl 50 % glycerol). All plasmid constructs were confirmed by DNA sequencing to rule out introduced bacterial mutations. An overview of all generated plasmid constructs can be found in section 2 Materials.

3.2 DNA sequencing

DNA sequencing reactions were done using BigDye terminator v1.1 and v3.1 cycle sequencing kit, the ABI Prism genetic analyzer 3130xl and 3130xl v3.0 data collection Software. Following sequencing reactions AcroPrep 96-well filter plates were filled with 45 µl illustra Sephadex G-50 DNA grade, fine, using the MultiScreen column loader and scraper. To each well 300 µl deionised water was added. The mixture was incubated at least 3 hours at 4 °C covered with the lid and centrifuged at 1613x g for 3 minutes on a multifuge 3 S-R using the MultiScreen centrifuge alignment frame and a corresponding 96-well plate. The water was discarded and subsequently, 20 µl of cycle sequencing reactions were pipetted onto the Sephadex columns to get rid off cycle sequencing reaction components. AcroPrep 96-well filter plates were centrifuged again as described and cleaned sequencing products were caught in round-bottom 96-well microplates. Hi-Di formamide (10 µl) was pipetted into 96-well PCR plates and 2 µl of the clean sequencing product was added. Plates were sealed with 96-well silicone rubber septa mats, spinned down and proceeded to sequencing analysis.

Plasmid constructs using the inducible siRNA expression vector pTER were verified by sequencing using the vector-intern BGH-reverse primer and constructs obtained by the inducible pcDNA4/TO expression vector were verified using the vector-intern BGH-reverse primer and whole *AAAS* cDNA-spanning primers: *AAAS*-forward primer for exon 2 (TA-WD-cd239-F) and reverse primer for exon 2 (*AAAS*-Ex2-280-R), forward primer for exon 6 (*AAAS*-Ex6-558-F), exon 11 (*AAAS*-Ex11-1104-F) and exon 16 (TA-WD-Exon 16/2-F) and *Hind*III-forward primer.

For sequencing of plasmids used for the investigation of nuclear import processes (pFP C1 or pFP N3) the following primers were used: the cloned cDNA in the pYP C1 construct (*LIG1*) was verified using JG 387-forward and -reverse primers and in the pYP N3 constructs (*APTX*

and *FTH*) using BK-PCMV-IE-forward and BK-SequFluo-reverse primers. For sequencing the fluorescent protein (YFP) of the fusion proteins in both plasmid constructs BK-SequFluo-forward 2 and -reverse 2 primers were used. All sequencing primers were generated using OLIGO Primer Analysis Software v7.60 and sequences were analysed using Contig Express Vector NTI Advance v10.3.0.

3.3 Cell culture and treatments

NCI-H295R1-TR cells containing a tetracycline response system, expressing a repressor binding to the tetracycline response element, were kindly provided by Enzo Lalli (Doghman et al., 2007; Nogueira et al., 2009). The cells were cultured in DMEM/F12 medium supplemented with 1 mM L-glutamine, 5 % Nu-serum, 1 % insulin-transferrin-selenium (ITS-G), 1 % antibiotic-antimycotic solution (100 U penicillin/ml, 0,1 mg/ml streptomycin sulphate and 0.25 µg/ml amphotericin B) and 5 µg/ml blasticidin S. The vector pcDNA6TR expressing the repressor, binding to the tetracycline response element on the expression plasmids, contained a blasticidin S resistance gene. Cells expressing the vector of choice will grow in the presence of 5 µg/ml blasticidin S. Cells were maintained in a 37 °C humidified atmosphere (5 % CO_2) using a BBD6220 Incubator.

For generation of NCI-H295R1-TR stably expressing *AAAS* shRNA (NCI-H295R1-TR *AAAS* knock-down) the cells were transfected with the two different pTER-*AAAS*1 and pTER-*AAAS*2 shRNA vectors or the pTER-scrambled shRNA vector as a control cell line (NCI-H295R1-TR scrambled shRNA).

For generation of NCI-H295R1-TR stably expressing h*AAAS* cDNA (NCI-H295R1-TR *AAAS* over-expression), the pcDNA4/TO-*AAAS* cDNA was transfected into NCI-H295R1-TR. NCI-H295R1-TR cells stably expressing empty pcDNA4/TO were generated in addition without PCR product insert as a control cell line (NCI-H295R1-TR pcDNA4/TO empty).

NCI-H295R1-TR cells with *AAAS* knock-down shRNA, scrambled shRNA, *AAAS* over - expression and pcDNA4/TO empty vector were selected and cultured with 100 µg/ml zeocin in culture media. Doxycyline hydrochloride (a tetracycline analogue) was used at 1 µg/ml for 48 hours to turn on the expression of the subsequent integrated gene or shRNA sequences. The most reliable sub-clones were selected and one clone per construct type was chosen (*AAAS* knock-down shRNA, scrambled shRNA, *AAAS* over-expression and pcDNA4/TO empty vector). Selected NCI-H295R1-TR cell lines were cultured in 6-well culture dishes at a density of 2x10^5 cells/well and treated 24 hours after seeding with doxycyline for 48 hours. In order to determine efficiency of *AAAS* knock-down, over-expression and expression of genes coding for steroidogenic enzymes total RNA was isolated from one well and used for real-time RT-PCR. In addition, whole protein was isolated from two wells and ALADIN expression was verified on protein level. Steroid production was determined by LC/MS-MS of the cell media of three wells. Experiments were repeated six times.

For analysis of oxidative stress response NCI-H295R1-TR *AAAS* knock-down, scrambled shRNA, *AAAS* over-expression and pcDNA4/TO empty cells were stimulated with 0.2 mM methyl viologen dichloride (paraquat) for 24 hours.

NCI-H295R cells stably expressing GFP-ALADIN fusion protein or GFP were kindly provided by Katrin Köhler. In order to generate these cells the γ-retroviral transfervectors pcz-CFG5.1-GFP-*AAAS* and pcz-CFG5.1-GFP were co-transfected with the packaging plasmids pHIT60 (a plasmid expressing murine leukaemia virus group-specific antigen and polymerase-integrase-replicase) which enable viral encapsulation and DNA integration and replication, respectively) and pMD.G (a plasmid expressing vesicular stomatitis virus protein G which facilitates viral entry into the host cell) into the packing cell line HEK 293T in order to produce pseudo retroviruses (Kind et al., 2009; Temme et al., 2003). NCI-H295R wild-type cells were transduced with pseudo retroviruses containing pcz-CFG5.1-GFP-*AAAS* and pcz-CFG5.1-GFP.

NCI-H295R wild-type cells and NCI-H295R cells stably expressing GFP-ALADIN fusion protein or GFP were cultured in DMEM/F12 medium supplemented with 1 mM L-glutamine, 5 % Nu-serum, 1 % ITS-G and 1 % antibiotic-antimycotic solution. Cells were maintained in a 37 °C humidified atmosphere (5 % CO2).

3.4 Stable and transient adrenal cell transfection

NCI-H295R1-TR cells were cultured in 6-well culture dishes containing medium supplemented with 5 µg/ml blasticidin S at a density of 1.6x10^5 cells/well 24 hours before subsequent transfections. Cells were counted with CASY TT - cell counter and analyzer system. Cells were transfected using X-tremeGENE HP DNA transfection reagent following the manufacturer's protocol. All plasmids were used at a concentration of 0.01 µg/µl diluted in pure DMEM/F12 at an optimised transfection ratio of 2:5. DNA-transfection reagent mixtures were left at room-temperature for 15 minutes and were given in drop wise manner to the cells. For stable transfections, pTER and pcDNA4/TO plasmid constructs (10 µg) were linearised prior transfections by digestion with *Pvu*I (20 U). At 50 % confluency after transfection cells were split 1:4 and sub-cultured in 6-well culture dishes containing medium supplemented with 100 µg/ml zeocin. Zeocin resistance was contained on pTER and on pcDNA4/TO and subsequently the resistance was expressed in those cells carrying the plasmid of interest. Clones appeared after approximately 4 weeks and were transferred each into one well of 24-well culture dishes by the use of PYREX 6x8 mm cloning cylinders. Clones were grown up and at a confluency of 70 % split at a ratio of 1:3.

For transient transfections of pYFP C1-*LIG1*, *APTX*-N3 and *FTH1*-N3, 10^5 cells of NCI-H295R1-TR *AAAS* knock-down, scrambled shRNA, *AAAS* over-expression and pcDNA4/TO empty cells were sub-cultured onto glass cover slips in 6-well culture dishes. During transfection 1 µg/ml doxycycline was added to the medium. After 24 hours the medium was changed and cells were grown for additional 24 hours in the presence of doxycycline.

3.5 RNA extraction, cDNA synthesis and quantitative real-time PCR using TaqMan

Total RNA was isolated directly from the well using the NucleoSpin RNA according to the protocol from the manufacturer using a Centrifuge 5417C. Purity of the RNA was assessed using Nanodrop spectrophotometer (ND-1000) and NanoDrop spectrophotometer ND-1000 software v3.5.2. RNA was stored at -80 °C until use. The amount of 500 ng of total RNA was reverse

transcribed with usage of the GoScript reverse transcription system following the protocols from the manufacturer and cDNA was stored at -20 °C.

Primers and probes for the quantitative amplification of the target sequence using TaqMan were designed using Primer Express 3.0 and compared to the human genome database for unique binding using BLAST search. The primer sequences, probes and gene accession numbers used for the amplification of specific target sequences are listed in section 2 Materials: ß-actin (*ACTB*), *AAAS*, *CYP11A1*, *CYP17A1*, *CYP21A2*, *GSR*, *POR* and *StAR*. Real-time PCR is a quantitative measurement of PCR amplification as it occurs during the exponential growth phase (exact doubling of product at every PCR cycle). TaqMan technology is based on the usage of two PCR primers and one probe which is labelled with a reporter dye and a quencher. During PCR primers and probe anneal to the target and during extension the Taq polymerase uses 5'-nuclease activity to degrade the reporter. The dye will be unquenched and emit fluorescence. The fluorescence is proportional to the amount of PCR product synthesised. A specific hybridisation is prerequisite for fluorescence emission and reduces background and especially false positive amplification products (Sherrill et al., 2004).

The qPCR amplifications were performed in triplicates using the GoTaq probe qPCR master mix according to the manufacturer's reaction parameters; using 20 µl total reaction volumes in 96-well PCR plates with 70 µm ultra clear pressure sensitive sealing films on an ABI 7300 fast real-time PCR system with the 7300 sequence detection software v1.3.1. The 20X primer stock solutions were prepared in a light insensitive tube as follows: 35.7 µl forward and reverse primer each (stock: 100 pmol/µl), 10 µl TaqMan probe (stock: 100 pmol/µl) and 118.6 µl nuclease-free water. As a reference dye 17 µl of carboxy-X-rhodamine was freshly added to each 1 ml tube of master mix. As housekeeping gene for normalisation *ACTB* was used. Positive controls contained a random mix of cDNA and negative controls contained nuclease-free water instead of cDNA.

In all real-time qPCR experiments relative gene expression was calculated using the C_t method using standard and semi-log plots of amplification curves. Subsequently, the measured mRNA of each sample was firstly normalised to the gene expression relative of *ACTB* and secondly to a calibrator. In each case the calibrator was the native doxycycline-uninduced sample. Finally, results were expressed either in gene expression relative to *ACTB* or in percentile change in gene expression relative to *ACTB* and calibrator as follows:

$$\% \; change = \frac{C_t \; sample}{C_t \; calibrator} * 100.$$

In all results repeatability was assessed by standard deviation of triplicate C_ts and reproducibility was verified by normalising all real-time RT-PCR experiments by the C_t of each positive control per run. The guidelines of the Minimum Information for Publication of Quantitative Real-Time PCR Experiments were followed in this work to allow more reliable interpretation of real-time RT-PCR results (Bustin et al., 2009; Bustin, 2010; Bustin et al., 2013).

3.6 Quantitative real-time PCR using a DNA-binding dye as reporter

Total RNA was extracted and reverse transcribed from NCI-H295R1-TR *AAAS* knock-down, scrambled shRNA, *AAAS* over-expression and pcDNA4/TO empty cells as described previously.

Primers for the amplification of the target sequence were designed using OLIGO primer analysis software v7.60 and compared to the human genome database for unique binding using BLAST search. All primer sequences and gene accession numbers used for the amplification of specific target sequences are listed in section 2 Materials: *CYP11B1*, 24-dehydrocholesterol reductase (*DHCR24*) and glyceraldehyde 3-phosphate dehydrogenase (*GAPDH*). During dye-based real-time PCR two primers were used and a double-stranded DNA-binding fluorophore. During PCR extension the dye will be integrated in the DNA, the target amplicon will increase and fluoresce. The fluorescence will be proportional to the amount of product but including non-specific amplified double-stranded DNA (false positives) (Sherrill et al., 2004; Wittwer et al., 2013).

The qPCR amplifications were performed in duplicate using the GoTaq qPCR master mix according to the manufacturer's reaction parameters and as described previously; using 20 µl total volumes. The 20X primer stock solutions were prepared as follows: 40 µl forward and reverse primer each (stock: 100 pmol/µl) and 120 µl nuclease-free water. As a reference dye carboxy-X-rhodamine was added to the qPCR reaction mixture. As housekeeping gene for normalisation *GAPDH* was used. Positive controls contained a random mix of cDNA and negative controls contained nuclease-free water instead of cDNA.

In all real-time qPCR experiments relative gene expression was calculated using the C_t method described previously. Results were presented in gene expression relative to GAPDH. In all results repeatability was assessed by standard deviation of duplicate C_ts and reproducibility was verified by normalising all real-time qPCR experiments by the C_t of each positive control per run. False positive measurements due to primer dimerisation during the amplification reaction were excluded by comparing the melting peaks of the negative controls with those of the samples. No secondary peak was observed in any of the PCR products which would indicate a secondary non-specific PCR product.

3.7 Chromatographic-mass spectrometric conditions and sample preparation

Steroids were isolated from 1 ml of NCI-H295R1-TR *AAAS* knock-down, scrambled shRNA, *AAAS* over-expression and pcDNA4/TO empty cell culture supernatant by liquid/liquid extraction using 3 ml of methyl tertiary butyl ether in borosilicate glass tubes. Samples were vortexed twice for 5 seconds at highest speed, spinned down and subsequently frozen at -20 °C for at least an hour. The top organic layer was poured off into a new clean and dry glass tube. The frozen aqueous layer was discarded. Samples were evaporated for 15 minutes at 55 °C and 0.5 bar using a nitrogen evaporator.

Samples were reconstituted in 200 µL of 50/50 methanol/water. They were analysed at the Centre for Endocrinology, Diabetes and Metabolism, School of Clinical & Experimental Medicine (Birmingham, United Kingdom) by LC/MS-MS on a Waters Xevo Mass Spectrometer with an Acquity ultra-Performance Liquid Chromatography system as described previously (Haring et al., 2012). Steroids were separated using a HSS T3 1.2 x 50 mm column by LC and identified in positive ionisation using electrospray ionisation mode by the mass analyser. The system set-up is described in Table 18.

Steroids were quantified by comparison to a calibration series ranging from 0.5 to 1000 ng/ml and set off against total protein content (µg) per well, which represents the cell number. Steroid concentrations were expressed in mMol/g total protein content and each sample was normalised to its native doxycycline-uninduced state giving the percentile change in steroid output as follows:

$$\%\ change = \frac{steroid\ conc.\ sample}{steroid\ conc.\ native} * 100.$$

All steroids were quantified using a suitable internal standard listed in Table 19. A set of steroids was considered covering the steroid bio-pathway; cortisol, cortisone, 11-deoxycortisol (compound S), corticosterone, androstenedione, testosterone, 5α-dihydrotestosterone, dehydroepiandrosterone, 17-hydroxyprogesterone (17OHP), deoxycorticosterone (DOC), progesterone, pregnenolone and 17-hydroxypregnenolone. Two mass transitions were required to positively quantify each steroid.

Table 18 – Liquid chromatography/mass spectrometry system parameters.

LC/MS SYSTEM SET-UP	CRITERIA
Capillary voltage	0.8-1.5 kV (depending on most recent tune file)
Collision energy	8-26 eV (depending on the mass transition)
Column	HSS T3, 1.8 µm, 1.2x50 mm column
Column temperature	60 °C
Cone voltage	14-30 V
Desolvation temperature	600 °C
Flow rate	0.6 ml/min
Injection volume	20 µL
Ionisation mode	Positive
Seal wash	10 % methanol
Solvent A1	Water (LC/MS grade) 0.1 % formic acid
Solvent B1	Methanol (LC/MS grade) 0.1 % formic acid
Solvents A2 and B2	50/50 methanol/water
Source	Electrospray source
Source temperature	150 °C
Strong wash	Solvent B
System	Waters Xevo mass spectrometer
uPLC	Acquity uPLC system
Weak wash	50/50 methanol/water

Table 19 – Mass transitions and retention times of steroids.

STEROID	ABBREVIATION	QUANTIFIER TRANSITION (precursor > product)	QUALIFIER TRANSITION (precursor > product)
11-deoxycortisol	S	347 > 97	347 > 109
11-deoxycortisol-d2	S-d2	349 > 97	349 > 109
17-hydroxypregnenolone	17OHPreg	297 > 279	297 > 159
17-hydroxypregnenolone-d3	17OHPreg-d3	336 > 300	336 > 105
17-hydroxyprogesterone	17OHP	331 > 97	331 > 109
17-hydroxyprogesterone-d8	17OHP-d8	339 > 100	339 > 113
Androstenedione	A'dione	287 > 97	287 > 109
Corticosterone	B	347 > 121	347 > 97
Corticosterone-d8	B-d8	355 > 125	355 > 100
Cortisol	F	363 > 121	363 > 97
Cortisol-d4	F-d4	367 > 121	367 > 331
Cortisone	E	361 > 163	361 > 121
Dehydroepiandrosterone	DHEA	289 > 253	289 > 271
Dehydroepiandrosterone-d6	DHEA-d6	277 > 219	277 > 259
Deoxycorticosterone	DOC	331 > 109	331 > 97
Dihydrotestosterone	DHT	291 > 255	291 > 159
Dihydrotestosterone-d3	DHT-d3	294 > 258	294 > 159
Pregnenolone	Preg	317 > 299	317 > 281
Pregnenolone-d4	Preg-d4	321 > 303	321 > 285
Progesterone	Prog	315 > 97	315 > 109
Progesterone-d9	Prog-d9	324 > 100	342 > 113
Testosterone	Test	289 > 97	289 > 109
Testosterone-d3	Test-d3	292 > 109	292 > 97

Steroids in italic represent internal standards.

3.8 Cell viability assay

For measurement of cell viability, NCI-H295R1-TR *AAAS* knock-down, scrambled shRNA, *AAAS* over-expression and pcDNA4/TO empty cells were sub-cultured at a density of 10^4 cells/well onto 96-well culture dishes. After 24 hours medium was added containing doxycycline. After another 48 hours one part of the cells was exposed to oxidative stress with 0.2 mM paraquat for 24 hours.

Cell viability was measured in triplicate in a final volume of 120 µl of paraquat-treated and untreated cells using CellTiter-Blue cell viability assay according to the manufacturer's protocol. Viable cells metabolised the redox dye resazurin to the red-fluorescent oxidation product resorufin by redox reactions. Non-viable cells did not produce a fluorescent metabolic end-product. Thus, the amount of resorufin was proportional to the amount of viable cells. Fluorescence emission at 590 nm of resorufin was measured after 4 hours using the Infinite 200 PRO multimode microplate reader and the Magellan - data analysis software v6.6. The experiments were repeated at least six times.

3.9 Measurement of total and oxidised glutathione

For measurement of GSH and its oxidised form ($GSSG$), NCI-H295R1-TR *AAAS* knock-down, scrambled shRNA, *AAAS* over-expression and pcDNA4/TO empty cells were sub-cultured at a density of 10^4 cells/well onto white-walled and white-bottomed 96-well culture dishes. After 24 hours the medium containing doxycyline was added. After another 48 hours cells were exposed to oxidative stress as described above.

The substrate luciferin-NT was converted to luciferin in a GSH-dependent reaction by glutathione-S-transferase. Luciferin was further used as substrate in a firefly luciferase reaction. Light emission was dependent on the amount of luciferin and in turn of GSH in the cell. Thus, the amount of detected light was proportional to the amount of GSH in the cell. Total GSH by converting all glutathione in the cell to GSH and $GSSG$ by blocking GSH were measured in triplicate using $GSH/GSSG$-Glo assay and the protocol recommended by the manufacturer. Luminescence was recorded after 15 minutes using the Mithras LB940 luminometer and the MikroWin 2000 software v4.29. An integration time of 0.5 sec for each 96-well-micro plate was used. The experiments were repeated at least five times.

3.10 Hydrogen peroxide assay

To detect H_2O_2 released from and within cells, NCI-H295R1-TR *AAAS* knock-down, scrambled shRNA, *AAAS* over-expression and pcDNA4/TO empty cells were sub-cultured at a density of 10^4 cells/well onto 96-well culture dishes. After 24 hours the medium containing doxycycline was added. After another 48 hours the cells were exposed to oxidative stress with 0.2 mM paraquat for 24 hours.

The concentration of H_2O_2 was measured in a final volume of 100 µl in triplicate of paraquat-treated and untreated cells using Amplex red hydrogen peroxide/peroxidase assay according to the manufacturer's protocol. Amplex red reagent reacts with H_2O_2 and produces the fluorescent oxidation product resorufin. Fluorescence emission at 590 nm of resorufin was measured after

5 hours using the Infinite 200 PRO multimode microplate reader and the Magellan - data analysis software v6.6. The experiments were repeated at least four times.

3.11 Nuclear import processes and microscopy

Transient transfected NCI-H295R1-TR *AAAS* knock-down, scrambled shRNA, *AAAS* over - expression and pcDNA4/TO empty cells grown on glass cover slips were washed three times with PBS, fixed with 4 % PFA in PBS for 10 minutes, followed by a three wash-step with PBS for 5 minutes and mounted onto 3x1 inch microscope slides with VECTASHIELD mounting medium for fluorescence without DAPI. For oxidative stress treatment cells were induced for another 24 hours with 0.2 mM paraquat before fixation.

Fluorescence was recorded using Axiovert 200 M and pictures taken using x40 objective, Axiocam MRm and filter set 38HE (excitation BP470/40, beam splitter FT 495, emission BP 525/50). Bright-field and fluorescence pictures were analysed using Fuji v1.48b (Fuji Is Just ImageJ). All input pictures were grey-scaled with auto exposure time for each picture. Cell cytosols and nuclei were analysed semi-automatically. Each cell cytosol of a series of pictures of a transient transfected cell type was measured automatically using the auto-threshold feature of ImageJ (Method Triangle) and the subsequent nucleus was marked manually. Region of interests (ROIs) of cytosols and nuclei were extracted on basis of the bright-field picture. These ROIs were transferred to the fluorescence picture and measured, giving the following data values for fluorescence intensity of cytosol and nucleus each: mean, median, minimum, maximum, area, standard deviation, percentage distribution, ratio ($\frac{mean_{nuc}}{mean_{cyt}}$) and especially for the nuclei, nucleus numbering (in order to verify and double-check the automatic process). Output values for fluorescence intensity of cytosols and nuclei ranged from 0 to 255; consequently, value 0 resembles no fluorescence intensity and value 255 maximum fluorescence intensity. Ratios were plotted in order to ascertain potential import impairment. The experiments were repeated twice.

3.12 Immunoblots

All cells were trypsinised, pelleted for 5 minutes at 220x g using a Biofuge primo R washed twice with PBS and centrifuged. Pellets (~10 µl) were subsequently lysed in 100 µl ice-cold lysis buffer containing 50 mM Tris (pH 7.4), 100 mM NaCl, 4 % sodium dodecyl sulfate, 1 % Triton X-100 and protease-phosphatase inhibitor (1 tablet/10 ml buffer, freshly prepared). Cell lysis and shearing was done using three times each a 20 G and a 30 G cannula. In order to avoid viscosity due to high DNA amount an additional step of 3 µl benzonase nuclease treatment for 30 minutes at 37 °C was done using a Thermomixer Comfort. Lysates were centrifuged at 15000x g using a Biofuge prime R for 5 minutes and the pellet was discarded. Protein concentration was measured using the colorimetric DC protein assay according to manufacturer's instructions. The biochemical assay exhibits an improved version of the method first described by Lowry (Lowry et al., 1951). Lysates were stored at -80 °C over-night.

Before loading 50 µg of protein per lane onto a NUPAGE bis-Tris mini gel samples were prepared with NUPAGE lithium dodecyl sulfate (LDS) sample buffer (4X), reducing agent (10X) and deionised water by heating the samples at 70 °C for 10 minutes using a Thermomixer Comfort.

LDS will denature the protein backbone and disulphide protein bonds will be reduced rendering the samples optimal for gel electrophoresis. After LDS-polyacrylamide gel electrophoresis (PAGE) separation (150 V for 1.5 hours) and electroblotting (30 V for 1.5 hours) onto Amersham hybond-enhanced chemiluminescence (ECL) nitrocellulose membrane (0.45 µm) non-specific binding of proteins to the membrane was blocked by incubation in PBS containing 3 % BSA at room-temperature using a Biometra WT16 rocking platform. The membrane was then probed with primary antibodies either anti-ALADIN (B-11): sc-374073 (1:100 in 3 % PBS/BSA), anti-POR (ab13513) (1:1000 in 5 % milk powder in PBS), anti-progesterone receptor membrane component 2 (anti-PGRMC2) (1:200 in 5 % PBS/milk powder) or anti-ACTB (clone AC-74) (1:20000 in 3 % PBS/BSA) over-night at 4 °C. Membranes were washed with 0.1 % Tween-20 in PBS for 30 minutes and secondary antibodies goat anti-mouse IgG conjugated to horseradish peroxidase (1:2000 in 3 % PBS/BSA) or goat anti-rabbit IgG conjugated to horseradish peroxidase (1:3000 in 5 % PBS/milk powder) were incubated one hour at room-temperature. Membranes were washed again for 30 minutes followed by detection using an Amersham ECL prime Western Blotting detection system using the protocol of the manufacturer. Blots were subsequently exposed to x-ray films and antigen bands visualised by autoradiography using Carestream Kodak autoradiography GPX replenisher/fixer.

3.13 Co-immunoprecipitation using agarose and sepharose beads

NCI-H295R wild-type cells and NCI-H295R cells stably transduced with GFP-ALADIN fusion protein or GFP were trypsinised and pelleted as described previously. Pellets ($\sim 10^7$ cells) were subsequently lysed with 200 µl of ice-cold lysis buffer containing 10 mM Tris (pH 7.5), 150 mM NaCl, 0.5 mM EDTA, 0.5 % NP-40 and protease-phosphatase inhibitor using a syringe as described previously. In order to avoid viscosity due to high DNA amount an additional step of 3 µl benzonase nuclease treatment was done, cell lysates were spinned and protein concentration was measured as described before. Lysates were stored at -80 °C until use.

For co-IP of GFP lysates from NCI-H295R cells expressing GFP-*AAAS* were used. Lysates from cells expressing GFP were used as negative control for all unspecific protein interactions due to the exogenous expression model using a GFP fusion protein. Bead slurry (25 µl) of GFP-Trap_A agarose beads, which are antibody fragments of alpaca against GFP bound to an agarose matrix, was equilibrated in 500 µl ice-cold dilution buffer containing 10 mM Tris (pH 7.5), 150 mM NaCl, 0.5 mM EDTA and protease-phosphatase inhibitor. Beads were spinned down at 2500x g for 2 minutes at 4 °C on a Fresco 17 centrifuge and washed twice with 500 µl ice-cold dilution buffer. Cell lysates (500 µg protein in dilution buffer adjusted to 500 µl) of NCI-H295R cells stably expressing GFP-ALADIN (27 + 59 kDa) or GFP (27 kDa) as control were added to the beads and gently resuspended by flipping the tube. The GFP and GFP-fusion proteins were bound over-night at constant mixing on a IDL TRM 50 rolling platform at 4°C. The tubes were spinned down and the supernatants were discarded. The beads were washed twice with 500 µl ice-cold dilution buffer and transferred to a new tube before the last wash step. The beads were gently resuspended in 60 µl NUPAGE LDS sample buffer (2X) and in order to dissociate the captured immunocomplexes from the beads, boiled at 95 °C for 10 minutes using a Thermomixer Comfort. The beads were collected by centrifugation at

2500x g for 2 minutes at 4 °C and Western Blot analysis was conducted with 20 µl of the eluate (referred to as bound fraction) as described previously. For Western Blot analysis besides eluates whole protein lysate (input), non-bound and wash fractions were used, in order to adjust co-IP methodology. The left 40 µl of the eluate was further processed for proteomic profiling using mass spectrometry (Figure 14). These experiments following mass spectrometry analysis were repeated three times.

For co-IP of ALADIN using lysates from NCI-H295R wild-type cells Protein G UltraLink Resin sepharose beads were used: 20 µl bead slurry was equilibrated in 500 µl ice-cold dilution buffer and spinned down at 2500x g for 2 minutes at 4 °C as described above. Beads were gently resuspended in ALADIN antibody (B-11): sc-374073 (2 µg/ml) and as negative control normal mouse IgG (2 µg/ml) in 200 µl dilution buffer. With the control experiment unspecific protein binding to IgG antibodies was ruled out. Antibody and IgGs were bound to the beads over-night at 4 °C in a Biometra OV3 rotation chamber. Beads were spinned down and washed once to get rid of excess antibody and IgGs. Cell lysates (500 µg protein in 500 µl dilution buffer) of NCI-H295R wild-type cells were added to the beads and gently resuspended by flipping the tube. The antigens were bound over-night to the antibody-beads-complex as described before. The tubes were spinned down and supernatants were discarded. The beads were washed four times and transferred to a new tube before the last wash step. The beads were gently resuspended in 60 µl sample buffer containing dilution buffer, NUPAGE LDS sample buffer (1X) and reducing agent (1X). The captured immunocomplexes were dissociated and the eluates were collected and processed by Western Blot analysis as described previously. The experiments were repeated three times. For Western Blot analysis besides eluates whole protein lysate (input), non-bound and wash fractions were used, in order to adjust co-IP methodology. In addition, the left 40 µl of the eluate after ALADIN co-IP and negative control using IgGs were further processed for proteomic profiling using mass spectrometry (Figure 14). These experiments following mass spectrometry analysis were conducted once.

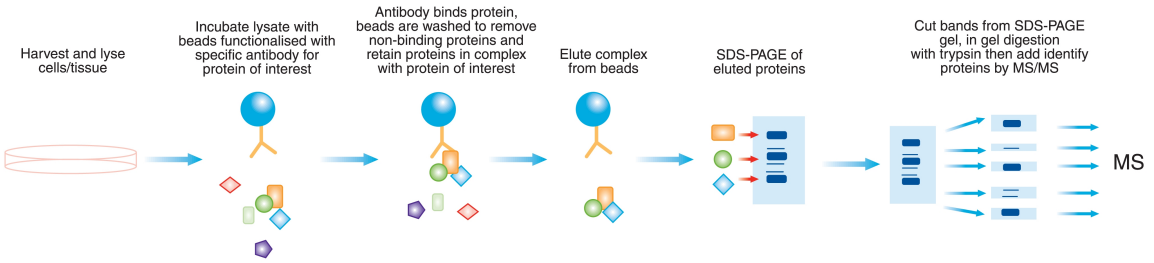

Figure 14 – Schematic presentation of co-immunoprecipitation followed by mass spectrometry.
After incubation of beads, equipped with a specific antibody, with cell lysate the protein of interest will bind to the antibody bound to the matrix. Unspecific protein-binding will be eliminated by wash steps and after elution (here, for facilitation, the antibody will not be eluted next to the immunocomplexes) the immunocomplexes will be separated using sodium/lithium dodecyl sulfate (SDS/LDS)-polyacrylamide gel electrophoresis (PAGE) and processed to mass spectrometry. The principles described here are the same for the co-immunoprecipitation (co-IP) method using lysates from NCI-H295R wild-type cells besides that an additional step for antibody binding is required (Australian Proteome Analysis Facility Ltd, 2015).

3.14 Proteomic profiling using mass spectrometry

Protein complexes of co-IPs using lysates from NCI-H295R cells expressing GFP-*AAAS*, lysates from NCI-H295R wild-type cell and controls were eluted and 40 µl of these fractions were load on the seventh lane after the protein marker Novex Sharp prestained protein standard of a NUPAGE bis-Tris mini gels. Gel electrophoresis was done as described previously followed by a wash-step of the gels in aqua dest. The gels were subsequently stained for 30 minutes in Coomassie staining solution containing 50 % methanol, 7.5 % acetic acid and 10 mg Coomassie brilliant blue R250. For controlled destaining an acetic acid solution containing 30 % methanol and 7.5 % acetic acid was used until the degree of preferred staining was achieved. The staining procedure was firstly described by Meyer and Lambert proposing a negatively charged protein-dye complex (Meyer and Lamberts, 1965). Finally, the gel was washed in aqua dest and further processed for mass spectrometry.

Entire gel lanes were cut into 40 slabs, each of which was in-gel digested with trypsin (Shevchenko et al., 2006). Gel analyses were performed at the Mass Spectrometry Facility at the Max Planck Institute for Molecular Cell Biology and Genetics (Dresden, Germany) on a nano high-performance liquid chromatograph Ultimate interfaced on-line to a LTQ Orbitrap Velos hybrid tandem mass spectrometer (Vasilj et al., 2012). Database search was performed against International Protein Index human database (downloaded in July 2010) and NCBI protein collection without species restriction (updated in June 2014) using MASCOT software v.2.2 under the following settings: enzyme specificity-trypsin; two miscleavages; mass tolerance 2.0 and 0.5 Da for precursor and fragments, respectively; variable modifications-deamidation of asparagine and glutamine, oxidation of methionine, acetyl of the protein N-terminus and propionamide of cysteine. Scaffold software v.4.3.2 was used to validate tandem mass spectrometer-based protein identifications. Peptide identifications were accepted if they could be established at greater than 95.0 % probability by the Peptide Prophet algorithm with Scaffold delta-mass correction (Keller et al., 2002), protein identifications at greater than 99.0 % and contained at least one (co-IP conducted with lysates from NCI-H295R wild-type cells) or two (co-IP conducted with lysates from NCI-H295R cells expressing GFP-*AAAS*) unique identified peptides (number of different amino acid sequences, regardless of any modification, that are associated only with this protein). Protein probabilities were assigned by the Protein Prophet algorithm (Nesvizhskii et al., 2003). The assumption Scaffold used for converting search engine results into peptide probabilities were examined manually using the MASCOT scoring function histogram. Proteins that contained similar peptides and could not be differentiated based on MS/MS analysis alone, were grouped to satisfy the principles of parsimony. Quantitative spectrum values were normalised to the total spectra.

3.15 Immunofluorescent staining

NCI-H295R wild type cells grown on glass cover slips were washed three times with PBS, fixed for 5 minutes with 2 % formaldehyde in PBS, permeabilised for 10 minutes with 0.5 % Triton-X-100 in PBS and fixed again for 5 minutes. Glass cover slips were washed three times with 0.1 % Triton-X-100 for 5 minutes and blocked for 30 minutes with 2 % PBS/BSA at room-temperature.

Primary antibodies ALADIN (B-11): sc-374073 (1:25 in 2 % PBS/BSA) or cytochrome P450 reductase (ab13513) (1:100 in 2 % PBS/BSA) were incubated at 4 °C over-night in a humidified chamber. Cells were washed again three times for 5 minutes and secondary antibodies alexa fluor 555 goat anti-mouse IgG and alexa fluor 488 goat anti-rabbi IgG (1:500 in 2 % PBS/BSA) were incubated one hour at room-temperature in the dark followed by a three wash-step for 5 minutes. Glass cover slips were mounted onto microscope slides with VECTASHIELD mounting medium for fluorescence with DAPI protected from light. Fluorescence was visualised using the laser scanning spectral confocal microscope TCS SP2 and pictures taken using x63 oil immersion objective, helium neon laser 543 nm, argon/argon krypton-laser 488 nm and diode 405 nm. The experiment was repeated at least three times.

3.16 Statistics

Statistical analyses were made using the open-source-software R i386 v2.15.0 and R Studio v0.98.1074. All values were expressed as a mean ± standard deviation. As assumption of normality (*goodness-of-fit*) the following tests were conducted: Shapiro-Wilk-test and Q-Q-Plot. Unpaired and paired Student's t-tests were used. During evaluation of the results a confidence interval α of 95 % and p values lower than 0.05 were considered as statistically significant.

Results are shown as box plots which give a fast and efficient overview about median, first and third quartile (50th, 25th and 75th percentile, respectively), interquartile range, minimal and maximal values and outliers. Box plots give an intuitive impression of position and statistical spread of the measurement.

4 Results

4.1 Generation of two different ALADIN expression models

In the first part of the results the cellular role of ALADIN was investigated by creating two experimental models using NCI-H295R1. These cells were engineered to either over-express or down-regulate *AAAS* by inducible stable transfection. Alterations in steroidogenic gene expression and functional consequences were determined. In addition, the role of ALADIN on cell viability and oxidative stress response was analysed in these distinct models.

Down-regulation and over-expression of *AAAS* was confirmed on mRNA level (Figure 15 A-B) (n=6; n gives the minimum number of independent experiments) and on protein level by Western Blot (Figure 15 C-D) (n=6). The establishment of stable doxcycline-inducible ALADIN knock-down and over-expression sub-clones of the adrenocortical cell line NCI-H295R1-TR was successful.

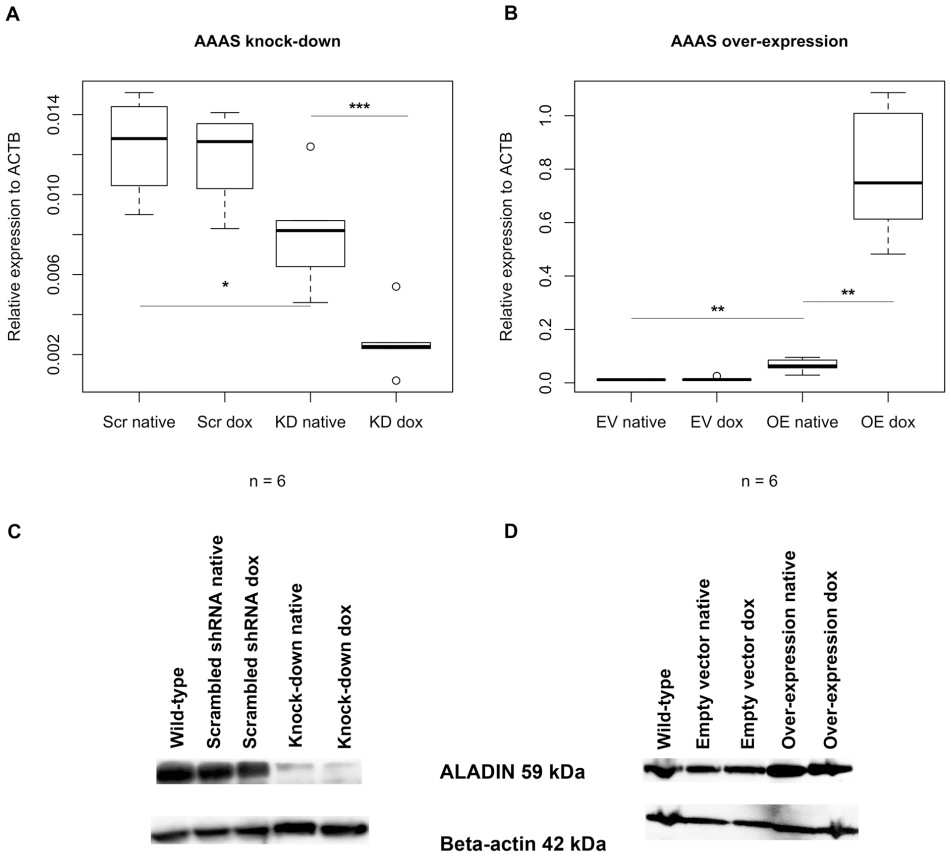

Figure 15 – Down-regulation and over-expression of *AAAS* on mRNA and protein level.
Knock-down and over-expression in stably transfected NCI-H295R1-TR cells was induced by treatment with doxycycline for 48 h: (A-B) Boxplots of down-regulation and over-expression of *AAAS* on mRNA level (TaqMan analysis) and (C-D) evidence of down-regulation and over-expression of *AAAS* on protein level (Western Blot). Scr, scrambled shRNA. KD, knock-down. EV, empty vector (= pcDNA4/TO). OE, over-expression. Native, without doxycycline induction. Dox, doxycycline induction. n, minimum number of independent experiments. P-values: * P < 0.05, ** P < 0.01, *** P < 0.001. Significant differences were measured with paired and unpaired Student's t-Test. Boxplot widths are proportional to the square root of the samples sizes. Whiskers indicate the range outside 1.5 times the inter-quartile range above the upper quartile and below the lower quartile. Outliers were plotted as dots (Jühlen et al., 2015).

Without doxycycline stimulation a partial *AAAS* knock-down and over-expression was observed when compared to the subsequent controls (Figure 15). Many of the positive results presented in this work were based on the doxycycline untreated cells and it had to be assumed that the T-REx system used as method of choice appeared to be leaky. The repressor-expressing plasmid pcDNA6TR seemed to be out-numbered in each cell model by the inducible expression vectors pTER for shRNA silencing and pcDNA4/TO for h*AAAS* cDNA over-expression which both contain the tetracycline-response element. In the doxycycline-uninduced state the amount of repressor produced seemed not to be enough in order to block expression of shRNA or h*AAAS* cDNA leading to the partial *AAAS* knock-down and over-expression described here.

4.2 Impairment of glucocorticoid and androgenic steroidogenesis and of POR by ALADIN deprivation

To investigate the effects of *AAAS* knock-down and over-expression on steroidogenesis mRNA expression of key enzymes involved in steroidogenesis was assessed including CYP11A1, CYP11B1, CYP17A1, CYP21A2, DHCR24, POR and StAR. In addition steroid production employing LC/MS-MS was measured in NCI-H295R1-TR *AAAS* knock-down and *AAAS* over-expression cells. With quantitative RT-PCR it was revealed that *AAAS* knock-down induced a significant down-regulation of the genes coding for enzymes involved in the glucocorticoid and androgenic pathways, i.e. 17α-hydroxylase/17,20lyase (*CYP17A1*) and 21-hydroxylase (*CYP21A2*) (n=6) (Figure 16 A). Expression of *StAR*, *CYP11A1*, *DHCR24* and *CYP11B1* was not affected in these cells (Figures 17 A, 18 A and 18 C). Similar effects were observed in the functional steroid output of the cells measured by LC/MS-MS. Changes in steroid production in *AAAS* knock-down cells were predominantly observed for 17OHP, compound S and androstenedione (n=6) (Figure 16 B), whereas only minor changes in the remaining ten steroids were observed. Thus, for simplification, the following results focus on those three steroids. There was no change in precursor metabolites of the mineralocorticoid pathway (DOC) (Figure 19 A). Furthermore it was seen that the ALADIN-dependent impairment of the glucocorticoid and androgenic pathways is accompanied by a down-regulation of the gene coding for POR, an enzyme managing electron transfer from $NADPH$ to CYP17A1 and CYP21A2 microsomal P450 hydroxylases (Figure 16 C). A decrease in *POR* gene expression was observed in knock-down cells prior to doxycycline treatment, most likely representing the partial *AAAS* knock-down presented in Figure 15 A and C.

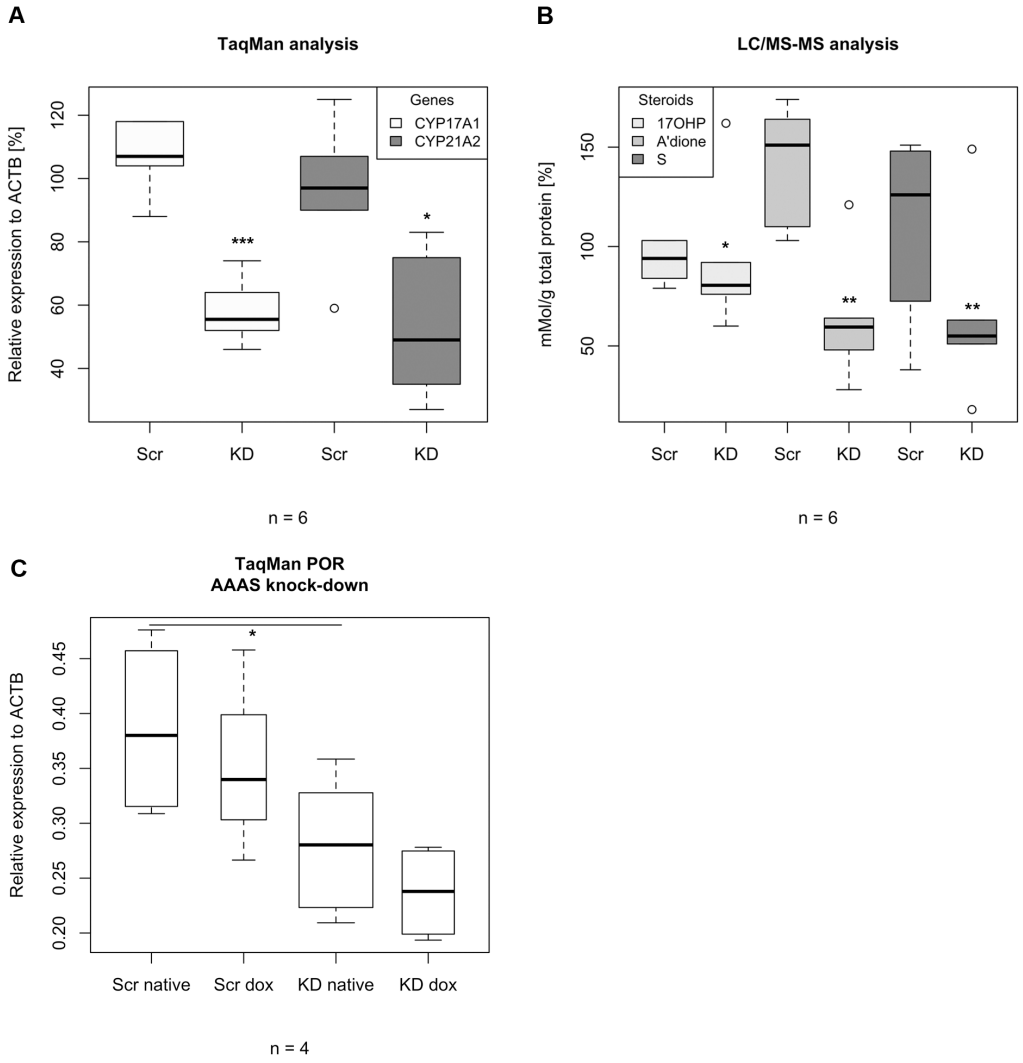

Figure 16 – TaqMan analyses (A and C) and LC/MS-MS (B) of stably transfected NCI-H295R1-TR *AAAS* knock-down cells.

Cells were treated for 48 h with doxycycline. Scr, scrambled shRNA. KD, knock-down. 17OHP, 17-hydroxyprogesterone. A'dione, androstenedione. Compound S, 11-deoxycortisol. n, minimum number of independent experiments. P-values: * P < 0.05, ** P < 0.01, *** P < 0.001. Significant differences were measured with paired and unpaired Student's t-Test. Boxplot widths are proportional to the square root of the samples sizes. Hundred percent boxes for native scrambled shRNA and knock-down are not shown. Whiskers indicate the range outside 1.5 times the inter-quartile range above the upper quartile and below the lower quartile. Outliers were plotted as dots (Jühlen et al., 2015).

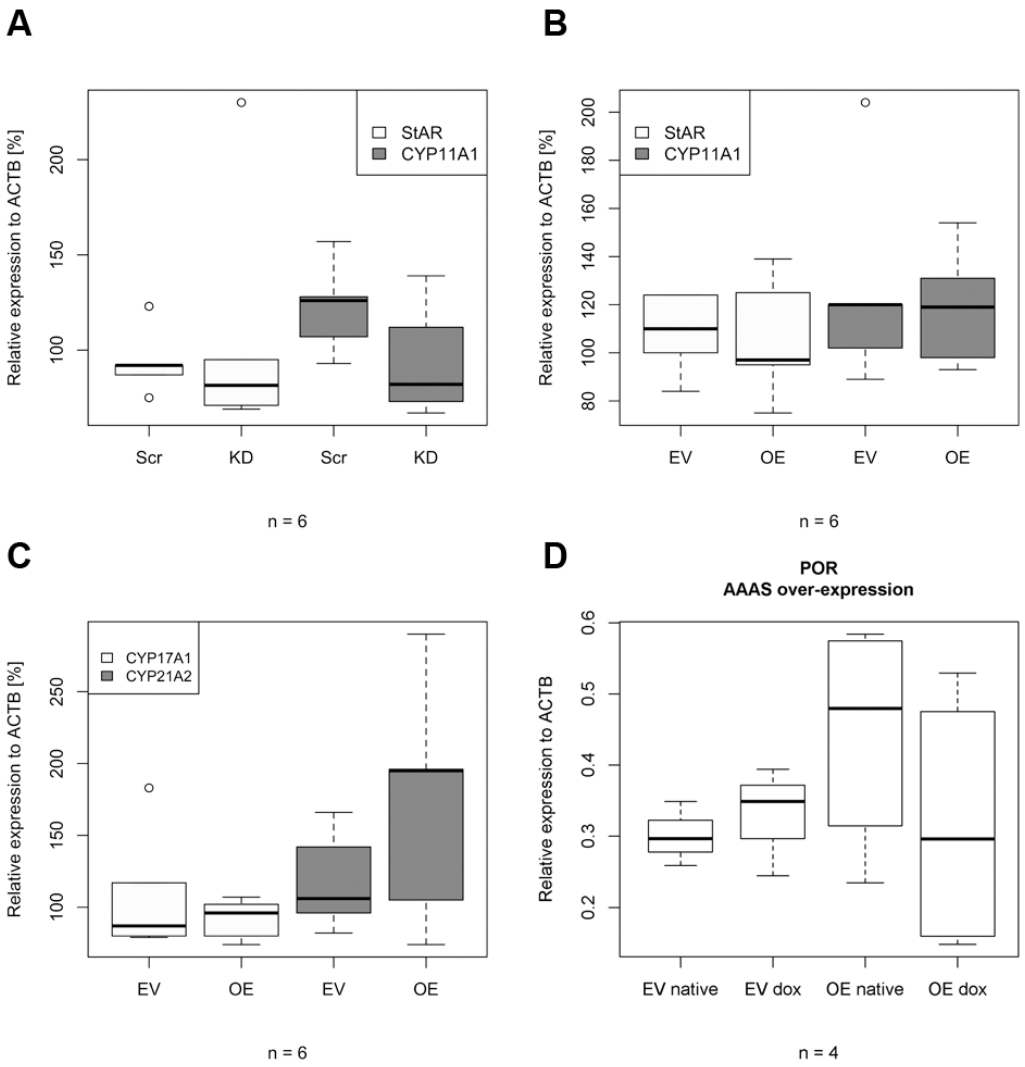

Figure 17 – TaqMan analyses of stably transfected NCI-H295R1-TR *AAAS* knock-down and over-expression cells.

(A-B) *StAR* and *CYP11A1* of *AAAS* knock-down and over-expression cells, (C) *CYP17A1* and *CYP21A2* and (D) *POR* of *AAAS* over-expression cells. Knock-down and over-expression in stably transfected NCI-H295R1-TR cells was induced by 48 h treatment with doxycycline. Scr, scrambled shRNA. KD, knock-down. EV, empty vector (=pcDNA4/TO). OE, over-expression. Native, without doxycycline induction. Dox, doxycyline induction. n, number of independent experiments. Boxplot widths are proportional to the square root of the samples sizes. Whiskers indicate the range outside 1.5 times the inter-quartile range above the upper quartile and below the lower quartile. Outliers were plotted as dots (Jühlen et al., 2015).

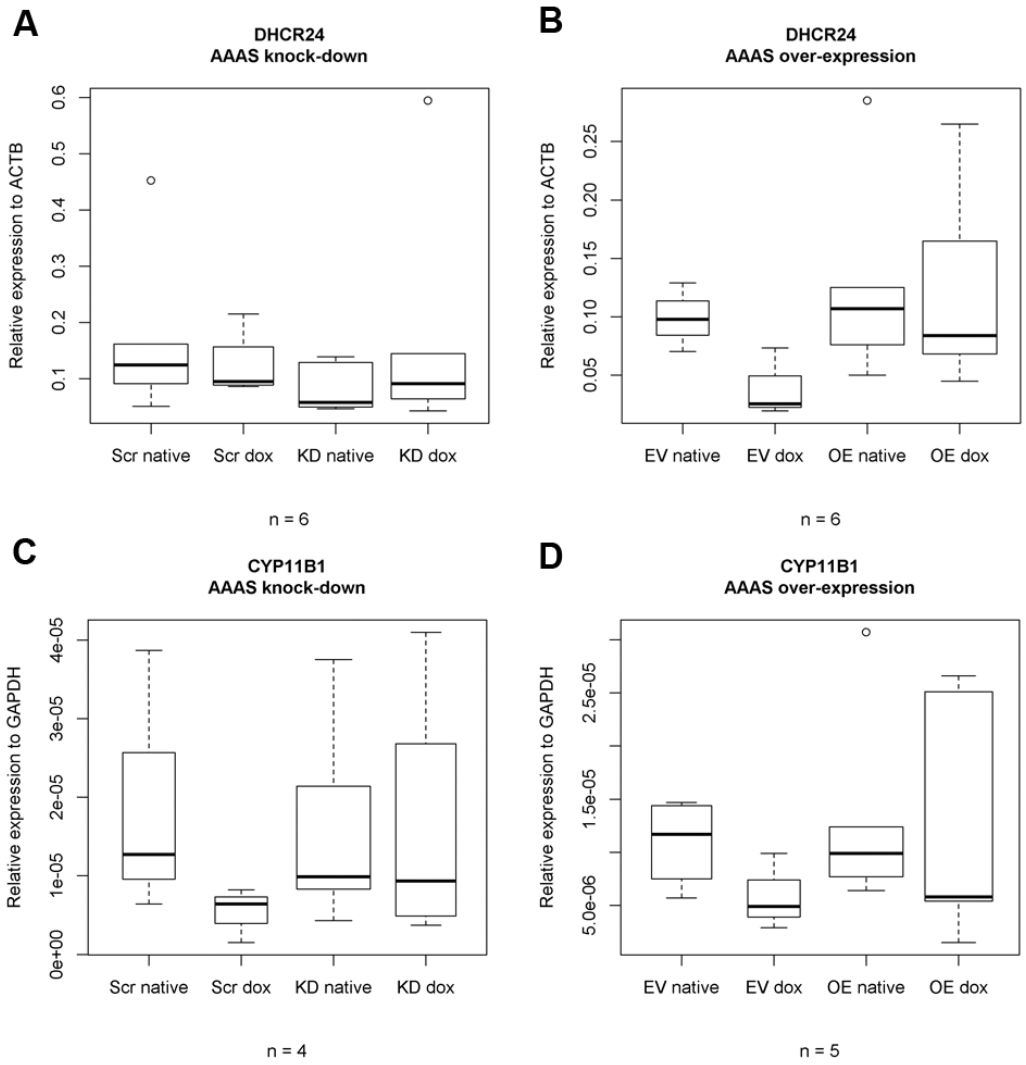

Figure 18 – Quantitative real-time PCR of stably transfected NCI-H295R1-TR *AAAS* knock-down and over-expression cells.

(A-B) *DHCR24* and (C-D) *CYP11B1* of *AAAS* knock-down and over-expression cells. Knock-down and over-expression in stably transfected NCI-H295R1-TR cells was induced by 48 h treatment with doxycycline. Scr, scrambled shRNA. KD, knock-down. EV, empty vector (=pcDNA4/TO). OE, over-expression. Native, without doxycycline induction. Dox, doxycycline induction. n, number of independent experiments. Boxplot widths are proportional to the square root of the samples sizes. Whiskers indicate the range outside 1.5 times the inter-quartile range above the upper quartile and below the lower quartile. Outliers were plotted as dots (Jühlen et al., 2015).

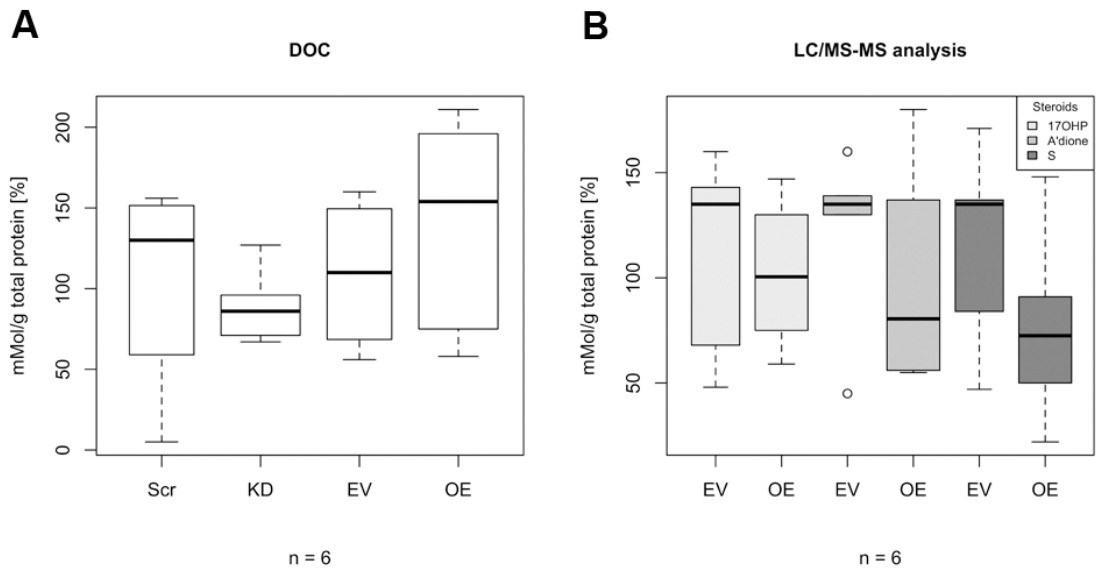

Figure 19 – LC/MS-MS of stably transfected NCI-H295R1-TR *AAAS* knock-down and over-expression cells.

(A) DOC of stably transfected NCI-H295R1-TR *AAAS* knock-down and over-expression cells and (B) 17OHP, a'dione and compound S of *AAAS* over-expression cells. Induction with doxycycline was done for 48 h. Scr, scrambled shRNA. KD, knock-down. EV, empty vector (=pcDNA4/TO). OE, over-expression. DOC, deoxycorticosterone. 17OHP, 17-hydroxyprogesterone. A'dione, androstenedione. Compound S, 11-deoxycortisol. n, number of independent experiments. Boxplot widths are proportional to the square root of the samples sizes. Whiskers indicate the range outside 1.5 times the inter-quartile range above the upper quartile and below the lower quartile. Outliers were plotted as dots (Jühlen et al., 2015).

AAAS over-expression in at least four triplicate experiments did not result in significant differences in expression of key enzymes involved in steroidogenesis and also did not impact on steroid production (Figures 17 B-D, 18 B, 18 D and 19, respectively).

4.3 Alteration of cellular redox homeostasis under exogenous oxidative stress

Cell viability in both the *AAAS* knock-down and over-expression models was investigated. To determine the role of ALADIN in redox homeostasis, it was ascertained how *AAAS* knock-down and over-expression affect the ratio between GSH and $GSSG$. When cells are exposed to increased levels of oxidative stress, $NADPH$ decreases and $GSSG$ accumulates. Consequently, the $GSH/GSSG$ ratio decreases which is a good indicator for cellular oxidative stress. $NADPH$ is used by GSR to generate the anti-oxidant GSH from its oxidised form $GSSG$. *GSR* expression was measured in both *AAAS* expression models in order to verify a GSR-dependent redox pathway disturbance leading to accumulation of $GSSG$.

4.3.1 Cell viability with and without exogenous oxidative stress

In NCI-H295R1-TR *AAAS* knock-down cells exposed to paraquat for 24 h (n=7) a significant decrease was observed in cell viability with oxidative stress compared to treated control cells was observed (Figure 20 A). Viability was not decreased after doxycycline treatment in scrambled shRNA-transfected cells. However, a decrease was seen in knock-down cells prior to doxycycline treatment, most likely representing the partial *AAAS* knock-down presented in Figure 15 A and C. The fully induced *AAAS* knock-down did not lead to a further decrease in cell viability after paraquat exposure. Cell viability without oxidative stress was not significantly altered.

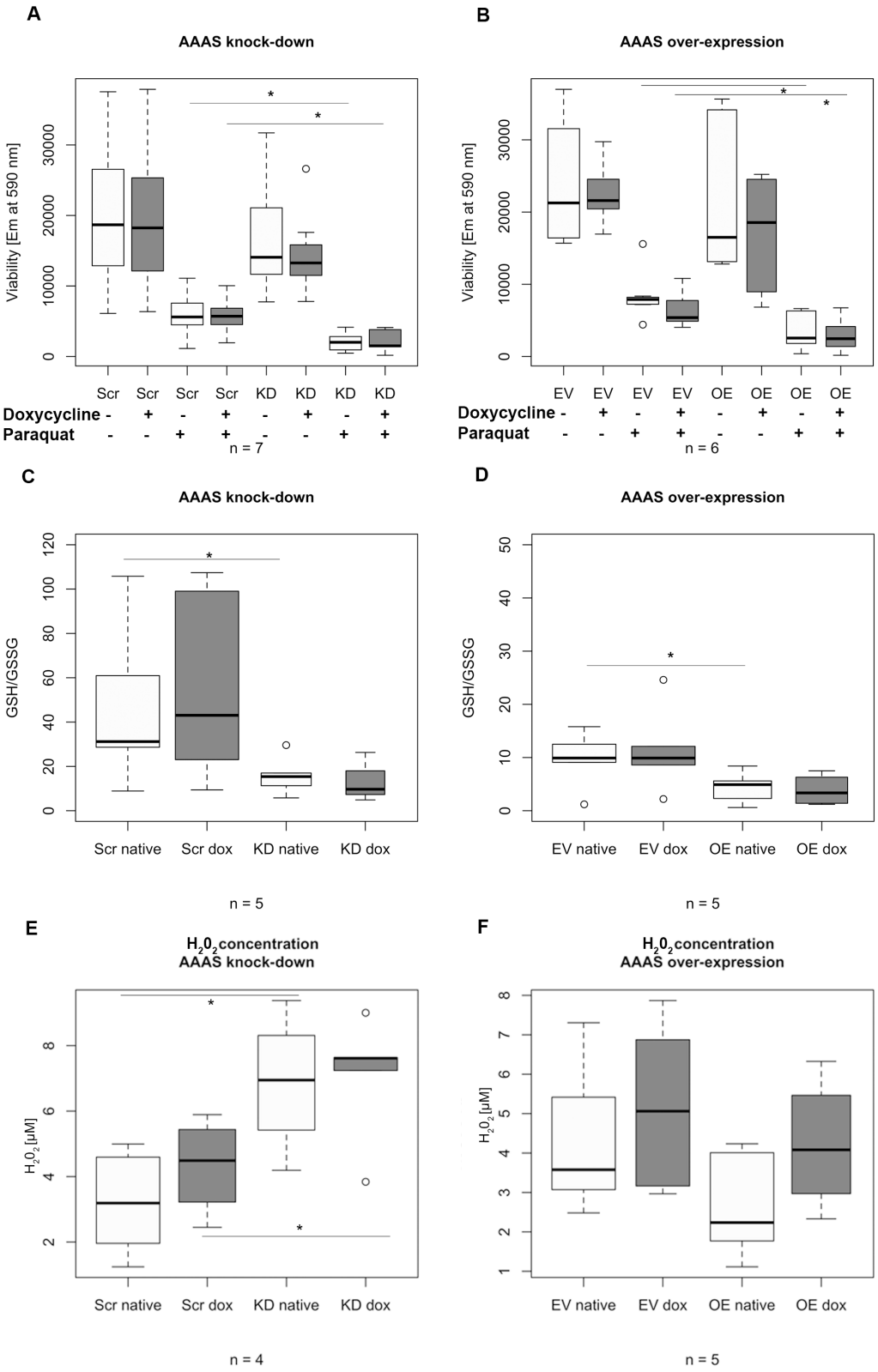

Figure 20 – Analysis of (A-B) cell viability, (C-D) glutathione ratios and (E-F) hydrogen peroxide production under oxidative stress.

ALADIN knock-down and over-expression in stably transfected NCI-H295R1-TR was induced by 48 h treatment with doxycycline and cells were additionally treated with 0.2 mM paraquat for 24 h. Em, fluorescence emission at 590 nm. GSH, reduced glutathione. $GSSG$, oxidised disulphide glutathione. H_2O_2, hydrogen peroxide. Scr, scrambled shRNA. KD, knock-down. EV, empty vector (=pcDNA4/TO). OE, over-expression. Native, without doxycycline induction. Dox, doxycycline induction. n, minimum number of independent experiments. P-values: * P < 0.05. Significant differences were measured with unpaired Student's t-Test. Boxplot widths are proportional to the square root of the samples sizes. Whiskers indicate the range outside 1.5 times the interquartile range above the upper quartile and below the lower quartile. Outliers were plotted as dots (Jühlen et al., 2015).

Surprisingly, in *AAAS* over-expressing cells similar effects were observed after paraquat treatment (n=6) (Figure 20 B). Viability was not altered after doxycycline induction in the control cells carrying the empty vector. However, cell viability was already significantly decreased after paraquat treatment in the native over-expression cells without the induction of doxycycline representing a partial *AAAS* over-expression shown in Figure 15 B and D. The fully induced over-expression cells did not reveal further alteration in viability after treatment with paraquat. Cell viability without oxidative stress did not result in any significant change.

4.3.2 $GSH/GSSG$ ratio with exogenous oxidative stress

$GSH/GSSG$ ratios were markedly decreased in NCI-H295R1-TR *AAAS* knock-down and over-expression cells after paraquat treatment for 24 h compared to treated control cells (n=5) (Figure 20 C and D).

However, in cells with the partial *AAAS* knock-down and over-expression without induction of doxycycline $GSH/GSSG$ ratios were already significantly down-regulated and no further impairment after doxycycline induction could be observed.

4.3.3 Hydrogen peroxide production with exogenous oxidative stress

In order to give further evidence that ALADIN is involved in the oxidative stress response of the cell H_2O_2 production was measured in stably transfected cells after exposure to oxidative stress. It was presumed that after oxidative stress treatment the oxidants $NADPH$ and GSH will decrease leading to a rise of H_2O_2. Cells presenting an impaired oxidative response concomitantly suffer from an increased ROS level and cellular damage.

Consistent with the results of cell viability analysis and $GSH/GSSG$ ratio in NCI-H295R1-TR *AAAS* knock-down cells after paraquat treatment a significantly increased level of H_2O_2 concentration in these cells compared to paraquat-treated control scrambled shRNA cells was seen (n=4) (Figure 20 E). After doxycycline induction in NCI-H295R1-TR *AAAS* knock-down cells no further significant increase of H_2O_2 concentration could be observed; the partial knock-down without induction of doxycycline shown in Figure 15 A and C is enough to disturb the oxidative response of the cell. In *AAAS* over-expressing cells with or without doxycycline induction significant changes in H_2O_2 concentration could not be observed after paraquat treatment compared to control cells carrying the empty vector (n=5) (Figure 20 F).

4.3.4 Gene expression of glutathione reductase

Analysis of the expression level of *GSR* showed that there was no significant change in expression level in NCI-H295R1-TR *AAAS* knock-down cells compared to scrambled-shRNA control cells with or without doxycycline (n=4) (Figure 21 A).

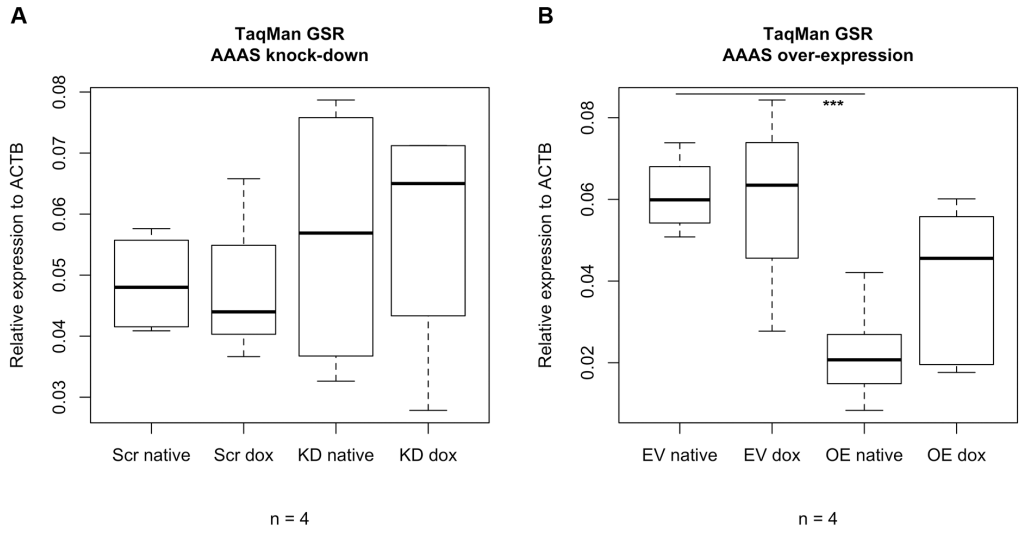

Figure 21 – TaqMan analyses of glutathione reductase of stably transfected NCI-H295R1-TR *AAAS* knock-down and over-expression cells.

Stably transfected NCI-H295R1-TR *AAAS* knock-down cells and over-expression were treated for 48 h with doxycycline. GSR, glutathione reductase. Scr, scrambled shRNA. KD, knock-down. EV, empty vector (=pcDNA4/TO). OE, over-expression. Native, without doxycycline induction. Dox, doxycycline induction. n, minimum number of independent experiments. P-values: *** P < 0.001. Significant differences were measured with unpaired Student's t-Test. Boxplot widths are proportional to the square root of the samples sizes. Hundred percent boxes for native scrambled shRNA and knock-down are not shown. Whiskers indicate the range outside 1.5 times the inter-quartile range above the upper quartile and below the lower quartile. Outliers were plotted as dots (Jühlen et al., 2015).

In contrast *GSR* expression level in NCI-H295R1-TR *AAAS* over-expression cells without induction of doxycycline was significantly reduced compared to control cells carrying the empty vector used for the over-expression vector construct (n=4) (Figure 21 B). Induction with doxycycline in *AAAS* over-expression cells increases the *GSR* expression level, but the increase was not statistically significant.

Overall, the results indicate that the redox response after *AAAS* knock-down in NCI-H295R1-TR under exogenous oxidative stress using paraquat is significantly impaired and leads to accumulation of hydrogen peroxide. The expression of *GSR* was not affected in *AAAS* knock-down cells under basal conditions, implying a normal prerequisite of anti-oxidant defence at *GSR* expression level when applying paraquat. *AAAS* over-expression cells suffer from decreased viability and glutathione levels under oxidative stress. In these cells the expression of *GSR* was reduced under basal conditions implying an increase of sensitivity during exogenous oxidative stress.

4.4 Disturbance of nuclear import of aprataxin, DNA ligase 1 and ferritin heavy chain 1

Using both the human adrenal NCI-H295R1-TR *AAAS* knock-down and over-expression models the potential impairment of the nuclear import of APTX, LIG1 and FTH1 was investigated. For this YFP-specific vectors transiently transfected into the cell lines were employed.

4.4.1 Nuclear import in *AAAS* knock-down cells

The nuclear import of APTX, LIG1 and FTH1 was markedly impaired after ALADIN deprivation (n=26, n=83 and n=51, respectively; n gives the minimum number of analysed cells per cell type) (Figures 22 A-C and 23). Nevertheless, nuclear import was not changed after doxycycline treatment but already in the native state without doxycycline induction probably reflecting a partial *AAAS* knock-down. The induced *AAAS* knock-down did not lead to a further decrease of nuclear import of APTX, LIG1 and FTH1 compared to the native state without doxycycline induction (Figure 22 A-C). Upon treatment with paraquat for 24 h a significant increase was found in nuclear import of FTH1 in scrambled-shRNA control cells and *AAAS* knock-down cells, but there was no significant difference between paraquat-treated scrambled-shRNA control cells and *AAAS* knock-down cells (n=26) (Figure 24 A).

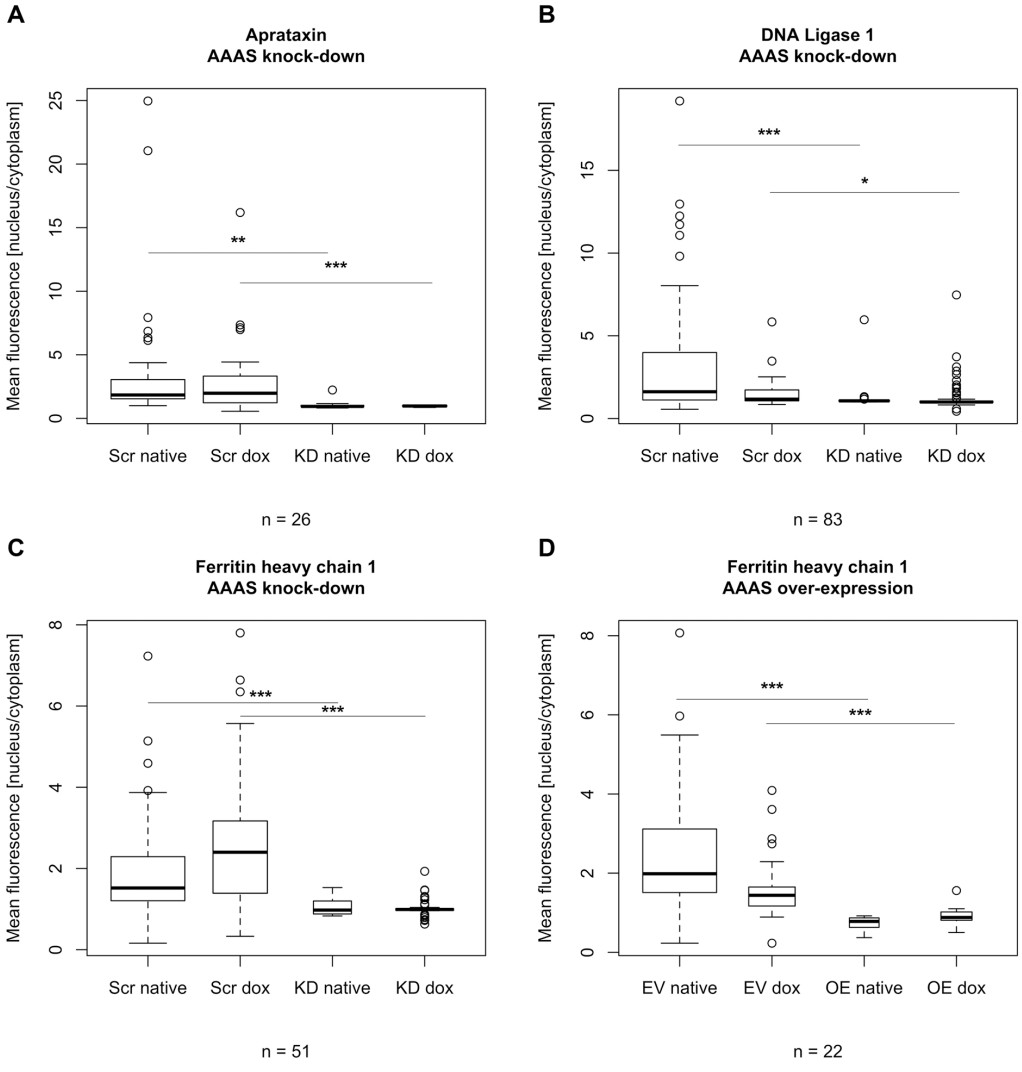

Figure 22 – Analyses of fluorescent microscopy of the nuclear import of aprataxin (A), DNA ligase 1 (B) and ferritin heavy chain 1 (C-D).

ALADIN knock-down and over-expression in stably transfected NCI-H295R1-TR cells was induced by 48 h treatment with doxycycline. Scr, scrambled shRNA. KD, knock-down. EV, empty vector (=pcDNA4/TO). OE, over-expression. Native, without doxycycline induction. Dox, doxycycline induction. n, minimum number of analysed cells per cell type. P-values: * P < 0.05, ** P < 0.01, *** P < 0.001. Significant differences were measured with unpaired Student's t-Test. Boxplot widths are proportional to the square root of the samples sizes. Whiskers indicate the range outside 1.5 times the inter-quartile range above the upper quartile and below the lower quartile. Outliers were plotted as dots. The experiment was repeated twice (Jühlen et al., 2015).

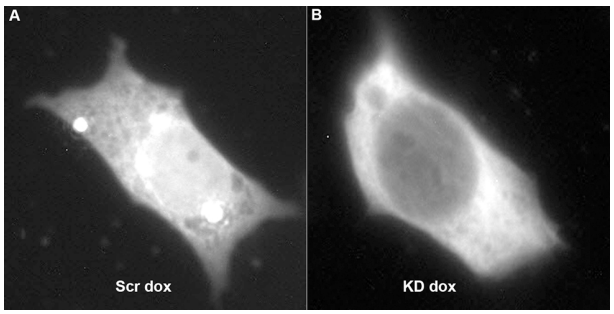

Figure 23 – Nuclear import of ferritin heavy chain 1-tagged YFP (pYFP-N3-*FTH1*).
Results of fluorescent microscopy of transiently transfected NCI-H295R1-TR scrambled shRNA and *AAAS* knock-down cells. NCI-H295R1-TR cells were treated for 48 h with doxycycline. Scr, scrambled shRNA. KD, knock-down. Dox, doxycycline induction (Jühlen et al., 2015).

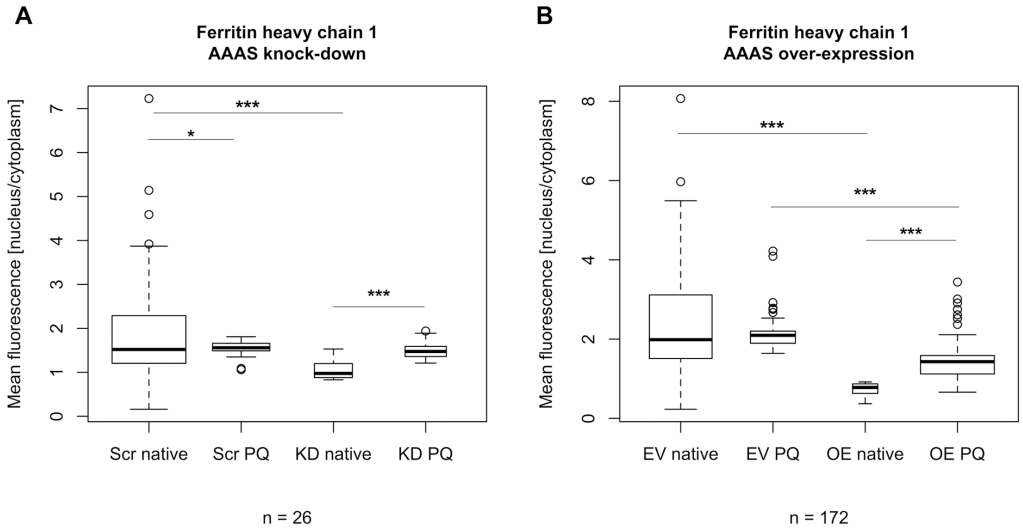

Figure 24 – Fluorescent microscopy of the nuclear import of ferritin heavy chain 1 after treatment with paraquat.
NCI-H295R1-TR cells were treated for 48 h with doxycycline. Scr, scrambled shRNA. KD, knock-down. EV, empty vector (=pcDNA4/TO). OE, over-expression. Native, without paraquat treatment. PQ, paraquat treatment. n, minimum number of analysed cells per cell type. P-values: * $P < 0.05$, *** $P < 0.001$. Significant differences were measured with unpaired Student's t-Test. Boxplot widths are proportional to the square root of the samples sizes. Whiskers indicate the range outside 1.5 times the inter-quartile range above the upper quartile and below the lower quartile. Outliers were plotted as dots. The experiment was repeated twice (Jühlen et al., 2015).

4.4.2 Nuclear import in *AAAS* over-expression cells

Cells over-expressing ALADIN did not show any change in nuclear import of APTX and LIG1 (n=55 and n=50, respectively) (Figure 25). Interestingly, the import of FTH1 was markedly impaired (n=22) (Figure 22 D). The nuclear import of FTH1 was already impaired in the doxycycline-untreated *AAAS* over-expressing cells and no further impairment could be observed after doxycycline induction. When treating control cells carrying the empty over-expression vector and *AAAS* over-expression cells with 0.2 mM paraquat for 24 h FTH1 was significantly imported into the nucleus (n=172) (Figure 24 B). There was a significant difference in FTH1 import after paraquat treatment between control and over-expressing cells.

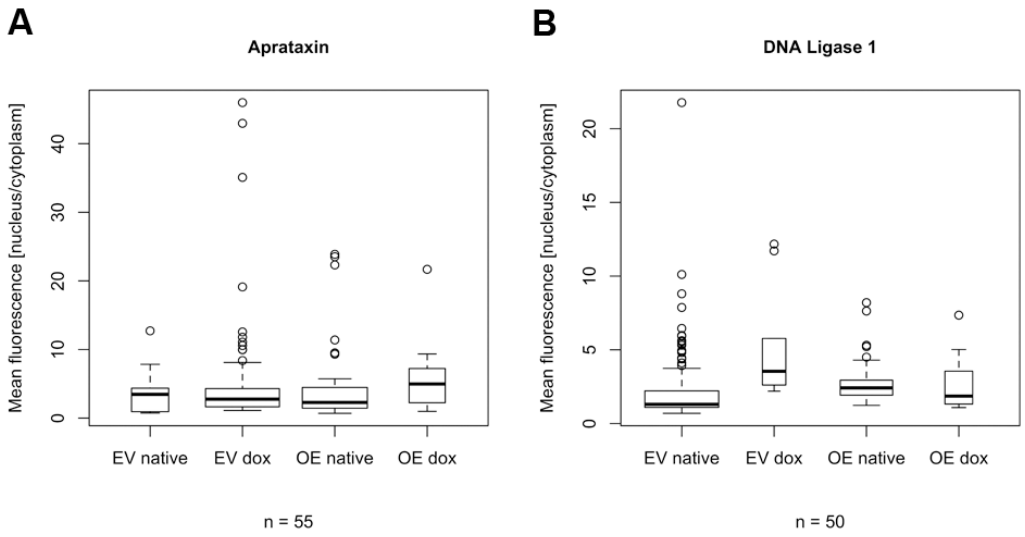

Figure 25 – Analyses of fluorescent microscopy of stably transfected NCI-H295R1-TR *AAAS* over-expression cells.

Nuclear import of (A) aprataxin and (B) DNA ligase 1. Induction with doxycycline was done for 48 h treatment. EV, empty vector (=pcDNA4/TO). OE, over-expression. Native, without doxycycline induction. Dox, doxycycline induction. n, minimum number of analysed cells per cell type. Boxplot widths are proportional to the square root of the samples sizes. Whiskers indicate the range outside 1.5 times the inter-quartile range above the upper quartile and below the lower quartile. Outliers were plotted as dots. The experiment was repeated twice (Jühlen et al., 2015).

4.5 ALADIN co-immunoprecipitation in an adrenal cell model expressing exogenous GFP-ALADIN and endogenous ALADIN

Co-IP was conducted in an adrenal cell model expressing exogenous GFP-ALADIN and endogenous ALADIN. For GFP-ALADIN co-IP whole cell lysates of NCI-H295R cells stably over-expressing the GFP-ALADIN fusion protein and as negative control NCI-H295R cells stably over-expressing the GFP protein were used. Efficient co-IP using GFP-Trap agarose beads is presented in Figure 26 A. Both over-expressed proteins, GFP-ALADIN and GFP, were successfully fished in the bound fractions of each specific cell lysate. No eluted GFP antibodies were detectable on the Western Blot due to the antibody's alpaca origin which was not recognised by the secondary antibody used. The experiments were repeated three times.

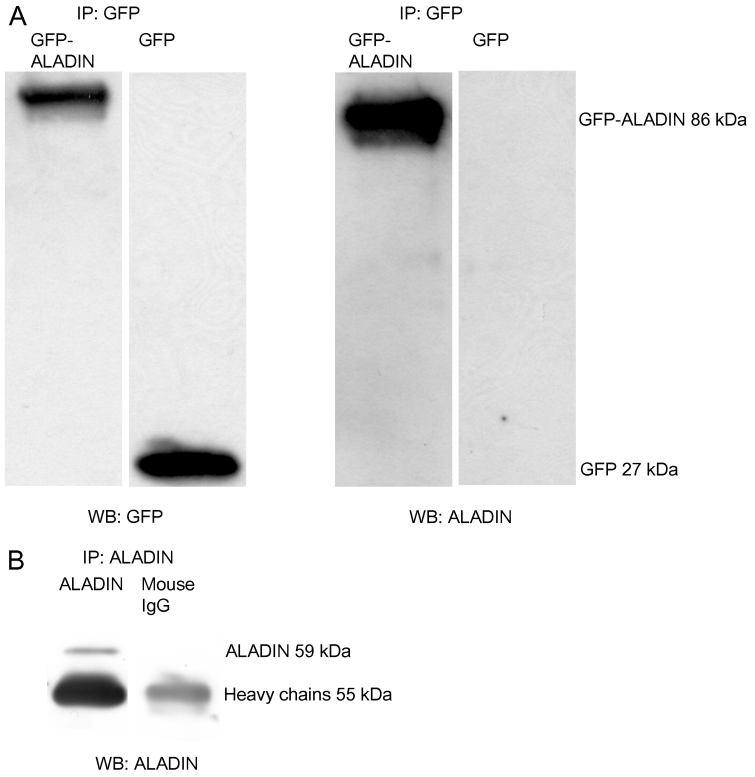

Figure 26 – Western Blot of bound fractions after co-immunoprecipitation of GFP (A) and of ALADIN (B).

(A) Whole cell lysates of GFP-ALADIN and GFP (as negative control) over-expressing NCI-H295R cells were prepared for GFP co-immunoprecipitation (co-IP). Primary antibodies against GFP and ALADIN were used for Western Blot. GFP-ALADIN fusion protein and GFP were found in each specific bound fraction implying efficient fishing of each of the proteins. No ALADIN was detectable in the control fraction of GFP co-IP. (B) Whole cell lysates of NCI-H295R wild-type cells were prepared for ALADIN co-IP. A mouse monoclonal antibody against ALADIN and normal mouse IgGs as negative control were used for co-IP. A primary antibody against ALADIN was used for Western Blot. ALADIN was found in the specific bound fraction implying efficient fishing of the protein. No ALADIN was detectable in the control fraction of normal mouse IgGs. The bound antibodies to the bead matrix were revealed on Western Blot: heavy chains appeared at the size of 55 kDa.

For co-IP of endogenous ALADIN whole cell lysates of NCI-H295R wild-type cells were prepared using Protein G UltraLink sepharose beads. A mouse monoclonal ALADIN antibody and normal mouse IgGs as negative control were coupled each to the sepharose beads and antigen was bound. Successful co-IP is shown in Figure 26 B. The protein was found in the bound fraction of the ALADIN co-IP, but the negative control remained empty implying no unspecific fishing of ALADIN. The bound and eluted antibodies to the beads were revealed on Western

Blot: heavy chains appeared at the size of 55 kDa (Figure 26 B). The co-IP and Western Blot was repeated three times.

Bound fractions of GFP-ALADIN co-IP (n=3) and of co-IP of endogenous ALADIN (n=1) were conducted for tandem mass spectrometry proteomic analyses. In GFP-ALADIN co-IP about 500 proteins or protein precursors were identified. Proteins simultaneously found in the negative control experiments were excluded and only those were selected which could be reproduced in all three independent GFP-ALADIN co-IP experiments. In co-IP analysis of endogenous ALADIN also about 500 proteins or precursors were detected and those excluded which were found in the negative control experiment. Proteomic results and identified proteins can be reviewed in Table 20 for GFP-ALADIN and Table 21 for endogenous ALADIN co-IP verified by GFP-ALADIN co-IP.

Table 20 – Functional classification of proteins identified by mass spectrometry analyses after co-immunoprecipitation of GFP-ALADIN.

PROTEIN	METABOLISM	GENE
CITRIC ACID CYCLE (CAC)/GLYCOLYSIS		
Tricarboxylate transport protein, mitochondrial*	CAC	*SLC25A1*
Mitochondrial 2-oxoglutarate/malate carrier protein	CAC	*SLC25A11*
2-oxoglutarate dehydrogenase, mitochondrial	CAC	*OGDH*
cDNA FLJ55072, highly similar to succinate dehydrogenase (ubiquinone) flavoprotein subunit, mitochondrial*	CAC, electron transport chain complex II	*SDHA*
Malate dehydrogenase	Malate/aspartate shuttle for CAC	*MDH1*
Malate dehydrogenase, mitochondrial	CAC	*MDH2*
Isoform 1 of adipocyte plasma membrane-associated protein*	Arylesterase activity, acetate synthesis	*APMAP*
6-phosphofructokinase type C	Glycolysis	*PFKP*
*6-phosphofructokinase, muscle type isoform 1**	Glycolysis	*PFKM*
Fructose-bisphosphate aldolase	Glycolysis	*ALDOA, ALDOB, ALDOC*
Glucose-6-phosphate isomerase	Glycolysis	*GPI*
Isoform of α-enolase*	Glycolysis	*ENO1*
LIPID METABOLISM/STEROIDOGENESIS		
Isoform 1 of lysophospholipid acyltransferase 7	Phospholipid metabolism	*MBOAT7*
Isoform 1 of trans-2,3-enoyl-CoA reductase	Fatty acid synthesis and elongation	*TECR*
Sterol O-acyltransferase 1	Cholesteryl ester formation	*SOAT1*
Sterol-4-α-carboxylate 3-dehydrogenase, decarboxylating*	Cholesterol biosynthesis	*NSDHL*
Progesterone receptor membrane component 2*	CYP P450 regulation	*PGRMC2*

PROTEIN PROCESSING		
cDNA FLJ61290, highly similar to neutral α-glucosidase AB*	Glycan metabolism, protein N-glycolsylation	*GANAB*
Dolichol-phosphate mannosyltransferase	Protein N-glycosylation	*DPM1*
Dolichyl-diphosphooligosaccharide–protein glycosyltransferase subunit 2*	Protein N-glycosylation	*RPN2*
Malectin	Protein N-glycosylation	*MLEC*
Isoform 1 of translocon-associated protein subunit α*	ER translocon complex	*SSR1*
Elongation factor 1-gamma*	Protein biosynthesis and anchorage	*EEF1G*
Elongation factor 2	Protein biosynthesis, translation, ribosomal translocation	*EEF2*
Glutaminyl-tRNA synthetase*	Protein biosynthesis	*QARS*
Lysosome-associated membrane glycoprotein 1*	Presents sugars to selectins	*LAMP1*
Lysosome membrane protein 2*	Lysosomal receptor	*SCARB2*
Protein ERGIC-53*	Protein recycling and sorting, mannose-specific	*LMAN1*
Perilipin-3 isoform 3*	Mannose-6 receptor transport	*PLIN3*
Isoform 1 of minor histocompatibility antigen H13	Intra-membrane proteolysis of signal peptides from a pre-protein	*HM13*
Protein disulphide-isomerase A3*	Protein processing	*PDIA3*
Protein disulphide-isomerase A4	Protein processing	*PDIA4*
Protein disulphide-isomerase*	Protein processing	*P4HB*
OTHER PATHWAYS		
14-3-3 protein eta	Universal signalling pathways	*YWHAH*
14-3-3 protein gamma	Universal signalling pathways	*YWHAG*
14-3-3 protein theta	Universal signalling pathways	*YWHAQ*
14-3-3 protein zeta/delta*	Universal signalling pathways	*YWHAZ*
Isoform long of 14-3-3 protein beta/alpha	Universal signalling pathways	*YWHAB*
EF-hand domain-containing protein D2	Calcium-binding	*EFHD2*
Galectin-7	Growth control	*LGALS7*

OTHER PATHWAYS		
Isoform 1 of protein SET	DNA-binding, inhibition of histone 4 deacetylation and DNA demethylation	*SET*
Isoform 2 of sarcoplasmic/endoplasmic reticulum calcium ATPase 2*	ER calcium-homeostasis	*ATP2A2*
Wolframin	ER calcium-homeostasis	*WFS1*
Isoform long (1) of sodium/potassium-transporting ATPase subunit α-1*	Sodium/potassium pump catalytic subunit	*ATP1A1*
LanC-like protein 1	G-Protein-coupled receptor-signalling, binds GSH	*LANCL1*
Microsomal glutathione S-transferase 3*	GSH metabolism, peroxidase activity	*MGST1*
Multidrug resistance protein 1*	ATPase	*ABCB1*
Isoform 2 of vacuolar-type proton ATPase 116 kDa subunit a isoform 1	Transferrin recycling, iron homeostasis	*ATP6V0A1*
Vacuolar-type proton ATPase 16 kDa proteolipid subunit	Transferrin recycling, iron homeostasis, pore subunit	*ATP6V0C*
Vacuolar-type proton ATPase catalytic subunit A*	Vacuolar ATPase, transferrin recycling, iron homeostasis	*ATP6V1A*
Vacuolar-type proton ATPase subunit d 1	Vacuolar ATPase, transferrin recycling, iron homeostasis	*ATP6V0D1*
MITOCHONDRIAL RESPIRATION		
*CDGSH iron-sulfur domain-containing protein 1**	Electron transport chain, oxidative phosphorylation	*CISD1*
Cytochrome c oxidase subunit 5A, mitochondrial*	Electron transport chain, cytochrome C oxidase complex IV	*COX5A*
Cytochrome c oxidase subunit 5B, mitochondrial*	Electron transport chain, cytochrome C oxidase complex IV	*COX5B*
Cytochrome c oxidase subunit 6C	Electron transport chain, cytochrome C oxidase complex IV	*COX6C*
Cytochrome c oxidase subunit 7a polypeptide 2 (liver) precursor	Electron transport chain, cytochrome C oxidase complex IV	*COX7A*

NUCLEO-CYTOPLASMIC TRANSPORT		
Isoform 1 of nucleoporin NDC1	NPC anchoring between nuclear envelope and soluble NUPs	*NDC1*
Importin subunit ß-1*	Nuclear protein import via NPC, nuclear localisation signal receptor	*KPNB1*
Isoform 1 of importin-5*	Nuclear protein import via NPC, nuclear localisation signal receptor	*IPO5*
GTP-binding nuclear protein Ran*	Nucleo-cytoplasmic import, RNA export, mitotic spindle-formation	*RAN*
Isoform 1 of exportin-2	Importin α re-export after cargo import	*CSE1L*
Isoform A1-B of heterogeneous nuclear ribonucleoprotein A1*	PolyA-mRNA export from nucleus	*HNRNPA1*
Isoform short of heterogeneous nuclear ribonucleoprotein U*	Nucleotide-binding, mRNA export	*HNRNPU*
MITOCHONDRIAL TRANSPORT		
Isoform 1 of mitochondrial import receptor subunit TOM40 homologue*	Mitochondrial precursor protein import	*TOM40*
Mitochondrial import receptor subunit TOM22 homologue	Mitochondrial precursor protein import	*TOM22*
Mitochondrial carrier homologue 2	Induces mitochondrial de-polarisation	*MTCH2*
Sideroflexin-1	Iron ion-transport in/out of mitochondria	*SFXN1*
OTHER TRANSPORT		
Ras-related protein Rab-10*	GOLGI-membrane, ER dynamics, phospholipid synthesis	*RAB10*
Ras-related protein Rab-11A*	GOLGI-membrane, cytokinesis	*RAB11A*
Ras-related protein Rab-1B*	ER-GOLGI transport	*RAB1B*
Ras-related protein Rab-2A*	ER-GOLGI transport	*RAB2A*
Ras-related protein Rab-3B	Vesicular transport	*RAB3B*
Ras-related protein Ral-A*	Cytokinesis	*RALA*
CILIA TRANSPORT		
T-complex protein 1 subunit beta	Chaperone, T-complex protein 1 ring complex, cilia vesicle transport	*CCT2*
T-complex protein 1 subunit delta*	Chaperone,cilia vesicle transport	*CCT4*

CILIA TRANSPORT		
T-complex protein 1 subunit epsilon	Chaperone,cilia vesicle transport	*CCT5*
T-complex protein 1 subunit eta isoform d	Chaperone,cilia vesicle transport	*CCT7*
T-complex protein 1 subunit gamma isoform b*	Chaperone,cilia vesicle transport	*CCT3*
T-complex protein 1 subunit zeta	Chaperone,cilia vesicle transport	*CCT6A*
STRUCTURE		
Coiled-coil-helix-coiled-coil-helix domain-containing protein 3, mitochondrial*	Mitochondrial contact site complex, mitochondrial cristae structure	*CHCHD3*
Fascin	Actin bundle formation	*FSCN1*
Filaggrin*	Keratin intermediate filaments	*FLG*
Isoform 1 of surfeit locus protein 4*	GOLGI-organisation	*SURF4*
Isoform ß-1A of integrin ß-1*	Cell adhesion, cytokinesis	*ITGB1*
Isoform DPI of desmoplakin*	Desmosomes	*DSP*
Keratin, type II cuticular Hb4	Universal signalling pathways	*KRT84*
Keratin, type II cytoskeletal 3*	Universal signalling pathways	*KRT3*
Keratin, type II cytoskeletal 6B*	Universal signalling pathways	*KRT6B*
Keratin, type II cytoskeletal 6C*	Universal signalling pathways	*KRT6C*
MARCKS-related protein	Actin cytoskeleton formation	MARCKSL1
Myristoylated alanine-rich C-kinase substrate	Actin-cross-linking	*MARCKS*

Whole cell lysates of GFP and GFP-ALADIN expressing NCI-H295R cells were used for co-immunoprecipitation (co-IP). Proteins not found in two independent GFP control co-IPs but found in all three independent GFP-ALADIN co-IPs are listed here. Proteins are grouped according to their biological function or cellular role using UniProt database. Proteins with an asterisk were identified simultaneously by GFP-ALADIN co-IP and by co-IP of endogenous ALADIN. Those in bold with an asterisk were found in none of the controls of both expression models. Proteins in italic were detected as another isoform or protein from the same group in co-IP of endogenous ALADIN.

Table 21 – Functional classification of proteins identified by mass spectrometry analyses after co-immunoprecipitation of endogenous ALADIN verified by proteins found at least once in exogenous GFP-ALADIN co-IP.

PROTEIN	METABOLISM	GENE
LIPID METABOLISM/STEROIDOGENESIS		
Isoform 1 of acylglycerol kinase, mitochondrial	Lipid and glycerolipid metabolism	AGK
Isoform 1 of NADH-cytochrome b5 reductase 3	CYP P450 regulation	CYB5R3
Progesterone receptor membrane component 2*	CYP P450 regulation	*PGRMC2*
PROTEIN PROCESSING		
Cathepsin D	Lysosomal acid protease	*CTSD*
Isoform 1 of serpin B3	Protease inhibitor	*SERPINB3*
Isoform 1 of translocon-associated protein subunit α	ER translocon complex	*SSR1*
Isoform LAMP-2A of Lysosome-associated membrane glycoprotein 2	Lysosomal metabolism	*LAMP2*
Protein ERGIC-53	Protein recycling and sorting, mannose-specific	*LMAN1*
Translocon-associated protein subunit delta precursor	ER translocon complex	*SSR4*
OTHER PATHWAYS		
14-3-3 protein zeta/delta	Universal signalling pathways	*YWHAZ*
Isoform 2 of sarcoplasmic/endoplasmic reticulum calcium ATPase 2	ER calcium-homeostasis	*ATP2A2*
Isoform long (1) of sodium/potassium-transporting ATPase subunit α-1	Sodium/potassium pump catalytic subunit	*ATP1A1*
MITOCHONDRIAL RESPIRATION		
CDGSH iron-sulfur domain-containing protein 2	Electron transport chain, oxidative phosphorylation	*CISD2*
NUCLEO-CYTOPLASMIC TRANSPORT		
Isoform 1 of importin-5	Nuclear protein import via NPC, nuclear localisation signal receptor	*IPO5*

Whole cell lysates of NCI-H295R wild-type cells were used for co-immunoprecipitation (co-IP). Proteins not found in the mouse normal IgG control co-IP but found in the ALADIN co-IP were compared to those found in the GFP-ALADIN co-IP (Table 20). Those which were found in both co-IP models (at least once) and in none of the controls are listed here. Proteins are grouped according to their biological function or cellular role using UniProt database. Proteins in italic were detected as another isoform or protein from the same group in the GFP-ALADIN co-IP.

In co-IP conducted with whole cell lysates of NCI-H295R cells stably over-expressing the GFP-ALADIN fusion protein 92 proteins not found in specific controls but in all three independent

experiments were detected (Table 20). Distinct proteins involved in the nucleo-cytoplasmic import of proteins and export of mRNA through NPCs were identified in the experiments. Among these were the nucleoporin NDC1, importin subunit ß-1, importin-5, GTP-binding nuclear protein Ran, exportin-2, heterogeneous nuclear ribonucleoprotein A1 and heterogeneous nuclear ribonucleoprotein U (HNRNPA1 and U). Well-known mitochondrial TOM (mitochondrial import receptor subunit TOM40 and mitochondrial import receptor subunit TOM22) were found. Several proteins or precursor polypeptides involved in different aerobic metabolism pathways (glycolysis, citric acid cycle (CAC), oxidative respiration chain) precipitated with ALADIN. Many of these proteins have mitochondrial destination and/or origin and are nuclear-encoded. Many glycolytic proteins of the cytosol feeding pyruvate into the mitochondrial TAC were recognised. Main transporters (tricarboxylate transport protein and mitochondrial 2-oxoglutarate/malate carrier protein) and players of the CAC (2-oxoglutarate dehydrogenase, succinate dehydrogenase and malate dehydrogenase) impact on the mitochondrial respiration chain. Of this mitochondrial electron transport chain cytochrome c oxidase subunit 5A, 5B, 6C and 7A precursor; all are components of cytochrome C oxidase complex IV, were found. In addition, some proteins involved in cholesterol synthesis and lipogenesis were identified. Concerning ALADIN being involved in impairment of steroidogenesis, POR (not in Table 20 or 21) and PGRMC2 of the proteomic analyses were of interest.

Reviewing proteins identified after co-IP using whole cell lysates of NCI-H295R wild-type cells (and not found in the specific control experiment) with those detected in the GFP-ALADIN co-IP (found at least once) cut down the total sum of possible interacting proteins to one sixth (14 proteins) (Table 21). Proteins distinct for regulating lipogenesis or steroidogenesis were acylglycerol kinase, NADH-cytochrome b5 reductase and PGRMC2. Several proteins involved in protein maturation or processing could be found; among those were proteins of the translocon complex in the ER membrane responsible for translocation-coupled translation: translocon-associated protein (TRAP) subunit α (SSR1) and TRAP subunit delta (SSR4). The nucleoporin NDC1 shown to interact with ALADIN (Kind et al., 2009; Yamazumi et al., 2009) could not be reproduced in endogenous ALADIN co-IP, but the nuclear localisation receptor importin-5 could be identified. Subunits of two specific ATPases, the first anchored within the ER membrane (sarcoplasmic/endoplasmic reticulum calcium ATPase 2) and the second integrated within the cell membrane (sodium/potassium-transporting ATPase), were repeatedly found.

4.6 ALADIN-dependent alteration in steroidogenesis requires an interaction with microsomal CYP P450 enzymes

4.6.1 PGRMC2 and POR precipitate with ALADIN in an exogenous and endogenous adrenal cell expression model

Proteins simultaneously identified in GFP-ALADIN co-IP and co-IP of endogenous ALADIN implying a specific connection to adrenocortical steroidogenesis were POR and PGRMC2 (Figure 27). Both are microsomal integral membrane proteins acting as regulators of several different CYP P450 enzymes; the first one extensively studied, the latter barely known. Even though POR was found in mass spectrometry to a small extent also in the co-IP negative controls it was mainly focussed on the protein since recent results showed a possible interaction be-

tween ALADIN and POR (Jühlen et al., 2015). Exclusive unique peptides of ALADIN, POR and PGRMC2 detected in tandem mass spectrometry after GFP-ALADIN and endogenous ALADIN co-IP are summarised in Figure 27. In the exogenous expression model sufficient ALADIN peptides could be identified, the analysis of endogenous ALADIN co-IP resulted in less detected peptides. Despite distinct methodological optimisation procedures using different protocols and antibodies, endogenous ALADIN co-IP had a low yield and measurement using tandem mass spectrometry was more difficult to process. Nevertheless, these results are presented here as well.

A

IPI00024143 (100%), 59.574,1 Da
Aladin
11 exclusive unique peptides, 11 exclusive unique spectra, 12 total spectra, 176/546 amino acids (32% coverage)

MCSLGLFPPP PPRGQVTLYE HNNELVTGSS YESPPPDFRG QWINLPVLQL
TKDPLKTPGR LDHGTRTAFI HHREQVWKRC INIWRDVGLF GVLNEIANSE
EEVFEWVKTA SGWALALCRW ASSLHGSLFP HLSLRSEDLI AEFAQVTNWS
SCCLRVFAWH PHTNKFAVAL LDDSVRVYNA SSTIVPSLKH RLQRNVASLA
WKPLSASVLA VACQSCILIW TLDPTSLSTR PSSGCAQVLS HPGHTPVTSL
AWAPSGGRLL SASPVDAAIR VWDVSTETCV PLPWFRGGGV TNLLWSPDGS
KILATTPSAV FRVWEAQMWT CERWPTLSGR CQTGCWSPDG SRLLFTVLGE
PLIYSLSFPE RCGEGKGCVG GAKSATIVAD LSETTIQTPD GEERLGGEAH
SMVWDPSGER LAVLMKGKPR VQDGKPVILL FRTRNSPVFE LLPCGIIQGE
PGAQPQLITF HPSFNKGALL SVGWSTGRIA HIPLYFVNAQ FPRFSPVLGR
AQEPPAGGGG SIHDLPLFTE TSPTSAPWDP LPGPPPVLPH SPHSHL

IPI00470467 (100%), 76.690,9 Da
NADPH--cytochrome P450 reductase
21 exclusive unique peptides, 22 exclusive unique spectra, 39 total spectra, 271/677 amino acids (40% coverage)

MGDSHVDTSS TVSEAVAEEV SLFSMTDMIL FSLIVGLLTY WFLFRKKKEE
VPEFTKIQTL TSSVRESSFV EKMKKTGRNI IVFYGSQTGT AEEFANRLSK
DAHRYGMRGM SADPEEYDLA DLSSLPEIDN ALVVFCMATY GEGDPTDNAQ
DFYDWLQETD VDLSGVKFAV FGLGNKTYEH FNAMGKYVDK RLEQLGAQRI
FELGLGDDDG NLEEDFITWR EQFWPAVCEH FGVEATGEES SIRQYELVVH
TDIDAAKVYM GEMGRLKSYE NQKPPFDAKN PFLAAVTTNR KLNQGTERHL
MHLELDISDS KIRYESGDHV AVYPANDSAL VNQLGKILGA DLDVVMSLNN
LDEESNKKHP FPCPTSYRTA LTYYLDITNP PRTNVLYELA QYASEPSEQE
LLRKMASSSG EGKELYLSWV VEARRHILAI LQDCPSLRPP IDHLCELLPR
LQARYYSIAS SSKVHPNSVH ICAVVVEYET KAGRINKGVA TNWLRAKEPA
GENGGRALVP MFVRKSQFRL PFKATTPVIM VGPGTGVAPF IGFIQERAWL
RQQGKEVGET LLYYGCRRSD EDYLYREELA QFHRDGALTQ LNVAFSREQS
HKVYVQHLLK QDREHLWKLI EGGAHIYVCG DARNMARDVQ NTFYDIVAEL
GAMEHAQAVD YIKKLMTKGR YSLDVWS

IPI00005202 (100%), 26.170,9 Da
progesterone receptor membrane component 2
2 exclusive unique peptides, 2 exclusive unique spectra, 2 total spectra, 20/247 amino acids (8% coverage)

MGGAGRGVGE GRGRGGGGRR WRAVMAAGDG DVKLGTLGSG SESSNDGGSE
SPGDAGAAAE GGGWAAAALA LLTGGGEMLL NVALVALVLL GAYRLWVRWG
RRGLGAGAGA GEESPATSLP RMKKRDFSLE QLRQYDGSRN PRILLAVNGK
VFDVTKGSKF YGPAGPYGIF AGRDASRGLA TFCLDKDALR DEYDDLSDLN
AVQMESVREW EMQFKEKYDY VGRLLKPGEE PSEYTDEEDT KDHNKQD

B

IPI00024143 (100%), 59.574,1 Da
Aladin
1 exclusive unique peptides, 1 exclusive unique spectra, 1 total spectra, 15/546 amino acids (3% coverage)

MCSLGLFPPP PPRGQVTLYE HNNELVTGSS YESPPPDFRG QWINLPVLQL
TKDPLKTPGR LDHGTRTAFI HHREQVWKRC INIWRDVGLF GVLNEIANSE
EEVFEWVKTA SGWALALCRW ASSLHGSLFP HLSLRSEDLI AEFAQVTNWS
SCCLRVFAWH PHTNKFAVAL LDDSVRVYNA SSTIVPSLKH RLQRNVASLA
WKPLSASVLA VACQSCILIW TLDPTSLSTR PSSGCAQVLS HPGHTPVTSL
AWAPSGGRLL SASPVDAAIR VWDVSTETCV PLPWFRGGGV TNLLWSPDGS
KILATTPSAV FRVWEAQMWT CERWPTLSGR CQTGCWSPDG SRLLFTVLGE
PLIYSLSFPE RCGEGKGCVG GAKSATIVAD LSETTIQTPD GEERLGGEAH
SMVWDPSGER LAVLMKGKPR VQDGKPVILL FRTRNSPVFE LLPCGIIQGE
PGAQPQLITF HPSFNKGALL SVGWSTGRIA HIPLYFVNAQ FPRFSPVLGR
AQEPPAGGGG SIHDLPLFTE TSPTSAPWDP LPGPPPVLPH SPHSHL

IPI00470467 (100%), 76.690,9 Da
NADPH--cytochrome P450 reductase
8 exclusive unique peptides, 9 exclusive unique spectra, 11 total spectra, 109/677 amino acids (16% coverage)

MGDSHVDTSS TVSEAVAEEV SLFSMTDMIL FSLIVGLLTY WFLFRKKKEE
VPEFTKIQTL TSSVRESSFV EKMKKTGRNI IVFYGSQTGT AEEFANRLSK
DAHRYGMRGM SADPEEYDLA DLSSLPEIDN ALVVFCMATY GEGDPTDNAQ
DFYDWLQETD VDLSGVKFAV FGLGNKTYEH FNAMGKYVDK RLEQLGAQRI
FELGLGDDDG NLEEDFITWR EQFWPAVCEH FGVEATGEES SIRQYELVVH
TDIDAAKVYM GEMGRLKSYE NQKPPFDAKN PFLAAVTTNR KLNQGTERHL
MHLELDISDS KIRYESGDHV AVYPANDSAL VNQLGKILGA DLDVVMSLNN
LDEESNKKHP FPCPTSYRTA LTYYLDITNP PRTNVLYELA QYASEPSEQE
LLRKMASSSG EGKELYLSWV VEARRHILAI LQDCPSLRPP IDHLCELLPR
LQARYYSIAS SSKVHPNSVH ICAVVVEYET KAGRINKGVA TNWLRAKEPA
GENGGRALVP MFVRKSQFRL PFKATTPVIM VGPGTGVAPF IGFIQERAWL
RQQGKEVGET LLYYGCRRSD EDYLYREELA QFHRDGALTQ LNVAFSREQS
HKVYVQHLLK QDREHLWKLI EGGAHIYVCG DARNMARDVQ NTFYDIVAEL
GAMEHAQAVD YIKKLMTKGR YSLDVWS

IPI00005202 (100%), 26.170,9 Da
progesterone receptor membrane component 2
1 exclusive unique peptides, 1 exclusive unique spectra, 1 total spectra, 14/247 amino acids (6% coverage)

MGGAGRGVGE GRGRGGGGRR WRAVMAAGDG DVKLGTLGSG SESSNDGGSE
SPGDAGAAAE GGGWAAAALA LLTGGGEMLL NVALVALVLL GAYRLWVRWG
RRGLGAGAGA GEESPATSLP RMKKRDFSLE QLRQYDGSRN PRILLAVNGK
VFDVTKGSKF YGPAGPYGIF AGRDASRGLA TFCLDKDALR DEYDDLSDLN
AVQMESVREW EMQFKEKYDY VGRLLKPGEE PSEYTDEEDT KDHNKQD

Figure 27 – Identified exclusive unique peptides of ALADIN, cytochrome P450 oxidoreductase and progesterone receptor membrane compartment 2.

Identified exclusive unique peptides (yellow) (number of different amino acid sequences, regardless of any modification, that are associated only with this protein) of cytochrome P450 oxidoreductase, progesterone receptor membrane compartment 2 and ALADIN after co-immunoprecipitation of whole cell lysates of GFP-ALADIN over-expressing (A) and of wild-type NCI-H295R cells (B). Peptide modifications are marked in green (oxidation of methionine (M)).

In Figure 28 A Western Blot verifications of positive POR binding in the GFP-ALADIN co-IP and co-IP of endogenous ALADIN is seen. Positiv PGRMC2 binding in the GFP-ALADIN co-IP is shown in Figure 28 B. In co-IP of endogenous ALADIN bound antibodies to the beads were revealed on Western Blot: light chains appeared at the size of 25 kDa disturbing efficient PGRMC2 verification at 26 kDa due to much background. This result is not shown here. Bound fractions of co-IPs were conducted for tandem mass spectrometry proteomic analyses as described before. The most minimal level of POR unique peptides was detected once of three in the specific negative control of GFP-ALADIN co-IP (two unique peptides) and five unique peptides were found in the specific negative control of endogenous ALADIN co-IP (Figure 27). This result could not be shown on Western Blot level where the negative controls remained empty for POR protein (Figure 28 A). The experiments were repeated three times.

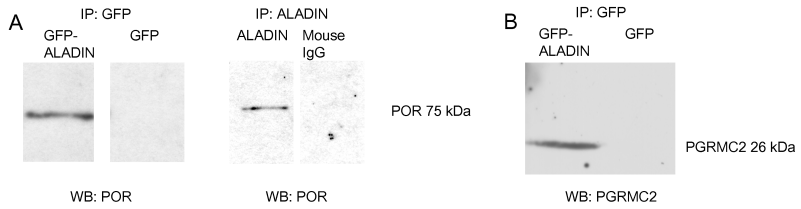

Figure 28 – Western Blot of bound fractions after GFP and ALADIN co-IP.
Whole cell lysates of GFP-ALADIN and GFP as negative control over-expressing NCI-H295R cells were prepared for GFP co-immunoprecipitation (co-IP). Whole cell lysates of NCI-H295R wild-type cells were prepared for ALADIN co-IP. A mouse monoclonal antibody against ALADIN and normal mouse IgGs as negative control were used for ALADIN co-IP. Primary antibodies against cytochrome P450 oxidoreductase (POR) (A) and progesterone receptor membrane compartment 2 (PGRMC2) (B) were used in Western Blots. POR and PGRMC2 were found in each specific bound fraction implying possible interaction with ALADIN. No POR and PGRMC2 were detectable in the fractions of the negative controls.

4.6.2 Immunofluorescent localisation of POR in adrenal cells

Further evidence of suggested interaction and communication should be given after immunofluorescent staining of ALADIN and POR in adrenal NCI-H295R cells. Primary antibodies against ALADIN and POR were proceeded for immunostaining. Secondary goat anti-mouse tagged with alexa fluor 555 (staining ALADIN) and anti-rabbit IgGs tagged with alexa fluor 488 (staining POR) were applied. Immunofluorescent staining of the NUP ALADIN appeared at the nuclear envelope at the proximity of NPCs. The microsomal POR localised to the central ER and to the perinuclear space between nuclear envelope and ER. An overlay of both immunostainings revealed co-localisation of ALADIN with POR at the perinuclear space (Figure 29) (n=3).

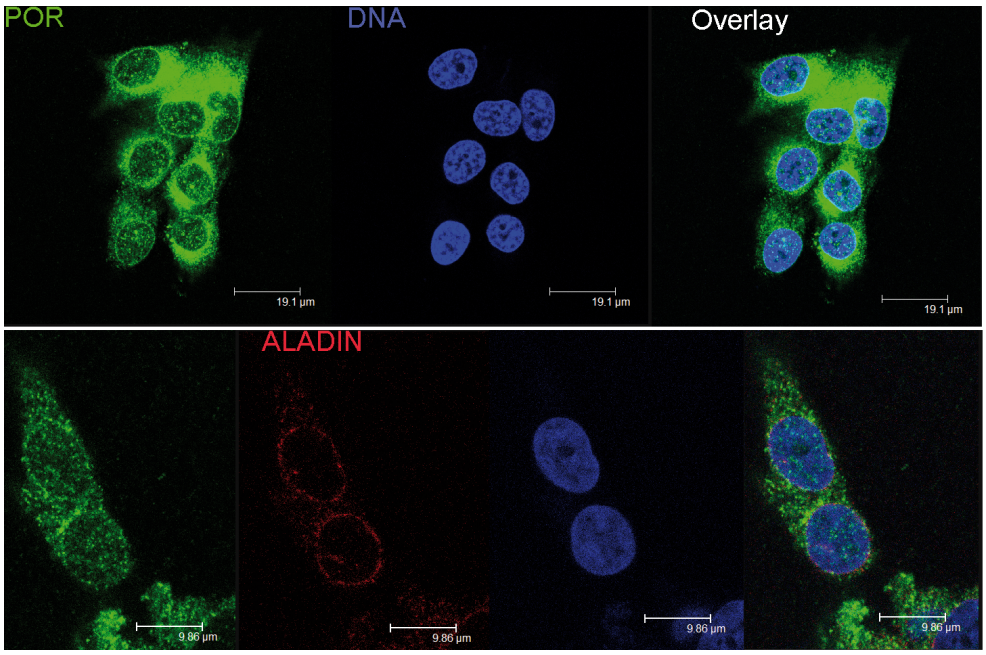

Figure 29 – Immunofluorescent staining of ALADIN and cytochrome P450 oxidoreductase in NCI-H295R wild-type cells.

Primary antibodies against ALADIN and cytochrome P450 oxidoreductase (POR), and secondary antibodies alexa fluor 555 goat anti-mouse IgG (ALADIN, red) and alexa fluor 488 goat anti-rabbit IgG (POR, green) were used for immunofluorescence. Nuclei were stained with DAPI (blue). Overlays are presented in the last column presenting co-localisation of ALADIN with POR at the perinuclear space.

5 Discussion

5.1 Role of ALADIN in human adrenocortical cells for oxidative stress response and steroidogenesis

Primarily in the first part of this work, the cellular role of ALADIN was investigated by creating two experimental expression systems using the human adrenocortical carcinoma cell line NCI-H295R1-TR that resembles the glucocorticoid producing adrenal zona fasciculata (Wang et al., 2012). These cells were successfully transformed to either over-express or down-regulate ALADIN by a doxycycline-inducible stable expression of either *AAAS*-shRNA (*AAAS* down-regulation) or *AAAS*-mRNA (*AAAS* over-expression).

In this study it is successfully demonstrated that *AAAS* knock-down firstly induces a significant down-regulation of genes coding for type II microsomal CYP enzymes involved in the glucocorticoid and androgen pathways of steroidogenesis, CYP17A1 and CYP21A2, and of the gene coding for their electron donor enzyme POR. Secondly, it is revealed that the functional output of these enzymes, i.e. precursor metabolites of the glucocorticoid and androgen pathways, was markedly decreased in ALADIN knock-down cells.

In triple A patients adrenal insufficiency may appear later in life than the other two symptoms and its development is gradually (Milenkovic et al., 2010). Glucocorticoid and androgen production is affected, consistent with the presented *in vitro* results where production of precursors involved in these pathways (17OHP, 11-deoxycortisol and androstenedione) was impaired. Fifteen percent of patients however show a deficiency in mineralocorticoid production (Clark and Weber, 1998; Tsigos, 1999). Precursor metabolites of the mineralocorticoid pathway (DOC) were not impaired in the experiments of this study. Mitochondrial aldosterone synthase encoded by *CYP11B2* exhibits 11ß-hydroxylase activity beside its activity to catalyse aldosterone from corticosterone by 18-hydroxylation. 11ß-hydroxylase activity is expressed by a closely related mitochondrial enzyme CYP11B1 in order to produce cortisol from 11-deoxycortisol (Kawamoto et al., 1992). Furthermore it was shown that CYP11B2 exhibits some activity to hydroxylate 11-deoxycortisol (Kawamoto et al., 1992; Bureik et al., 2002). Thus, it can be assumed that 11-deoxycortisol can serve as a substrate for aldosterone production. The relative preservation of mineralocorticoid production in triple A patients resembles the lower production of aldosterone compared to cortisol. This may save the zona glomerulosa from cell degeneration as it is seen for the other zones (Clark and Weber, 1998).

Even though Prasad et al. already provided some evidence that lentivirally transduced ALADIN-deficient adrenal cells show an alteration in steroidogenesis due to a decrease of expression of *StAR* and *CYP11B1* (Prasad et al., 2013), in this work stable transfection for *AAAS* knock-down (and over-expression) was employed and the effects on steroidogenic enzyme expression and steroid production comprehensively investigated. In this work, by using tandem mass spectrometry for multiple steroid identification and quantitation strong evidence for a significant functional impairment of the glucocorticoid and androgenic pathways in ALADIN-deficient cells is provided. Our findings lead further to the exact mechanism how ALADIN deficiency affects steroidogenesis and elucidates more details about the pathogenesis in triple A syndrome. These results therefore significantly add to the understanding of the role of ALADIN for adrenal steroidogenesis.

Many of the results are demonstrated in the partial *AAAS* knock-down state, i.e. the doxycycline-uninduced state in which too little repressor is produced to efficiently block *AAAS*-shRNA expression leading to a premature *AAAS* knock-down. Nevertheless, the amount of *AAAS*-shRNA produced is enough to silence partly *AAAS* gene expression and to exert a pathogenic phenotype in the adrenal cells. Adenoviral transduction in primary bovine adrenocortical cells has been shown to result in the impairment of steroidogenesis and alteration of cell morphology (Alesci et al., 2002). With regard to human adrenocortical cells Matkovic et al. could show that adenoviral infection leads to alteration in steroidogenesis, presumably not due to viral transgene expression but rather due to viral structure encounter (Matkovic et al., 2009). One can therefore assume that the discrepancies in the findings between Prasad et al. and this work lie primarily in the alternative cell model (transduction and stable transfection) and to some extent in the experimental sample sizes especially for steroid analyses. Additionally, the zona fasciculata sub-strain 1 of NCI-H295R cells (Wang et al., 2012) which resembles one of the zones most degenerated in triple A patients (Clark and Weber, 1998) is different from the cells used by Prasad and colleagues.

It was also ascertained that after *AAAS* knock-down in NCI-H295R1-TR cells not only cellular $NADPH$ and $GSH/GSSG$ levels were significantly decreased under oxidative stress using paraquat but also that the concentration of cellular hydrogen peroxide was elevated. *GSR* expression was not altered under basal conditions suggesting that the increase in sensitivity to oxidative stress in these cells was not the result of low *GSR* expression. These findings imply that ALADIN knock-down cells have an altered redox homeostasis and, hence, are more sensitive to oxidative stress (Figure 30).

In order to further address the involvement of ALADIN in the oxidative stress response the impairment of the nuclear import of proteins that protect the nucleus against ROS was analysed. The nuclear import of APTX, LIG1 and FTH1 was markedly decreased after ALADIN depletion. It can therefore be concluded as previously shown in fibroblast cells deriving from triple A syndrome patients (Kind et al., 2010; Storr et al., 2009; Hirano et al., 2006) that ALADIN is involved in oxidative stress responses and import of these proteins also in adrenocortical cells.

In addition, it was recently observed that fibroblast cells of triple A patients show an altered down-regulation or induction of genes associated with oxidative stress and antioxidant defence (Koehler et al., 2013). APTX and DNA ligases work concomitantly together in order to initiate and repair DNA in multiple pathways and upon various deleterious factors, especially ROS-mediated damage (Rass et al., 2007). Neurological disorders (early-onset ataxia with oculomotor apraxia and hypoalbuminemia, MIM #208920) caused by mutations in *APTX* are probably caused by accumulation of unrepaired DNA strand breaks resulting from abortive DNA ligation, especially generated by oxidation (Rass et al., 2007; Ahel et al., 2006). Another possibility of abortive DNA ligation (including LIG1) is during ribonucleotide excision repair. It has been shown that adenylated RNA-DNA lesions are resolved by APTX and that accumulation of these lesions is associated with neurologic diseases (Tumbale et al., 2014).

Triple A syndrome is commonly associated with a variety of neurologic impairments, presumably due to an increasing number of RNA-DNA lesions in patients' neurons. APTX and LIG1 both contain a nuclear localisation signal and are thought to be translocated into the nucleus by a karyopherin-α/β-mediated pathway through NPCs. Hirano et al. presented that

nuclear import of APTX and LIG1 is impaired when treating patient fibroblasts and control cells with L-buthionine-(S,R)-sulfoximine (BSO), a glutathione-depleting agent, but single-stranded DNA breaks increased only in patient cells (Hirano et al., 2006). Increased oxidative stress by BSO seems to intensify nuclear import impairment in patient fibroblasts seen by accumulation of single-stranded DNA breaks. These findings in patient fibroblasts are now confirmed by our results in ALADIN knock-down adrenal cells which were also depleted of GSH and show impaired nuclear import of APTX and LIG1.

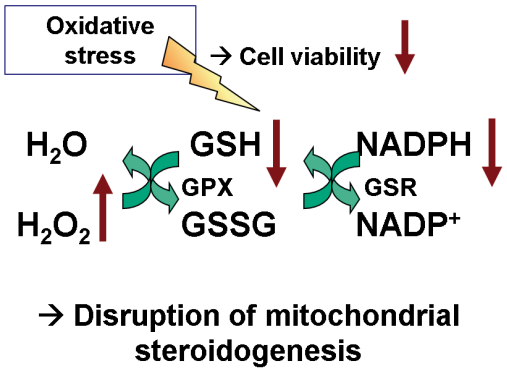

Figure 30 – Increase of cellular susceptibility to oxidative stress after *AAAS* knock-down in NCI-H295R1-TR.

Deprivation of ALADIN in human adrenocortical cells leads to decreased levels of $NADPH$ and concomitantly affects the buffer amount of reduced glutathione (GSH) and increases hydrogen peroxide (H_2O_2). $GSSG$, oxidised glutathione disulphide. GPX, glutathione peroxidase. GSR, glutathione reductase (Jühlen et al., 2015).

In *AAAS* over-expressing cells, neither steroidogenic enzyme expression nor steroid production was altered. Surprisingly, similar to ALADIN deprivation, over-expressing cells showed a significant impairment of cell viability and $GSH/GSSG$ ratio under oxidative stress, but cellular H_2O_2 concentration was not increased. In addition it is presented that over-expressing cells have a decreased expression of *GSR* which explains the decreased $GSH/GSSG$ ratio.

These results suggest that *AAAS* over-expression cells do not have an impaired redox potential and are able to detoxify an increased level of ROS after paraquat treatment in contrast to *AAAS* knock-down cells. In addition, it explains the finding that *AAAS* over-expression cells do not show an alteration in steroidogenesis but rather behave like control cells. The impaired cell viability and decreased expression of *GSR* may be caused by cell stress due to an increased ALADIN protein synthesis and significant accumulation in the cytosol and ER.

Cellular ER stress has been recently reported to cause increased protein folding-stress. Initial protein maturation takes place at the ER and is of importance of proper protein folding. Increased protein synthesis and folding, especially in specialised secretory cells, introduces a high level of stress and a particular challenge for the cell. If the ER machinery is working over-strained an excess of synthesised proteins will be sensed causing a stop of translation, ultimately leading to cell death (Hetz, 2012). I therefore hypothesise that this phenomenon accounts for our *AAAS* over-expressing cells.

AAAS over-expressing cells did not show any change in nuclear import of APTX or LIG1. In addition, the import of FTH1 was significantly decreased after *AAAS* over-expression. These results together with the ALADIN knock-down results confirm the previously reported finding that ALADIN is involved in the nuclear import of FTH1 (Storr et al., 2009).

FTH1 is an iron chelator and its intrinsic ferroxidase activity is an important player in the cellular antioxidant defence system by converting ferrous iron to its ferric storage form which can act in the Fenton reaction as a ROS scavenger. FTH1 is shown to have transcriptional regulatory activity which explains its translocation to the nucleus besides protecting the DNA from ROS. Regarding its nuclear import, it is known that FTH1 enters the nucleus through NPCs, but no obvious nuclear localisation signal has been found so far. It is rather thought to be shuttled by a chaperon molecule to the NPC and into the nucleus (Misaggi et al., 2014; Thompson et al., 2002; Alkhateeb and Connor, 2010). In corneal epithelial cells it was presented that FTH1 not passively diffuses into the nucleus but is rather shuttled by a chaperon molecule, called ferritoid. This molecule seems to be highly specific for this cell type (Cai et al., 2008; Cai and Linsenmayer, 2001).

In this study it is presented that *AAAS* over-expression leads to a significant accumulation of ALADIN in the cytoplasm; most likely due to a lack of binding sites of ALADIN at the nuclear pore complexes. Consequently, mislocalisation of ALADIN in the cytoplasm leads to a decrease of nuclear import and subsequent retention of FTH1 in the cytoplasm. After treating ALADIN knock-down and over-expression cells with paraquat for 24 h an increase of nuclear import of FTH1 was observed. However, this import was significant diminished in the over-expression model in comparison to paraquat treated control cells. In the knock-down model this effect was not obvious, probably due to an insufficient total loss of ALADIN at the nuclear pore. Thus, it is assumed here that FTH1 is withheld in the cytoplasm by ALADIN in the over-expression cells. It still remains to be clarified how FTH1 is translocated into the nucleus and how this protein interacts with ALADIN.

As a conclusion for the first part of this work, the results of the knock-down experiments in the human cell line NCI-H295R1 are in accordance with the pathology in triple A syndrome patients. They show an alteration in adrenal steroidogenesis, especially the glucocorticoid and androgenic pathways, and an impairment in the cellular response to oxidative stress.

No such adrenal phenotype has so far been shown in *AAAS* knock-out mice (Huebner et al., 2006). Mice predominantly have a zona glomerulosa, the aldosterone producing part of the adrenal cortex which seems to escape cellular damage by ALADIN deprivation (Clark and Weber, 1998; Huebner et al., 2006). The presented results suggest that alteration in adrenal steroidogenesis in humans through POR is accompanied by a defective redox potential and homeostasis due to ALADIN deficiency which is more elucidated in the second part of this work.

The presence of ALADIN seems to be of high significance for detoxification of ROS in adrenocortical cells and puts weight on the genuine susceptibility of this organ to oxidative stress. This study shows that these processes affect adrenal cells and are likely to be causally linked to the adrenal phenotype in triple A syndrome patients. It merits further research if ALADIN deficiency preferentially affects cell-type specific transport and damage, because, as seen in classic triple A syndrome patients, mainly cells of the adrenal cortex and of the nervous system are damaged. It is recently investigated by Carvalhal and colleagues that ALADIN is involved in Aurora A-kinase-dependent cell division (personal communication Sara Carvalhal

et al, Dundee, 2015). Therefore, it can be assumed that cells damaged in triple A syndrome not only have a unique metabolism but also a specific type of cell division.

In addition, a new role for the glucocorticoid receptor (GR), belonging to the nuclear hormone receptor superfamily, has been established. Ligand-binding to the quiescent cytosolic GR induces transformation, translocation in the nucleus and regulation of DNA transcription leading to altered metabolism, immunity and cell fate. Besides these tasks the GR has been discovered to co-ordinate mitotic progression and chromosome segregation by aggregating to mitotic spindles, interestingly dependent on Aurora A. This action does neither require ligand-binding nor transcriptional regulation (Matthews et al., 2015). Based on these recent results, the role of ALADIN in mitosis awaits further studies and may add to the pathogenetic mechanisms in triple A syndrome.

5.2 Involvement of ALADIN in translocation of specific nuclear-encoded mitochondrial precursors through the nuclear pore complex

In the second part of this study co-IP analyses of two ALADIN expression models wild-type ALADIN and GFP-ALADIN over-expression using NCI-H295R adrenal cells followed by mass spectrometry provided an experimental approach to aim for new interaction partners of ALADIN and for elucidation of further pathways involved in the pathogenesis of triple A syndrome.

Astonishingly in co-IP with lysates of GFP-ALADIN-expressing NCI-H295R cells followed by mass spectrometry, a huge part of those proteins being identified were proteins of mitochondrial destination or origin. In addition, two specific heterogeneous nuclear ribonucleoproteins, HNRNPA1 and U, precipitated with ALADIN. These chaperone proteins are responsible for precursor (pre-) mRNA processing, metabolism and mature mRNA nuclear export.

The small nuclear GTPase Ran was also detected in co-IP with lysates of GFP-ALADIN-expressing cells. Ran cycling between bound GTP in the nucleus and GDP in the cytoplasm adjusts import and export between nucleus and cytosol. Ran-GTP carries a specific cargo containing a nuclear export signal bound to a receptor (e.g. mRNA coated with a myriad of proteins forming the messenger ribonucleoprotein (mRNP) particle) and is transferred through the NPC to the cytosol. Ran-GDP releases its cargo on the cytoplasmic site of the NPC and GTP is hydrolysed to GDP by a Ran-GTP-activating protein (Figure 31). Some pathways for RNA export through NPCs are described in the following. Many of those pathways use Ran cycling as the shuttle mechanism (Cole and Scarcelli, 2006; Katahira, 2015; Okamura et al., 2015).

Pre-mRNA undergoes splicing, 5'-capping and cleavage/polyadenylation at the 3'-end before being exported as mature mRNA from the nucleus. Association with factors involved in nuclear export is conducted during transcription and pre-mRNA processing, ultimately forming the mRNP particle. Functional and mature mRNA is then encountered by the transcription machinery in the cytoplasm (Katahira, 2015). Small non-coding RNAs (transfer RNA and micro RNA) are exported from the nucleus by proteins of the importin/karyopherin-β family comprising the prototypical transport receptors. This mechanism uses Ran cycling (Cole and Scarcelli, 2006; Katahira, 2015).

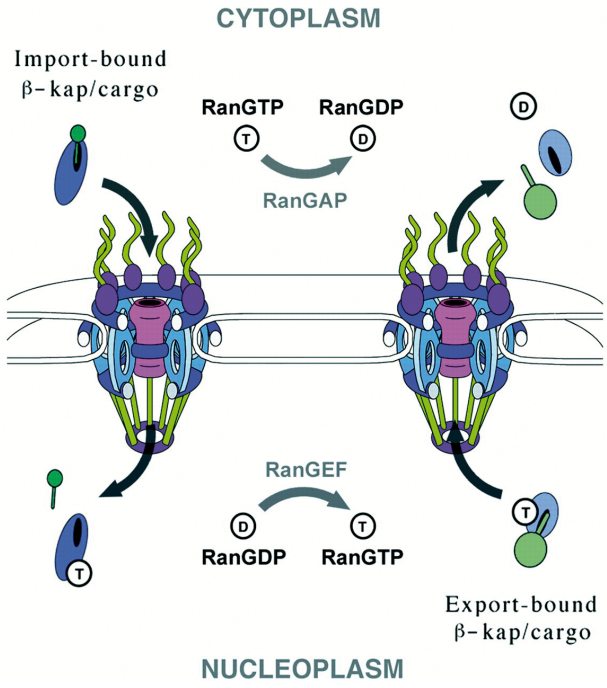

Figure 31 – The Ran cycle.
Depending on its subcellular localisation Ran cycles between GTP- and GDP-bound states. During import (left) karyopherins (importins) in the cytoplasm bind to cargoes containing a nuclear localisation signal and are transferred through nuclear pore complexes to the nucleus. Ran-GTP binds to importins and releases the cargo. The Ran-GTP-importin complex is then recycled to the cytoplasm where it is disrupted after GTP hydrolysis by a Ran-GTP-activating protein. During export (right) nuclear Ran-GTP stabilised by RanGEF binds a cargo containing a nuclear export signal bound to exportins and is translocated through the nuclear pore complex to the cytosol. Ran-GDP releases its cargo on the cytoplasmic site and GTP is hydrolysed to GDP. D, Ran-GDP. T, Ran-GTP. β-kap, importin/karyopherin-β. RanGEF, Ran guanine exchange factor (Rout and Aitchison, 2001).

Nuclear export of mRNA does not comprise importin/karyopherin-β proteins but rather an evolutionarily conserved heterodimeric transport receptor Tap-p15. In order to bind and to direct to different mRNAs the conserved transcription-export complex and several serine-arginine rich proteins associate with the transport receptor. Tap-p15 bound to its mRNA-cargo makes contact with FG-repeats of distinct NUPs and upon escape to the cytoplasm dissociates from its cargo in order to avoid re-entering of the mRNA into the nucleus (Cole and Scarcelli, 2006; Katahira, 2015). This pathway does not directly depend on Ran cycle, but p15 is shown to bind Ran-GTP and is thought to assist export of other RNA and proteins (Black et al., 1999). Transport receptor Tap-p15 co-ordinates bulk mRNA export but certain groups of mRNAs are exported via Crm1.

Crm1 belongs to the importin/karyopherin-β family and depends on adaptor proteins being able to bind RNA. Export of nuclear RNA mediated by Crm1 involves Ran cycle (Okamura et al., 2015). NUPs of the cytoplasmic filaments rich in FG-repeats are thought to be essentially involved in mRNA export in yeast. In metazoa these NUPs are shown to have the same location and are essentially thought to have the same function (NUP214, NUP88 and NUP358) (Fahrenkrog, 2014; Cole and Scarcelli, 2006). Ran cycle is an essential player of RNA export from the nucleus and is involved in a myriad of export mechanisms. In the GFP-ALADIN overexpression model Ran, importin-5 and heterogeneous nuclear ribonucleoprotein A1 and U were shown to co-precipitate with ALADIN. This highlights the assumption that ALADIN is involved in the export of especially mRNA.

Based on the fact that ALADIN seems to be involved in the export of mature mRNA from the nucleus the finding of mitochondrial precursors like COX7A and succinate dehydrogenase precursor in co-IP with lysates of GFP-ALADIN-expressing cells raises the question of cytoplasmic transport from the nucleus to the mitochondria of nuclear-encoded mRNA. There is evidence in lower eukaryotes like *Saccharomyces cerevisiae* that nuclear-encoded mitochondrial products are passed to the organelle either in form of nascent polypeptide-associated complexes (NACs) or as RNP particles which are thought to be co-translationally transported. The first group is synthesised in the cytoplasm prior mitochondrial import through TOM-translocase of the inner mitochondrial membrane (TIM23) pathway. Mitochondrial precursor proteins are equipped with a N-terminal mitochondrial targeting sequence rich in positively charged residues interacting with the TOM-TIM23 pore carrying many negatively charged amino acids (Tarassov et al., 2007; Ding et al., 2009).

Regarding the co-translational transport of mitochondrial products most studies in yeast revealed that the mRNA is transported within the cytoplasm to the mitochondrial surface either by passive diffusion or active transport occupied by the micro cytoskeleton or translocation associated within the ER in a signal recognition particle (SRP)-dependent manner (Figure 32) (Ding et al., 2009). SRP is a RNP complex binding early in the translation process and targeting the mRNA-ribosome-nascent polypeptide chain to the ER. Recognition is achieved by topogenic hydrophobic signals in the peptide precursor chain. A receptor associated with the ER membrane, the SRP receptor, mediates targeting of the complex and induces binding of the ribosome to the translocation channel (Sec61 complex). After docking of the complex to the translocation channel the protein is secreted across or into the ER membrane (Figure 33) (Reid and Nicchitta, 2015).

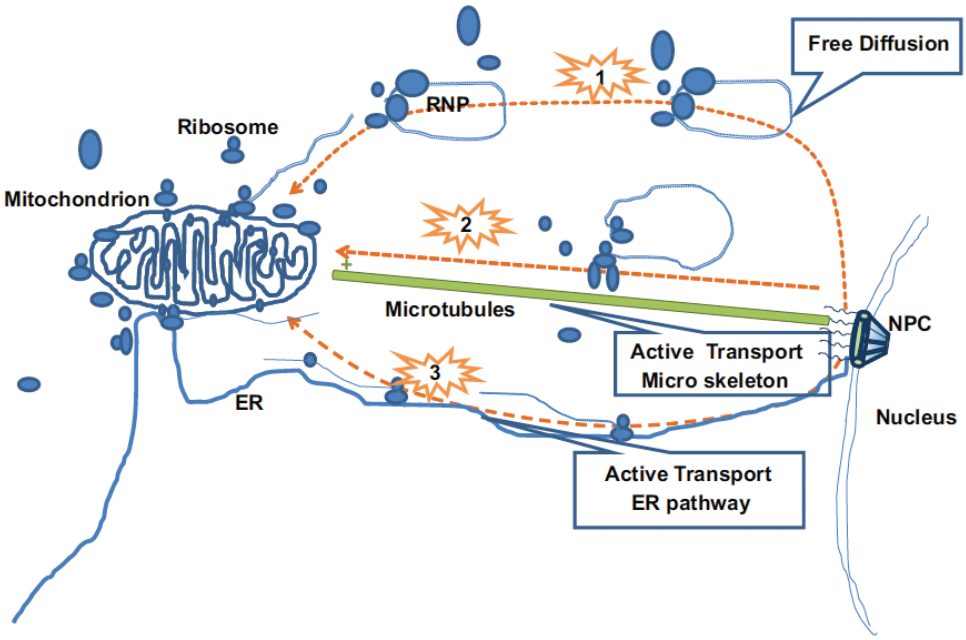

Figure 32 – Transport of nuclear-encoded mitochondrial mRNA in the cytoplasm.
The three different pathways are numbered. Nuclear-encoded mitochondrial mRNA exported through the nuclear pore complex (NPC) is thought to be either transported by (1) free diffusion of ribonucleoprotein (RNP) particles to the mitochondrial surface, (2) molecular motors on the cytoskeleton (microtubules) or (3) active transport along the endoplasmic reticulum (ER) (Ding et al., 2009).

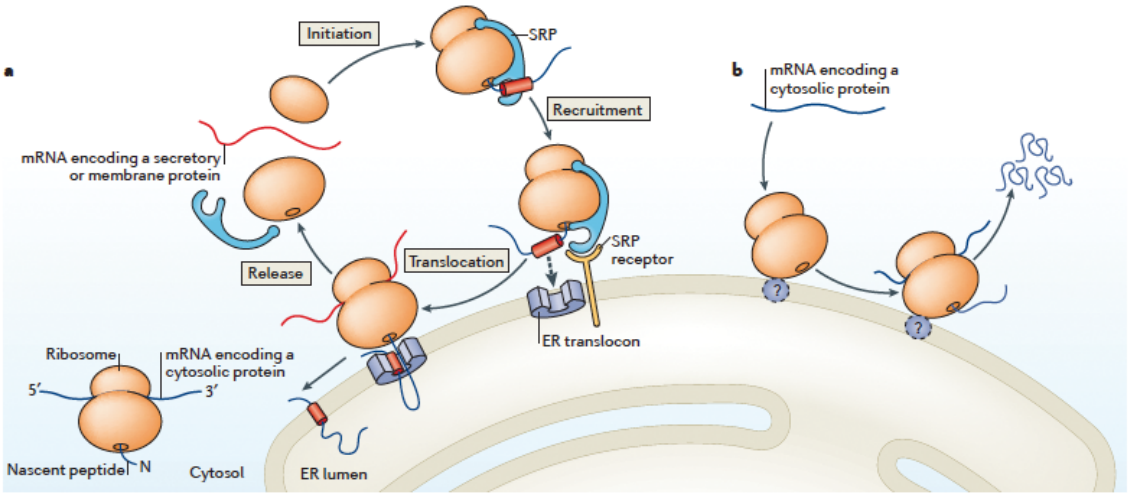

Figure 33 – The model for translational compartmentalisation.

Cytosolic proteins which lack a topogenic signal at their N-terminus targeting them to the endoplasmic reticulum (ER) are translated in the cytosol. Proteins encoded by mRNAs containing a signal peptide or a transmembrane domain at their N-terminus (secretory or integral membrane proteins) are co-translationally targeted to the ER by the signal recognition particle (SRP) pathway and SRP receptor in the ER membrane (Reid and Nicchitta, 2015, modified).

Fifty percent of mRNA encoding mitochondrial proteins are translated in the proximity of mitochondria. Such mRNA is called mitochondrially localised mRNA (MLR). Those MLRs are as well thought to be translocated via TOM-TIM23 pathway (Tarassov et al., 2007; Ding et al., 2009). With MLR calculations in yeast using bioinformatics mRNAs targeted for mitochondria have been divided into different groups: MLR class I localises to mitochondria (I-1 strictly and I-2 partly dependent on the translation regulatory protein Puf3p), class II localises to mitochondria (Puf3p independent) and class III does not localise to mitochondria (Figure 34).

MLR class	Number of genes	Typical gene	Class characteristics	
Class I-1	83	*COX17*	mRNA mitochondrial localization strictly dependent upon Puf3p and highly sensitive to cycloheximide	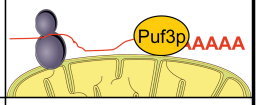
Class I-2	173	*TOM20*	mRNA mitochondrial localization only partially dependent upon Puf3p and weakly sensitive to cycloheximide	
Class II	224	*ATP2*	mRNA mitochondrial localization Puf3p independent and weakly sensitive to cycloheximide	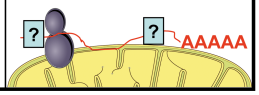

Figure 34 – Sub-classification of mitochondrially localised mRNA according to their Puf3p dependence in yeast.

Mitochondrially localised mRNAs (MLRs) are distinguished in two main classes, class I and class II, by the presence or absence of at least one pumilio family 3 (PUF3) motif in the mRNA 3'-UTR, respectively. Class I-1 is thought to depend solely on Puf3p for their mitochondrial localisation and is highly sensitive for cycloheximide which is believed to solidify mRNA-ribosome complexes. Class I-2 seems to depend also on other transacting factors besides Puf3p (here symbolised as question mark) (Saint-Georges et al., 2008).

Puf3p belongs to the Pumilio family (PUF) and it is shown to bind as a trans-acting factor to a consensus motif in 3'-UTR of mRNA encoding mitochondrial yeast products. Puf3p is a mitochondrial RNA-binding protein at the cytosolic face of the outer mitochondrial membrane

with multiple functions (Garcia-Rodriguez et al., 2007; Jackson et al., 2004; Gerber et al., 2004). The protein seems to mediate transport and stability of a specific set of nuclear-encoded mitochondrial mRNAs thereby affecting mitochondrial biogenesis (Saint-Georges et al., 2008).

In this study, structural proteins of mitochondrial respiration complex IV COX5A, 5B, 6C and 7A were shown to co-immunoprecipitate with ALADIN in lysates of human adrenocortical cells expressing GFP-ALADIN. These nuclear-encoded mitochondrial proteins are non-MLRs (class III). They are thought to be synthesised on cytosolic free ribosomes and precursor protein import shall most likely occur through TOM-TIM23 pathway.

Additionally, identified components of the CAC among these 2-oxoglutarate dehydrogenase, succinate dehydrogenase (mitochondrial respiration complex II) and malate dehydrogenase are MLR class II, class I-2 and class III, respectively. 2-oxoglutarate and succinate dehydrogenase are translated in the vicinity of mitochondria and mRNA translation is partly dependent on Puf3p in the case of succinate dehydrogenase (Saint-Georges et al., 2008; Perocchi et al., 2006).

The result suggests that ALADIN, probably in an oligomeric protein complex, seems to take part in the transport of nuclear-encoded mitochondrial proteins in either way; as NACs (for all MLR class III) or co-translationally as RNP complex (class II and I). ALADIN is likely to build large multimeric protein complexes due to its several WD repeats (Tullio-Pelet et al., 2000; Rabut et al., 2004). Remarkably, precursor proteins of two identified proteins were found in mass spectrometry analysis (COX7A and succinate dehydrogenase precursor); underlying the suggestion that ALADIN takes part in the translocation of mitochondrial precursors. More evidence that ALADIN is involved in the transport of nuclear-encoded mitochondrial proteins is raised by the fact that several subunits of the mitochondrial TOM complex (TOM40, TOM22 and TOM70) and the ER membrane-associated TRAP subunit α (SSR1) were found after GFP-ALADIN co-IP and mass spectrometry.

These findings emphasise the hypothesis that transport of nuclear-encoded mitochondrial proteins may specifically involve ALADIN. NACs synthesised in the cytosol and RNP complexes transported through the translocon channel are imported into the mitochondria through the TOM complex (Tarassov et al., 2007; Ding et al., 2009). Furthermore, the glycolytic enzyme enolase-2 was shown to be a chaperone to facilitate tRNA import into mitochondria (Brandina et al., 2006; Entelis et al., 2006). Enolase-1 co-precipitated with ALADIN in the GFP-ALADIN expression model. This enzyme has not yet been shown to be involved in cytoplasmic RNA transport to mitochondria, but it localises to the organelle in rat cardiomyocytes which suggests a possible interaction (Gao et al., 2014).

In co-IP of endogenous ALADIN proteins of mitochondrial destination or origin could not be verified to be simultaneously detected in both ALADIN expression models. The fusion protein in the GFP-ALADIN over-expression model in NCI-H295R cells is not only localised to the nuclear pore but also to the cytoplasm (data not shown). False localisation could lead to false positive results or abolish real protein connections when looking for ALADIN-interacting proteins. In order to verify results produced by co-IP with lysates of GFP-ALADIN expressing NCI-H295R cells sepharose beads were coated with an antibody against ALADIN and co-IP with lysates of NCI-H295R cells was conducted.

Since ALADIN is expressed at a very low level in the cell and exclusively at the NPC (eight ALADIN proteins per NPC (Cronshaw et al., 2002)), co-IP of endogenous ALADIN was chal-

lenging. This method was successfully established but in mass spectrometry remarkably less ALADIN was detected compared to the GFP-ALADIN expression model. Thus, not all proteins detected in GFP-ALADIN co-IP could be verified in endogenous co-IP. Detection especially of proteins of mitochondrial destination could have been abolished in the wild-type model since co-IP of ALADIN was not as efficient as in the GFP-ALADIN expression model.

The assumption that GFP-ALADIN co-IP would detect an increased number of false positive proteins could be raised but was tried to ruled out by repetition and reproduction of the experiment. Only those proteins detected in all three co-IPs with lysates of GFP-ALADIN expressing NCI-H295R cells were conducted for further analysis and grouped as a possible positive match to look at. In GFP-ALADIN co-IP SSR1 is identified and SSR1 and SSR4 (TRAP subunit delta) were both detected after co-IP of ALADIN. Both proteins closely associate with the Sec61 translocation channel translocating nascent chains of secretory proteins across the ER membrane into the lumen (Gorlich et al., 1990).

This supports the hypothesis that ALADIN is closely involved in targeting the nuclear exported mRNA-ribosome-nascent polypeptide chain to the ER. If and how ALADIN plays a role in establishing nuclear mRNA targeting to the ER, shall be investigated in future research and may further characterise the perhaps predominant function of ALADIN in cell metabolism.

5.3 ALADIN-dependent alteration in steroidogenesis postulates an interaction with microsomal CYP P450 regulators

In wild-type ALADIN and GFP-ALADIN over-expression co-IP analyses followed by mass spectrometry POR was one of the proteins identified to interact with ALADIN. It seemed reasonable to discover this possible interaction in more detail because it is shown that deprivation of ALADIN leads to impairment of glucocorticoid and androgenic steroidogenesis and of cytochrome P450 oxidoreductase (Jühlen et al., 2015).

Co-IP studies showed that ALADIN precipitated with the microsomal flavoprotein and in co-localisation immunofluorescent studies both proteins appear at the same perinuclear ER. In the GFP-ALADIN over-expression model POR co-precipitated with ALADIN. This result could be shown after mass spectrometry analyses and on Western Blot. In order to verify results produced by GFP-ALADIN co-IP, wild-type ALADIN co-IP was conducted. ALADIN is expressed at very low levels in the cell and exclusively at the NPC (Cronshaw et al., 2002). This made endogenous ALADIN co-IP challenging. The method was successfully established but in mass spectrometry less ALADIN was detected compared to the GFP-ALADIN over-expression model. Nevertheless, POR could be efficiently reproduced as a potential interaction partner of ALADIN. Negative controls for both co-IPs showed low levels of detected peptides exclusively belonging to POR. This result could not be shown on Western Blot level since protein/peptide amounts of POR in the negative control were either too low to be detected by antibody or this result was unspecifically identified by mass spectrometry analyses.

All microsomal P450s need POR for their catalytic activity. The steroid output can be diminished even if the specific CYP P450 enzyme activity is unchanged (Fluck and Pandey, 2011). This was shown in ALADIN-deficient cells where the steroid output and gene expression of microsomal CYP17A1 and CYP21A2 hydroxylases was decreased accompanied by minimised

POR gene expression (Jühlen et al., 2015). Interestingly, CYP21A2 hydroxylase was also detected in mass spectrometry to co-precipitate with ALADIN after co-IP of endogenous ALADIN (data not shown). This underlines the fact that POR might be a possible target for ALADIN-dependent alteration in adrenal steroidogenesis.

CYP P450s are heme-containing enzymes metabolising endogenous compounds or xenobiotics. These enzymes are mainly localised to the membrane of the ER or at lower levels to the inner mitochondrial membrane. Nevertheless, they have also been identified in other sub-cellular compartments: at the outer nuclear membrane, in GOLGI subunits, at the plasma membrane or in peroxisomes. Anchorage of CYP P450s to membranes is achieved by a hydrophobic tail at the N-terminus; thereby exposing the catalytic domain and the rest of the enzyme to the cytoplasm or the mitochondrial matrix.

Transcription of CYP P450 mRNAs is SRP-dependent and translation occurs on membrane-free ribosomes with hydrophobic N-terminus acting as topogenic signal (Figure 33). Translation is stopped by binding of the SRP and only resumed when the complex consisting of SRP, ribosome and nascent protein chain is bound to the SRP receptor anchored in the ER membrane. Upon binding of the complex SRP is released and the growing polypeptide chain of the CYP P450 enzyme is transferred through the Sec61 translocon complex into the ER. Translocation of the polypeptide is immediately stopped when the N-terminus meets the translocation channel. The remainder of the protein is in the following translated on the cytoplasmic site of the ER membrane (Neve and Ingelman-Sundberg, 2008; Seliskar and Rozman, 2007).

The hydrophobic N-terminus of CYP P450s leading SRP-dependent translation of the protein has also been shown to be sufficient for ER retention mechanisms of the mature protein. In addition, large immobile oligomeric complexes built of, for example POR and $CYPb_5$, were also thought to be excluded from ER exit sites and consequently, lead to retention of the proteins in the ER. Beside these hypotheses other possible mechanism exist resulting in retention in the ER but the exact mechanism of restrict ER localisation of many CYP P450s remains to be identified (Neve and Ingelman-Sundberg, 2008; Seliskar and Rozman, 2007).

Non-genomic, membrane-associated progesterone receptors (MAPRs) are also restricted to the ER and are thought to regulate the activity of CYP P450 enzymes. The first identified MAPR, PGRMC1, gained wide-spread attention (Falkenstein et al., 1996). PGRMC1 is a cytochrome-related protein with several implications in cancer. In my work, PGRMC2 was shown to interact with ALADIN in GFP-ALADIN co-IP studies and in co-IP of endogenous ALADIN followed by application of mass spectrometry. The protein is mainly localised to the ER membrane, is the second member of the MAPR family and barely investigated compared to its homologue brother PGRMC1.

There is evidence that both MAPRs probably have emerged from a common gene (Wendler and Wehling, 2013; Keator et al., 2012). *PGRMC1* lies on the X-chromosome whereas the gene for PGRMC2 resides on chromosome 4. Their protein structure is made up of a N-terminal extracellular domain followed by a transmembrane region and a cytoplasmic domain. Despite their close relation, there are differences in protein expression and function. Both proteins are involved in regulation of ovarian follicle development and therefore imply a neuroendocrine function (Wendler and Wehling, 2013; Keator et al., 2012). Deficiency of either MAPRs decreases the anti-apoptotic and/or anti-mitotic action of progesterone, although PGRMC2 seems to be

important for anti-mitotic actions of the steroid. Furthermore, MAPRs exert some progesterone-independent actions (Peluso et al., 2014). Depletion of either PGRMC1 or PGRMC2 leads to increased entry into cell cycle. Both proteins localise to the mitotic spindle and seem to exploit a distinct role during metaphase of mitosis by binding to each other, thereby suppressing entry into cell cycle. This effect is thought to be synergistic and does not seem to be additive (Peluso et al., 2014).

PGRMC2 is proven to act on mitosis and is recently shown by Griffin and co-workers to interact with the cyclin-dependent kinase 11b (p58), a kinase regulating G0 to G1 transition in mitosis. Interestingly, the expression of the MAPR was seen to be cell cycle-dependent with reduced expression between G0 and G1. This event could facilitate entry into cell cycle by releasing PGRMC2 inhibition (Griffin et al., 2014).

It is additionally known that PGRMC2 alters activity of CYP3A4 as possible electron donor, and binds CYP21A2, most likely through its $CYPb_5$-similar heme-binding domain (Wendler and Wehling, 2013; Albrecht et al., 2012). Up to now PGRMC2 shall await more investigations besides its role as tumour suppressor, migration inhibitor and of note, activity regulator of CYP P450 enzymes (Wendler and Wehling, 2013). ALADIN possibly interacts with the nuclear small GTPase Ran. This enzyme is investigated not only to be involved in nucleo-cytoplasmic transport but also exhibits a distinct role during mitosis (Clarke and Zhang, 2008). Cell-cycle control can be postulated to be one common pathway of PGRMC2 and ALADIN. Further research is warranted to elucidate the involvement of ALADIN in mitosis and meiosis.

5.4 Conclusion

Increased sensitivity to oxidative stress, especially in the adrenal, is a significant hallmark of the pathogenesis of triple A syndrome. In co-IP using an ALADIN over-expression model in the human adrenocortical cell line NCI-H295R complexes of the mitochondrial respiration chain (IV and II) and of the CAC were found. But ALADIN presumably does not localise to mitochondria as shown for the cytoplasmic filament RANBP2/NUP358 thereby acting on mitochondrial energy homeostasis (Aslanukov et al., 2006; Cho et al., 2007).

This implies that ALADIN co-ordinates the shuttle of nuclear-encoded mitochondrial proteins exiting the nucleus through the NPC. Support of this hypothesis is provided in this work; not only in the second division but also evidenced as secondary effects in the first part of the results, seen as increased sensitivity to oxidative stress in adrenocortical carcinoma cells (Jühlen et al., 2015). Attenuation of aerobic mitochondrial respiration through a deficient mRNA transport pathway of either components of the respiration chain or of the CAC, that feeds to a great part in mitochondrial respiration by donating $NADH$, ultimately leads to increased levels of oxidative stress as seen in triple A patient fibroblasts and adrenocortical cells *in vitro* (Kind et al., 2010; Prasad et al., 2013; Jühlen et al., 2015; Storr et al., 2009; Hirano et al., 2006).

Importantly, vacuolar acidification has also been coupled to mitochondrial respiration chain by Perocchi and co-workers but the mechanism remains to be determined (Perocchi et al., 2006). Vacuolar-type proton ATPase, an enzyme involved in vacuolar acidification by using ATP and pumping protons in intracellular compartments, seems to be connected to ALADIN as different subunits of this multi-complex enzyme co-precipitated with the nucleoporin in this work. These findings on the exclusive task of ALADIN for the translocation of nuclear-encoded mitochondrial precursors gives important insights in the distinct role of the nucleoporin and deserves a huge degree of future investigations.

In the future it needs to be investigated how ALADIN affects the expression of *POR* and why the nucleoporin co-localises with the microsomal flavoprotein at the perinuclear ER. Conclusively, the answer on this question can elucidate a significant role of ALADIN but merits more research. SRP-dependent translation of nuclear-encoded mitochondrial precursors and of microsomal-residing CYP P450s, is crucial for both protein processing and translocation.

Given the relationship between ALADIN and PGRMC2, POR is not the only microsomal CYP P450 enzyme possibly interacting with ALADIN. There is first evidence that PGRMC2 is cytochrome-related and, like POR, acts as electron donor for specific CYP P450 (Wendler and Wehling, 2013; Albrecht et al., 2012). As an integral ER membrane protein, PGRMC2 presumably also depends on translation involving SRP. The mechanism of SRP-dependent targeting to the ER could be a hallmark of the involvement of ALADIN. Given the relationship among ALADIN and SRP-dependent translation this mechanism would justify and explain glucocorticoid insufficiency and mitochondrial dysfunction seen after ALADIN deprivation.

6 Summary

Autosomal recessive triple A syndrome is caused by mutations in the *AAAS* gene encoding the protein ALADIN. The disorder manifests with the triad of adrenocorticotropic hormone-resistant adrenal insufficiency, achalasia of the stomach cardia and impaired tear production (alacrima) in combination with progressive neurological impairment of the central, peripheral and autonomic nervous systems. ALADIN is part of the nuclear pore complex acting as a scaffold nucleoporin. In this work the role of ALADIN in the human adrenocortical tumour cell line NCI-H295R1 was investigated. These cells were engineered to either over-express or down-regulate *AAAS* by inducible stable transfection. Alterations in steroidogenic gene expression and functional consequences were determined. In addition, the role of ALADIN on cell viability and oxidative stress response was analysed. Using both the human adrenal NCI-H295R1-TR *AAAS* knock-down and over-expression models the potential impairment of the nuclear import of aprataxin, DNA ligase 1 and ferritin heavy chain 1 was investigated. For this YFP-specific vectors transiently transfected into the cell lines were employed.

The findings indicate that *AAAS* knock-down induces a down-regulation of genes coding for type II microsomal cytochrome P450 hydroxylases CYP17A1 and CYP21A2 and their electron donor enzyme cytochrome P450 oxidoreductase, thereby decreasing biosynthesis of precursor metabolites required for glucocorticoid and androgen production. Furthermore I demonstrate that ALADIN deficiency leads to increased susceptibility to oxidative stress and alteration in redox homeostasis after paraquat treatment. Finally, I show significantly impaired nuclear import of DNA ligase 1, aprataxin and ferritin heavy chain 1 in ALADIN knock-down cells. I conclude that down-regulating ALADIN results in decreased oxidative stress response leading to alteration in steroidogenesis, highlighting the knock-down cell model as an important *in vitro* tool for studying the adrenal phenotype in triple A syndrome.

In an approach to identify new interaction partners of ALADIN, co-immunoprecipitation followed by proteome analyses using mass spectrometry was conducted in a GFP-ALADIN over-expression model using the human adrenocortical tumor cell line NCI-H295R. These results were verified in co-immunoprecipitation assays of endogenous ALADIN using NCI-H295R wild-type cells. The results suggest a possible interaction between ALADIN and microsomal flavoprotein cytochrome P450 oxidoreductase and progesterone receptor membrane compartment 2. Co-localisation analyses of these findings were done using immunofluorescence. The data are suggestive for an involvement of ALADIN in the export of nuclear-encoded mitochondrial proteins.

Regulation of adrenocortical steroidogenesis is complex and there is increasing evidence that oxidative stress due to ROS accumulation and mitochondria are significantly involved. Furthermore, there may be an important cross-talk between functional organelles comprising nucleus, ER and mitochondria which presumably involves lipid metabolism. The goal of this work was to elucidate the function of ALADIN for the cellular oxidative stress response and its possible consequences for adrenocortical steroidogenesis in triple A syndrome patients.

7 Zusammenfassung

Mutationen im *AAAS* Gen verursachen die autosomal rezessive Krankheit Triple-A-Syndrom. *AAAS* kodiert das Nukleoporin ALADIN, welches Bestandteil des nukleären Porenkomplexes ist. Phänotypische Charakteristika des Triple-A-Syndroms sind Nebennierenrinden-Insuffizienz, Achalasie des unteren Speiseröhrenschließmuskels und eine fehlende Tränenproduktion (Alakrimie). Diese Symptome sind kombiniert mit progredienten neurologischen Störungen des zentralen, peripheren und autonomen Nervensystems. In dieser Arbeit wurde die Rolle von ALADIN in der humanen Karzinom-Zelllinie NCI-H295R1 untersucht. Diese Nebennierenrinden-Zellen wurden stabil transfiziert und mit einem induzierbaren Expressionssystem modifiziert, so dass sie *AAAS* entweder überexprimierten oder herunterregulierten. In NCI-H295R1-Zellen wurden Veränderungen der Genexpression von Enzymen der Steroidogenese und funktionelle Konsequenzen der Überexpression oder Herunterregulation von ALADIN gemessen. Des Weiteren wurde die Rolle von ALADIN auf die Zellviabilität und die Redox-Homöostase analysiert. ALADIN überexprimierende und herunterregulierte Zellen wurden verwendet, um die potentielle Behinderung des nukleären Imports von Proteinen zu untersuchen, welche den Zellkern gegen oxidativen Stress schützen (z.B. Aprataxin, DNA-Ligase 1 und Ferritin Heavy Chain 1). Dazu wurden YFP-spezifische Vektoren transient in diese Zellen gebracht.

Mit den Ergebnissen dieser Arbeit wurde gezeigt, dass die Herunterregulation von *AAAS* eine Verminderung der Genexpression von CYP17A1 und CYP21A2 und deren Elektronendonor Cytochrom P450 Oxidoreduktase bewirken. Die Biosynthese der Vorläufermetabolite von Kortisol und Aldosteron ist in diesen Zellen ebenfalls vermindert. Des Weiteren zeigen die ALADIN-defizienten NCI-H295R1-Zellen eine erhöhte Sensitivität gegenüber oxidativem Stress und eine veränderte Redox-Homöostase nach der Behandlung mit Paraquat. Darüber hinaus konnte in dieser Studie auch gezeigt werden, dass herunterregulierte ALADIN NCI-H295R1-Zellen einen verminderten Zellkernimport von Aprataxin, DNA-Ligase 1 und Ferritin heavy chain 1 besitzen. Aus diesen Ergebnissen kann geschlussfolgert werden, dass ALADIN-defiziente Nebennierenzellen eine verminderte Stressantwort auf oxidativen Stress besitzen; dies führt schlussendlich zu einer veränderten Steroidogenese. Das beschriebene ALADIN knock-down Modell in NCI-H295R1-Zellen ist ein wichtiges *in vitro* Werkzeug, um die Pathogenese der Nebennierenveränderungen im Triple-A-Syndrom zu erforschen.

Neue Interaktionspartner von ALADIN wurden mit Hilfe von Co-Immunpräzipitation gefolgt von Proteom-Analysen durch Massenspektrometrie in einem GFP-ALADIN Überexpressionsmodell in NCI-H295R charakterisiert. Die Ergebnisse wurden durch Experimente auf endogenem Niveau in NCI-H295R-Wildtypzellen verifiziert. Mit diesen Daten wird in dieser Arbeit erstmals eine Interaktion zwischen ALADIN und dem Flavoprotein Cytochrom P450 Oxidoreduktase und Progesterone Receptor Membrane Compartment 2 nachgewiesen. Diese Ergebnisse wurden mit Co-Lokalisierungsanalysen durch Immunfluoreszenzfärbung von ALADIN und Cytochrome P450 Oxidoreduktase ergänzt. Außerdem gibt die Arbeit Hinweise darauf, dass ALADIN als Nukleoporin an dem nuklearen Export mitochondrialer Vorläuferproteine beteiligt ist.

Die Regulation der Steroidogenese in der Nebennierenrinde ist komplex und es existieren zahlreiche Hinweise darauf, dass oxidativer Stress aufgrund der Ansammlung reaktiver

Sauerstoffradikale und. dass die Mitochondrien involviert sind. Außerdem ist ein funktionelles Zusammenspiel verschiedener Organellen, darunter Nukleus, ER und Mitochondrien, von großer Bedeutung. Das Ziel dieser Arbeit war die Identifizierung der Funktion von ALADIN in der zellulären oxidativen Stressantwort und die möglichen Konsequenzen für die Steroidogenese in der Nebennierenrinden in Triple-A-Syndrom-Patienten.

Anlage 1

Technische Universität Dresden
Medizinische Fakultät Carl Gustav Carus
Promotionsordnung vom 24. Juli 2011

Erklärungen zur Eröffnung des Promotionsverfahrens

1. Hiermit versichere ich, dass ich die vorliegende Arbeit ohne unzulässige Hilfe Dritter und ohne Benutzung anderer als der angegebenen Hilfsmittel angefertigt habe; die aus fremden Quellen direkt oder indirekt übernommenen Gedanken sind als solche kenntlich gemacht.

2. Bei der Auswahl und Auswertung des Materials sowie bei der Herstellung des Manuskripts habe ich Unterstützungsleistungen von folgenden Personen erhalten:

   Prof. Dr. med. Angela Hübner

   Dr. rer. nat. Katrin Köhler

   Dr. Angela E. Taylor

   PhD Anna Shevchenko

3. Weitere Personen waren an der geistigen Herstellung der vorliegenden Arbeit nicht beteiligt. Insbesondere habe ich nicht die Hilfe eines kommerziellen Promotionsberaters in Anspruch genommen. Dritte haben von mir weder unmittelbar noch mittelbar geldwerte Leistungen für Arbeiten erhalten, die im Zusammenhang mit dem Inhalt der vorgelegten Dissertation stehen.

4. Die Arbeit wurde bisher weder im Inland noch im Ausland in gleicher oder ähnlicher Form einer anderen Prüfungsbehörde vorgelegt.

5. Die Inhalte dieser Dissertation wurden in folgender Form veröffentlicht:

   Jühlen R, Idkowiak J, Taylor AE, Kind B, Arlt W, Huebner A, Koehler K. 2015. Role of ALADIN in human adrenocortical cells for oxidative stress response and steroidogenesis. PLoS One 10:e0124582.

6. Ich bestätige, dass es keine zurückliegenden erfolglosen Promotionsverfahren gab.

7. Ich bestätige, dass ich die Promotionsordnung der Medizinischen Fakultät der Technischen Universität Dresden anerkenne.

8. Ich habe die Zitierrichtlinien für Dissertationen an der Medizinischen Fakultät der Technischen Universität Dresden zur Kenntnis genommen und befolgt.

Dresden, 28.07.2015

Unterschrift des Doktoranden
Formblatt 1.2.1, Seite 1-1, erstellt 18.10.2013

Anlage 2

Hiermit bestätige ich die Einhaltung der folgenden aktuellen gesetzlichen Vorgaben im Rahmen meiner Dissertation

☐ das zustimmende Votum der Ethikkommission bei Klinischen Studien, epidemiologischen Untersuchungen mit Personenbezug oder Sachverhalten, die das Medizinproduktegesetz betreffen
Aktenzeichen der zuständigen Ethikkommission

☐ die Einhaltung der Bestimmungen des Tierschutzgesetzes
Aktenzeichen der Genehmigungsbehörde zum Vorhaben/zur Mitwirkung

☒ die Einhaltung des Gentechnikgesetzes
Projektnummer AZ56-8811.72/40

☒ die Einhaltung von Datenschutzbestimmungen der Medizinischen Fakultät und des Universitätsklinikums Carl Gustav Carus.

Dresden, 28.07.2015

Unterschrift des Doktoranden

References

Ahel I, Rass U, El-Khamisy SF, Katyal S, Clements PM, McKinnon PJ, Caldecott KW, West SC. 2006. The neurodegenerative disease protein aprataxin resolves abortive DNA ligation intermediates. Nature 443:713-716.

Alber F, Dokudovskaya S, Veenhoff LM, Zhang W, Kipper J, Devos D, Suprapto A, Karni-Schmidt O, Williams R, Chait BT, Sali A, Rout MP. 2007. The molecular architecture of the nuclear pore complex. Nature 450:695-701.

Albrecht C, Huck V, Wehling M, Wendler A. 2012. In vitro inhibition of SKOV-3 cell migration as a distinctive feature of progesterone receptor membrane component type 2 versus type 1. Steroids 77:1543-1550.

Alesci S, Ramsey WJ, Bornstein SR, Chrousos GP, Hornsby PJ, Benvenga S, Trimarchi F, Ehrhart-Bornstein M. 2002. Adenoviral vectors can impair adrenocortical steroidogenesis: Clinical implications for natural infections and gene therapy. Proc Natl Acad Sci U S A 99:7484-7489.

Alkhateeb AA, Connor JR. 2010. Nuclear ferritin: A new role for ferritin in cell biology. Biochim Biophys Acta 1800:793-797.

Allgrove J, Clayden GS, Grant DB, Macaulay JC. 1978. Familial glucocorticoid deficiency with achalasia of the cardia and deficient tear production. Lancet 1:1284-1286.

Arlt W, Walker EA, Draper N, Ivison HE, Ride JP, Hammer F, Chalder SM, Borucka-Mankiewicz M, Hauffa BP, Malunowicz EM, Stewart PM, Shackleton CH. 2004. Congenital adrenal hyperplasia caused by mutant P450 oxidoreductase and human androgen synthesis: Analytical study. Lancet 363:2128-2135.

Aslanukov A, Bhowmick R, Guruju M, Oswald J, Raz D, Bush RA, Sieving PA, Lu X, Bock CB, Ferreira PA. 2006. RanBP2 modulates Cox11 and hexokinase I activities and haploinsufficiency of RanBP2 causes deficits in glucose metabolism. PLoS Genet 2:e177.

Australian Proteome Analysis Facility Ltd. 2015. [last updated: 04.06.2015, last reviewed: 01.04.2015] URL: www.proteome.or.au.

Axelrod J, Reisine TD. 1984. Stress hormones: Their interaction and regulation. Science 224:452-459.

Basel-Vanagaite L, Muncher L, Straussberg R, Pasmanik-Chor M, Yahav M, Rainshtein L, Walsh CA, Magal N, Taub E, Drasinover V, Shalev H, Attia R, Rechavi G, Simon AJ, Shohat M. 2006. Mutated nup62 causes autosomal recessive infantile bilateral striatal necrosis. Ann Neurol 60:214-222.

Beck M, Forster F, Ecke M, Plitzko JM, Melchior F, Gerisch G, Baumeister W, Medalia O. 2004. Nuclear pore complex structure and dynamics revealed by cryoelectron tomography. Science 306:1387-1390.

Beck M, Lucic V, Forster F, Baumeister W, Medalia O. 2007. Snapshots of nuclear pore complexes in action captured by cryo-electron tomography. Nature 449:611-615.

Becker T, Bottinger L, Pfanner N. 2012. Mitochondrial protein import: From transport pathways to an integrated network. Trends Biochem Sci 37:85-91.

Bernstein E, Caudy AA, Hammond SM, Hannon GJ. 2001. Role for a bidentate ribonuclease in the initiation step of RNA interference. Nature 409:363-366.

Black BE, Levesque L, Holaska JM, Wood TC, Paschal BM. 1999. Identification of an NTF2-related factor that binds ran-GTP and regulates nuclear protein export. Mol Cell Biol 19:8616-8624.

Brandina I, Graham J, Lemaitre-Guillier C, Entelis N, Krasheninnikov I, Sweetlove L, Tarassov I, Martin RP. 2006. Enolase takes part in a macromolecular complex associated to mitochondria in yeast. Biochim Biophys Acta 1757:1217-1228.

Bui KH, von Appen A, DiGuilio AL, Ori A, Sparks L, Mackmull MT, Bock T, Hagen W, Andres-Pons A, Glavy JS, Beck M. 2013. Integrated structural analysis of the human nuclear pore complex scaffold. Cell 155:1233-1243.

Bureik M, Lisurek M, Bernhardt R. 2002. The human steroid hydroxylases CYP1B1 and CYP11B2. Biol Chem 383:1537-1551.

Bustin SA. 2010. Why the need for qPCR publication guidelines?–the case for MIQE. Methods 50:217-226.

Bustin SA, Benes V, Garson J, Hellemans J, Huggett J, Kubista M, Mueller R, Nolan T, Pfaffl MW, Shipley G, Wittwer CT, Schjerling P, Day PJ, Abreu M, Aguado B, Beaulieu JF, Beckers A, Bogaert S, Browne JA, Carrasco-Ramiro F, Ceelen L, Ciborowski K, Cornillie P, Coulon S, Cuypers A, De Brouwer S, De Ceuninck L, De Craene J, De Naeyer H, De Spiegelaere W, Deckers K, Dheedene A, Durinck K, Ferreira-Teixeira M, Fieuw A, Gallup JM, Gonzalo-Flores S, Goossens K, Heindryckx F, Herring E, Hoenicka H, Icardi L, Jaggi R, Javad F, Karampelias M, Kibenge F, Kibenge M, Kumps C, Lambertz I, Lammens T, Markey A, Messiaen P, Mets E, Morais S, Mudarra-Rubio A, Nakiwala J, Nelis H, Olsvik PA, Perez-Novo C, Plusquin M, Remans T, Rihani A, Rodrigues-Santos P, Rondou P, Sanders R, Schmidt-Bleek K, Skovgaard K, Smeets K, Tabera L, Toegel S, Van Acker T, Van den Broeck W, Van der Meulen J, Van Gele M, Van Peer G, Van Poucke M, Van Roy N, Vergult S, Wauman J, Tshuikina-Wiklander M, Willems E, Zaccara S, Zeka F, Vandesompele J. 2013. The need for transparency and good practices in the qPCR literature. Nat Methods 10:1063-1067.

Bustin SA, Benes V, Garson JA, Hellemans J, Huggett J, Kubista M, Mueller R, Nolan T, Pfaffl MW, Shipley GL, Vandesompele J, Wittwer CT. 2009. The MIQE guidelines: Minimum information for publication of quantitative real-time PCR experiments. Clin Chem 55:611-622.

Cai C, Ching A, Lagace C, Linsenmayer T. 2008. Nuclear ferritin-mediated protection of corneal epithelial cells from oxidative damage to DNA. Dev Dyn 237:2676-2683.

Cai CX, Linsenmayer TF. 2001. Nuclear translocation of ferritin in corneal epithelial cells. J Cell Sci 114:2327-2334.

Capelson M, Doucet C, Hetzer MW. 2010. Nuclear pore complexes: Guardians of the nuclear genome. Cold Spring Harb Symp Quant Biol 75:585-597.

Chacinska A, Koehler CM, Milenkovic D, Lithgow T, Pfanner N. 2009. Importing mitochondrial proteins: Machineries and mechanisms. Cell 138:628-644.

Cho KI, Cai Y, Yi H, Yeh A, Aslanukov A, Ferreira PA. 2007. Association of the kinesin-binding domain of RanBP2 to KIF5B and KIF5C determines mitochondria localization and function. Traffic 8:1722-1735.

Clark AJ, Chan LF, Chung TT, Metherell LA. 2009. The genetics of familial glucocorticoid deficiency. Best Pract Res Clin Endocrinol Metab 23:159-165.

Clark AJ, Weber A. 1998. Adrenocorticotropin insensitivity syndromes. Endocr Rev 19:828-843.

Clarke PR, Zhang C. 2008. Spatial and temporal coordination of mitosis by ran GTPase. Nat Rev Mol Cell Biol 9:464-477.

Cole CN, Scarcelli JJ. 2006. Transport of messenger RNA from the nucleus to the cytoplasm. Curr Opin Cell Biol 18:299-306.

Cronshaw JM, Krutchinsky AN, Zhang W, Chait BT, Matunis MJ. 2002. Proteomic analysis of the mammalian nuclear pore complex. J Cell Biol 158:915-927.

Cronshaw JM, Matunis MJ. 2003. The nuclear pore complex protein ALADIN is mislocalized in triple A syndrome. Proc Natl Acad Sci U S A 100:5823-5827.

D'Angelo MA, Hetzer MW. 2008. Structure, dynamics and function of nuclear pore complexes. Trends Cell Biol 18:456-466.

De Brito OM, Scorrano L. 2008. Mitofusin 2 tethers endoplasmic reticulum to mitochondria. Nature 456:605-610.

Dekant W. 2009. The role of biotransformation and bioactivation in toxicity. In: Lurch A, editor. Molecular, clinical and environmental toxicology, volume 1: Molecular toxicology. Birkhäuser Basel. p 57-86.

Devos D, Dokudovskaya S, Williams R, Alber F, Eswar N, Chait BT, Rout MP, Sali A. 2006. Simple fold composition and modular architecture of the nuclear pore complex. Proc Natl Acad Sci U S A 103:2172-2177.

Ding D, Dave KR, Bhattacharya SK. 2009. On message ribonucleic acids targeting to mitochondria. Biochemistry Insights 2:71-81.

Doghman M, Karpova T, Rodrigues GA, Arhatte M, De Moura J, Cavalli LR, Virolle V, Barbry P, Zambetti GP, Figueiredo BC, Heckert LL, Lalli E. 2007. Increased steroidogenic factor-1 dosage triggers adrenocortical cell proliferation and cancer. Mol Endocrinol 21:2968-2987.

Duarte A, Castillo AF, Podesta EJ, Poderoso C. 2014. Mitochondrial fusion and ERK activity regulate steroidogenic acute regulatory protein localization in mitochondria. PLoS One 9:e100387.

Duarte A, Poderoso C, Cooke M, Soria G, Cornejo Maciel F, Gottifredi V, Podesta EJ. 2012. Mitochondrial fusion is essential for steroid biosynthesis. PLoS One 7:e45829.

Ehrhart-Bornstein M, Hinson JP, Bornstein SR, Scherbaum WA, Vinson GP. 1998. Intraadrenal interactions in the regulation of adrenocortical steroidogenesis. Endocr Rev 19:101-143.

Enss K, Danker T, Schlune A, Buchholz I, Oberleithner H. 2003. Passive transport of macromolecules through xenopus laevis nuclear envelope. J Membr Biol 196:147-155.

Entelis N, Brandina I, Kamenski P, Krasheninnikov IA, Martin RP, Tarassov I. 2006. A glycolytic enzyme, enolase, is recruited as a cofactor of tRNA targeting toward mitochondria in saccharomyces cerevisiae. Genes Dev 20:1609-1620.

Fahrenkrog B. 2014. Nucleoporin gene fusions and hematopoietic malignancies. New Journal of Science vol. 2014, Article ID 468306.

Falkenstein E, Meyer C, Eisen C, Scriba PC, Wehling M. 1996. Full-length cDNA sequence of a progesterone membrane-binding protein from porcine vascular smooth muscle cells. Biochem Biophys Res Commun 229:86-89.

Finsterer J. 2008. Leigh and leigh-like syndrome in children and adults. Pediatr Neurol 39:223-235.

Fiserova J, Kiseleva E, Goldberg MW. 2009. Nuclear envelope and nuclear pore complex structure and organization in tobacco BY-2 cells. Plant J 59:243-255.

Fluck CE, Nicolo C, Pandey AV. 2007. Clinical, structural and functional implications of mutations and polymorphisms in human $NADPH$ P450 oxidoreductase. Fundam Clin Pharmacol 21:399-410.

Fluck CE, Pandey AV. 2011. Clinical and biochemical consequences of p450 oxidoreductase deficiency. Endocr Dev 20:63-79.

Fluck CE, Tajima T, Pandey AV, Arlt W, Okuhara K, Verge CF, Jabs EW, Mendonca BB, Fujieda K, Miller WL. 2004. Mutant P450 oxidoreductase causes disordered steroidogenesis with and without antley-bixler syndrome. Nat Genet 36:228-230.

Forss-Petter S, Werner H, Berger J, Lassmann H, Molzer B, Schwab MH, Bernheimer H, Zimmermann F, Nave KA. 1997. Targeted inactivation of the X-linked adrenoleukodystrophy gene in mice. J Neurosci Res 50:829-843.

Fourcade S, Lopez-Erauskin J, Galino J, Duval C, Naudi A, Jove M, Kemp S, Villarroya F, Ferrer I, Pamplona R, Portero-Otin M, Pujol A. 2008. Early oxidative damage underlying neurodegeneration in X-adrenoleukodystrophy. Hum Mol Genet 17:1762-1773.

Frenkiel-Krispin D, Maco B, Aebi U, Medalia O. 2010. Structural analysis of a metazoan nuclear pore complex reveals a fused concentric ring architecture. J Mol Biol 395:578-586.

Galino J, Ruiz M, Fourcade S, Schluter A, Lopez-Erauskin J, Guilera C, Jove M, Naudi A, Garcia-Arumi E, Andreu AL, Starkov AA, Pamplona R, Ferrer I, Portero-Otin M, Pujol A. 2011. Oxidative damage compromises energy metabolism in the axonal degeneration mouse model of X-adrenoleukodystrophy. Antioxid Redox Signal 15:2095-2107.

Gao S, Li H, Cai Y, Ye JT, Liu ZP, Lu J, Huang XY, Feng XJ, Gao H, Chen SR, Li M, Liu PQ. 2014. Mitochondrial binding of alpha-enolase stabilizes mitochondrial membrane: Its role in doxorubicin-induced cardiomyocyte apoptosis. Arch Biochem Biophys 542:46-55.

Garcia-Rodriguez LJ, Gay AC, Pon LA. 2007. Puf3p, a pumilio family RNA binding protein, localizes to mitochondria and regulates mitochondrial biogenesis and motility in budding yeast. J Cell Biol 176:197-207.

Gerber AP, Herschlag D, Brown PO. 2004. Extensive association of functionally and cytotopically related mRNAs with puf family RNA-binding proteins in yeast. PLoS Biol 2:e79.

Gineau L, Cognet C, Kara N, Lach FP, Dunne J, Veturi U, Picard C, Trouillet C, Eidenschenk C, Aoufouchi S, Alcais A, Smith O, Geissmann F, Feighery C, Abel L, Smogorzewska A, Stillman B, Vivier E, Casanova JL, Jouanguy E. 2012. Partial MCM4 deficiency in patients with growth retardation, adrenal insufficiency, and natural killer cell deficiency. J Clin Invest 122:821-832.

Gorlich D, Prehn S, Hartmann E, Herz J, Otto A, Kraft R, Wiedmann M, Knespel S, Dobberstein B, Rapoport TA. 1990. The signal sequence receptor has a second subunit and is part of a translocation complex in the endoplasmic reticulum as probed by bifunctional reagents. J Cell Biol 111:2283-2294.

Grant DB, Dunger DB, Smith I, Hyland K. 1992. Familial glucocorticoid deficiency with achalasia of the cardia associated with mixed neuropathy, long-tract degeneration and mild dementia. Eur J Pediatr 151:85-89.

Griffin D, Liu X, Pru C, Pru JK, Peluso JJ. 2014. Expression of progesterone receptor membrane component-2 within the immature rat ovary and its role in regulating mitosis and apoptosis of spontaneously immortalized granulosa cells. Biol Reprod 91:36.

Gu J, Weng Y, Zhang QY, Cui H, Behr M, Wu L, Yang W, Zhang L, Ding X. 2003. Liver-specific deletion of the $NADPH$-cytochrome P450 reductase gene: Impact on plasma cholesterol homeostasis and the function and regulation of microsomal cytochrome P450 and heme oxygenase. J Biol Chem 278:25895-25901.

Han TS, Walker BR, Arlt W, Ross RJ. 2014. Treatment and health outcomes in adults with congenital adrenal hyperplasia. Nat Rev Endocrinol 10:115-124.

Handschug K, Sperling S, Yoon SJ, Hennig S, Clark AJ, Huebner A. 2001. Triple A syndrome is caused by mutations in AAAS, a new WD-repeat protein gene. Hum Mol Genet 10:283-290.

Haring R, Wallaschofski H, Teumer A, Kroemer H, Taylor AE, Shackleton CH, Nauck M, Volker U, Homuth G, Arlt W. 2012. A SULT2A1 genetic variant identified by GWAS as associated with low serum DHEAS does not impact on the actual DHEA/DHEAS ratio. J Mol Endocrinol 50:73-77.

Hetz C. 2012. The unfolded protein response: Controlling cell fate decisions under ER stress and beyond. Nat Rev Mol Cell Biol 13:89-102.

Hirano M, Furiya Y, Asai H, Yasui A, Ueno S. 2006. ALADINI482S causes selective failure of nuclear protein import and hypersensitivity to oxidative stress in triple A syndrome. Proc Natl Acad Sci U S A 103:2298-2303.

Huang N, Pandey AV, Agrawal V, Reardon W, Lapunzina PD, Mowat D, Jabs EW, Van Vliet G, Sack J, Fluck CE, Miller WL. 2005. Diversity and function of mutations in P450 oxidoreductase in patients with Antley-Bixler syndrome and disordered steroidogenesis. Am J Hum Genet 76:729-749.

Huebner A, Kaindl AM, Braun R, Handschug K. 2002. New insights into the molecular basis of the triple A syndrome. Endocr Res 28:733-739.

Huebner A, Mann P, Rohde E, Kaindl AM, Witt M, Verkade P, Jakubiczka S, Menschikowski M, Stoltenburg-Didinger G, Koehler K. 2006. Mice lacking the nuclear pore complex protein ALADIN show female infertility but fail to develop a phenotype resembling human triple A syndrome. Mol Cell Biol 26:1879-1887.

Hughes CR, Chung TT, Habeb AM, Kelestimur F, Clark AJ, Metherell LA. 2010. Missense mutations in the melanocortin 2 receptor accessory protein that lead to late onset familial glucocorticoid deficiency type 2. J Clin Endocrinol Metab 95:3497-3501.

Hughes CR, Guasti L, Meimaridou E, Chuang CH, Schimenti JC, King PJ, Costigan C, Clark AJ, Metherell LA. 2012. MCM4 mutation causes adrenal failure, short stature, and natural killer cell deficiency in humans. J Clin Invest 122:814-820.

Invitrogen Life Technologies. 2011. T-REx System - A Tetracycline-Regulated Expression System for Mammalian Cells. User Guide MAN0000105.

Invitrogen Life Technologies. 2015. siRNA target finder (Ambion). [last updated: 2015, last reviewed: 20.07.2015] URL: http://www.ambion.com/techlib/misc/siRNA_finder.html

Ivashchenko O, Van Veldhoven PP, Brees C, Ho YS, Terlecky SR, Fransen M. 2011. Intraperoxisomal redox balance in mammalian cells: Oxidative stress and interorganellar cross-talk. Mol Biol Cell 22:1440-1451.

Jackson JS,Jr, Houshmandi SS, Lopez Leban F, Olivas WM. 2004. Recruitment of the Puf3 protein to its mRNA target for regulation of mRNA decay in yeast. Rna 10:1625-1636.

Jühlen R, Idkowiak J, Taylor AE, Kind B, Arlt W, Huebner A, Koehler K. 2015. Role of ALADIN in human adrenocortical cells for oxidative stress response and steroidogenesis. PLoS One 10:e0124582.

Katahira J. 2015. Nuclear export of messenger RNA. Genes (Basel) 6:163-184.

Kawamoto T, Mitsuuchi Y, Toda K, Yokoyama Y, Miyahara K, Miura S, Ohnishi T, Ichikawa Y, Nakao K, Imura H. 1992. Role of steroid 11 beta-hydroxylase and steroid 18-hydroxylase in the biosynthesis of glucocorticoids and mineralocorticoids in humans. Proc Natl Acad Sci U S A 89:1458-1462.

Keator CS, Mah K, Slayden OD. 2012. Alterations in progesterone receptor membrane component 2 (PGRMC2) in the endometrium of macaques afflicted with advanced endometriosis. Mol Hum Reprod 18:308-319.

Keller A, Nesvizhskii AI, Kolker E, Aebersold R. 2002. Empirical statistical model to estimate the accuracy of peptide identifications made by MS/MS and database search. Anal Chem 74:5383-5392.

Kind B, Koehler K, Krumbholz M, Landgraf D, Huebner A. 2010. Intracellular ROS level is increased in fibroblasts of triple A syndrome patients. J Mol Med (Berl) 88:1233-1242.

Kind B, Koehler K, Lorenz M, Huebner A. 2009. The nuclear pore complex protein ALADIN is anchored via NDC1 but not via POM121 and GP210 in the nuclear envelope. Biochem Biophys Res Commun 390:205-210.

Kiseleva E, Allen TD, Rutherford S, Bucci M, Wente SR, Goldberg MW. 2004. Yeast nuclear pore complexes have a cytoplasmic ring and internal filaments. J Struct Biol 145:272-288.

Koehler K, Brockmann K, Krumbholz M, Kind B, Bonnemann C, Gartner J, Huebner A. 2008. Axonal neuropathy with unusual pattern of amyotrophy and alacrima associated with a novel AAAS mutation p.Leu430Phe. Eur J Hum Genet 16:1499-1506.

Koehler K, End K, Kind B, Landgraf D, Mitzscherling P, Huebner A. 2013. Changes in differential gene expression in fibroblast cells from patients with triple A syndrome under oxidative stress. Horm Metab Res 45:102-108.

Kornmann B, Currie E, Collins SR, Schuldiner M, Nunnari J, Weissman JS, Walter P. 2009. An ER-mitochondria tethering complex revealed by a synthetic biology screen. Science 325:477-481.

Krumbholz M, Koehler K, Huebner A. 2006. Cellular localization of 17 natural mutant variants of ALADIN protein in triple A syndrome - shedding light on an unexpected splice mutation. Biochem Cell Biol 84:243-249.

Lahiri S, Chao JT, Tavassoli S, Wong AK, Choudhary V, Young BP, Loewen CJ, Prinz WA. 2014. A conserved endoplasmic reticulum membrane protein complex (EMC) facilitates phospholipid transfer from the ER to mitochondria. PLoS Biol 12:e1001969.

Lanes R, Plotnick LP, Bynum TE, Lee PA, Casella JF, Fox CE, Kowarski AA, Migeon CJ. 1980. Glucocorticoid and partial mineralocorticoid deficiency associated with achalasia. J Clin Endocrinol Metab 50:268-270.

Lim RY, Ullman KS, Fahrenkrog B. 2008. Biology and biophysics of the nuclear pore complex and its components. Int Rev Cell Mol Biol 267:299-342.

Lowry OH, Rosebrough NJ, Farr AL, Randall RJ. 1951. Protein measurement with the folin phenol reagent. J Biol Chem 193:265-275.

Maimon T, Elad N, Dahan I, Medalia O. 2012. The human nuclear pore complex as revealed by cryo-electron tomography. Structure 20:998-1006.

Matkovic U, Pacenti M, Trevisan M, Palu G, Barzon L. 2009. Investigation on human adrenocortical cell response to adenovirus and adenoviral vector infection. J Cell Physiol 220:45-57.

Matthews LC, Berry AA, Morgan DJ, Poolman TM, Bauer K, Kramer F, Spiller DG, Richardson RV, Chapman KE, Farrow SN, Norman MR, Williamson AJ, Whetton AD, Taylor SS, Tuckermann JP, White MR, Ray DW. 2015. Glucocorticoid receptor regulates accurate chromosome segregation and is associated with malignancy. Proc Natl Acad Sci U S A 112:5479-5484.

Meimaridou E, Hughes CR, Kowalczyk J, Guasti L, Chapple JP, King PJ, Chan LF, Clark AJ, Metherell LA. 2013. Familial glucocorticoid deficiency: New genes and mechanisms. Mol Cell Endocrinol 371:195-200.

Meimaridou E, Kowalczyk J, Guasti L, Hughes CR, Wagner F, Frommolt P, Nurnberg P, Mann NP, Banerjee R, Saka HN, Chapple JP, King PJ, Clark AJ, Metherell LA. 2012. Mutations in NNT encoding nicotinamide nucleotide transhydrogenase cause familial glucocorticoid deficiency. Nat Genet 44:740-742.

Metherell LA, Chapple JP, Cooray S, David A, Becker C, Ruschendorf F, Naville D, Begeot M, Khoo B, Nurnberg P, Huebner A, Cheetham ME, Clark AJ. 2005. Mutations in MRAP, encoding a new interacting partner of the ACTH receptor, cause familial glucocorticoid deficiency type 2. Nat Genet 37:166-170.

Metherell LA, Naville D, Halaby G, Begeot M, Huebner A, Nurnberg G, Nurnberg P, Green J, Tomlinson JW, Krone NP, Lin L, Racine M, Berney DM, Achermann JC, Arlt W, Clark AJ. 2009. Nonclassic lipoid congenital adrenal hyperplasia masquerading as familial glucocorticoid deficiency. J Clin Endocrinol Metab 94:3865-3871.

Meyer TS, Lamberts BL. 1965. Use of coomassie brilliant blue R250 for the electrophoresis of microgram quantities of parotid saliva proteins on acrylamide-gel strips. Biochim Biophys Acta 107:144-145.

Mick DU, Fox TD, Rehling P. 2011. Inventory control: Cytochrome c oxidase assembly regulates mitochondrial translation. Nat Rev Mol Cell Biol 12:14-20.

Milenkovic T, Zdravkovic D, Savic N, Todorovic S, Mitrovic K, Koehler K, Huebner A. 2010. Triple A syndrome: 32 years experience of a single centre (1977-2008). Eur J Pediatr 169:1323-1328.

Miller WL, Agrawal V, Sandee D, Tee MK, Huang N, Choi JH, Morrissey K, Giacomini KM. 2011. Consequences of POR mutations and polymorphisms. Mol Cell Endocrinol 336:174-179.

Miller WL, Bose HS. 2011. Early steps in steroidogenesis: Intracellular cholesterol trafficking. J Lipid Res 52:2111-2135.

Miller WL, Huang N, Fluck CE, Pandey AV. 2004. P450 oxidoreductase deficiency. Lancet 364:1663.

Misaggi R, Di Sanzo M, Cosentino C, Bond HM, Scumaci D, Romeo F, Stellato C, Giurato G, Weisz A, Quaresima B, Barni T, Amato F, Viglietto G, Morrone G, Cuda G, Faniello MC, Costanzo F. 2014. Identification of H ferritin-dependent and independent genes in K562 differentiating cells by targeted gene silencing and expression profiling. Gene 535:327-335.

Mohr D, Frey S, Fischer T, Guttler T, Gorlich D. 2009. Characterisation of the passive permeability barrier of nuclear pore complexes. Embo J 28:2541-2553.

Moser HW. 1997. Adrenoleukodystrophy: Phenotype, genetics, pathogenesis and therapy. Brain 120 (Pt 8):1485-1508.

Moser HW, Loes DJ, Melhem ER, Raymond GV, Bezman L, Cox CS, Lu SE. 2000. X-linked adrenoleukodystrophy: Overview and prognosis as a function of age and brain magnetic resonance imaging abnormality. A study involving 372 patients. Neuropediatrics 31:227-239.

Moser HW, Raymond GV, Dubey P. 2005. Adrenoleukodystrophy: New approaches to a neurodegenerative disease. Jama 294:3131-3134.

Neilson DE, Adams MD, Orr CM, Schelling DK, Eiben RM, Kerr DS, Anderson J, Bassuk AG, Bye AM, Childs AM, Clarke A, Crow YJ, Di Rocco M, Dohna-Schwake C, Dueckers G, Fasano AE, Gika AD, Gionnis D, Gorman MP, Grattan-Smith PJ, Hackenberg A, Kuster A, Lentschig MG, Lopez-Laso E, Marco EJ, Mastroyianni S, Perrier J, Schmitt-Mechelke T, Servidei S, Skardoutsou A, Uldall P, van der Knaap MS, Goglin KC, Tefft DL, Aubin C, de Jager P, Hafler D, Warman ML. 2009. Infection-triggered familial or recurrent cases of acute necrotizing encephalopathy caused by mutations in a component of the nuclear pore, RANBP2. Am J Hum Genet 84:44-51.

Nelson DR. 2009. The cytochrome p450 homepage. Hum Genomics 4:59-65.

Nesvizhskii AI, Keller A, Kolker E, Aebersold R. 2003. A statistical model for identifying proteins by tandem mass spectrometry. Anal Chem 75:4646-4658.

Neve EP, Ingelman-Sundberg M. 2008. Intracellular transport and localization of microsomal cytochrome P450. Anal Bioanal Chem 392:1075-1084.

Nogueira EF, Xing Y, Morris CA, Rainey WE. 2009. Role of angiotensin II-induced rapid response genes in the regulation of enzymes needed for aldosterone synthesis. J Mol Endocrinol 42:319-330.

Novoselova TV, Rath SR, Carpenter K, Pachter N, Dickinson JE, Price G, Chan LF, Choong CS, Metherell LA. 2014. NNT pseudoexon activation as a novel mechanism for disease in two siblings with familial glucocorticoid deficiency. J Clin Endocrinol Metab jc20143641.

Okamura M, Inose H, Masuda S. 2015. RNA export through the NPC in eukaryotes. Genes (Basel) 6:124-149.

O'Riordan SM, Lynch SA, Hindmarsh PC, Chan LF, Clark AJ, Costigan C. 2008. A novel variant of familial glucocorticoid deficiency prevalent among the irish traveler population. J Clin Endocrinol Metab 93:2896-2899.

Pandey AV, Fluck CE. 2013. $NADPH$ P450 oxidoreductase: Structure, function, and pathology of diseases. Pharmacol Ther 138:229-254.

Pandey AV, Fluck CE, Huang N, Tajima T, Fujieda K, Miller WL. 2004. P450 oxidoreductase deficiency: A new disorder of steroidogenesis affecting all microsomal P450 enzymes. Endocr Res 30:881-888.

Pandey AV, Sproll P. 2014. Pharmacogenomics of human P450 oxidoreductase. Front Pharmacol 5:103.

Pante N, Kann M. 2002. Nuclear pore complex is able to transport macromolecules with diameters of about 39 nm. Mol Biol Cell 13:425-434.

Peluso JJ, Griffin D, Liu X, Horne M. 2014. Progesterone receptor membrane component-1 (PGRMC1) and PGRMC-2 interact to suppress entry into the cell cycle in spontaneously immortalized rat granulosa cells. Biol Reprod 91:104.

Perocchi F, Jensen LJ, Gagneur J, Ahting U, von Mering C, Bork P, Prokisch H, Steinmetz LM. 2006. Assessing systems properties of yeast mitochondria through an interaction map of the organelle. PLoS Genet 2:e170.

Peterson RE, Imperato-McGinley J, Gautier T, Shackleton C. 1985. Male pseudohermaphroditism due to multiple defects in steroid-biosynthetic microsomal mixed-function oxidases. A new variant of congenital adrenal hyperplasia. N Engl J Med 313:1182-1191.

Pohorecky LA, Wurtman RJ. 1971. Adrenocortical control of epinephrine synthesis. Pharmacol Rev 23:1-35.

Powers JM, Pei Z, Heinzer AK, Deering R, Moser AB, Moser HW, Watkins PA, Smith KD. 2005. Adreno-leukodystrophy: Oxidative stress of mice and men. J Neuropathol Exp Neurol 64:1067-1079.

Prasad R, Chan LF, Hughes CR, Kaski JP, Kowalczyk JC, Savage MO, Peters CJ, Nathwani N, Clark AJ, Storr HL, Metherell LA. 2014a. Thioredoxin reductase 2 (TXNRD2) mutation associated with familial glucocorticoid deficiency (FGD). J Clin Endocrinol Metab 99:e1556-63.

Prasad R, Kowalczyk JC, Meimaridou E, Storr HL, Metherell LA. 2014b. Oxidative stress and adrenocortical insufficiency. J Endocrinol 221:r63-73.

Prasad R, Metherell LA, Clark AJ, Storr HL. 2013. Deficiency of ALADIN impairs redox homeostasis in human adrenal cells and inhibits steroidogenesis. Endocrinology 154:3209-3218.

Rabut G, Doye V, Ellenberg J. 2004. Mapping the dynamic organization of the nuclear pore complex inside single living cells. Nat Cell Biol 6:1114-1121.

Rapoport R, Sklan D, Hanukoglu I. 1995. Electron leakage from the adrenal cortex mitochondrial P450scc and P450c11 systems: $NADPH$ and steroid dependence. Arch Biochem Biophys 317:412-416.

Rass U, Ahel I, West SC. 2007. Actions of aprataxin in multiple DNA repair pathways. J Biol Chem 282:9469-9474.

Reid DW, Nicchitta CV. 2015. Diversity and selectivity in mRNA translation on the endoplasmic reticulum. Nat Rev Neurosci 16:221-231.

Reshmi-Skarja S, Huebner A, Handschug K, Finegold DN, Clark AJ, Gollin SM. 2003. Chromosomal fragility in patients with triple A syndrome. Am J Med Genet A 117A:30-36. Riddick DS, Ding X, Wolf CR, Porter TD, Pandey AV, Zhang QY, Gu J, Finn RD, Ronseaux S, McLaughlin LA, Henderson CJ, Zou L, Fluck CE. 2013. $NADPH$-cytochrome P450 oxidoreductase: Roles in physiology, pharmacology, and toxicology. Drug Metab Dispos 41:12-23.

Rout MP, Aitchison JD. 2001. The nuclear pore complex as a transport machine. J Biol Chem 276:16593-16596.

Saint-Georges Y, Garcia M, Delaveau T, Jourdren L, Le Crom S, Lemoine S, Tanty V, Devaux F, Jacq C. 2008. Yeast mitochondrial biogenesis: A role for the PUF RNA-binding protein Puf3p in mRNA localization. PLoS One 3:e2293.

Schmidt O, Pfanner N, Meisinger C. 2010. Mitochondrial protein import: From proteomics to functional mechanisms. Nat Rev Mol Cell Biol 11:655-667.

Schwartz TU. 2005. Modularity within the architecture of the nuclear pore complex. Curr Opin Struct Biol 15:221-226.

Seliskar M, Rozman D. 2007. Mammalian cytochromes P450–importance of tissue specificity. Biochim Biophys Acta 1770:458-466.

Shen AL, O'Leary KA, Kasper CB. 2002. Association of multiple developmental defects and embryonic lethality with loss of microsomal $NADPH$-cytochrome P450 oxidoreductase. J Biol Chem 277:6536-6541.

Sherrill CB, Marshall DJ, Moser MJ, Larsen CA, Daude-Snow L, Jurczyk S, Shapiro G, Prudent JR. 2004. Nucleic acid analysis using an expanded genetic alphabet to quench fluorescence. J Am Chem Soc 126:4550-4556.

Shevchenko A, Tomas H, Havlis J, Olsen JV, Mann M. 2006. In-gel digestion for mass spectrometric characterization of proteins and proteomes. Nat Protoc 1:2856-2860.

Stoffler D, Feja B, Fahrenkrog B, Walz J, Typke D, Aebi U. 2003. Cryo-electron tomography provides novel insights into nuclear pore architecture: Implications for nucleocytoplasmic transport. J Mol Biol 328:119-130.

Storr HL, Kind B, Parfitt DA, Chapple JP, Lorenz M, Koehler K, Huebner A, Clark AJ. 2009. Deficiency of ferritin heavy-chain nuclear import in triple a syndrome implies nuclear oxidative damage as the primary disease mechanism. Mol Endocrinol 23:2086-2094.

Suntharalingam M, Wente SR. 2003. Peering through the pore: Nuclear pore complex structure, assembly, and function. Dev Cell 4:775-789.

Tarassov I, Kamenski P, Kolesnikova O, Karicheva O, Martin RP, Krasheninnikov IA, Entelis N. 2007. Import of nuclear DNA-encoded RNAs into mitochondria and mitochondrial translation. Cell Cycle 6:2473-2477.

Temme A, Rieger M, Reber F, Lindemann D, Weigle B, Diestelkoetter-Bachert P, Ehninger G, Tatsuka M, Terada Y, Rieber EP. 2003. Localization, dynamics, and function of survivin revealed by expression of functional survivinDsRed fusion proteins in the living cell. Mol Biol Cell 14:78-92.

Thompson KJ, Fried MG, Ye Z, Boyer P, Connor JR. 2002. Regulation, mechanisms and proposed function of ferritin translocation to cell nuclei. J Cell Sci 115:2165-2177.

Tsigos C. 1999. Isolated glucocorticoid deficiency and ACTH receptor mutations. Arch Med Res 30:475-480.

Tullio-Pelet A, Salomon R, Hadj-Rabia S, Mugnier C, de Laet MH, Chaouachi B, Bakiri F, Brottier P, Cattolico L, Penet C, Begeot M, Naville D, Nicolino M, Chaussain JL, Weissenbach J, Munnich A, Lyonnet S. 2000. Mutant WD-repeat protein in triple-A syndrome. Nat Genet 26:332-335.

Tumbale P, Williams JS, Schellenberg MJ, Kunkel TA, Williams RS. 2014. Aprataxin resolves adenylated RNA-DNA junctions to maintain genome integrity. Nature 506:111-115.

U.S. National Library of Medicine. 2015. Basic local alignment tool. [last updated: 05.03.2015, last reviewed: 13.07.2015] URL: http://blast.ncbi.nlm.nih.gov/Blast.cgi.

van de Wetering M, Oving I, Muncan V, Pon Fong MT, Brantjes H, van Leenen D, Holstege FC, Brummelkamp TR, Agami R, Clevers H. 2003. Specific inhibition of gene expression using a stably integrated, inducible small-interfering-RNA vector. EMBO Rep 4:609-615. Vasilj A, Gentzel M, Ueberham E, Gebhardt R, Shevchenko A. 2012. Tissue proteomics by one-dimensional gel electrophoresis combined with label-free protein quantification. J Proteome Res 11:3680-3689.

Wang T, Rowland JG, Parmar J, Nesterova M, Seki T, Rainey WE. 2012. Comparison of aldosterone production among human adrenocortical cell lines. Horm Metab Res 44:245-250.

Webb TR, Clark AJ. 2010. Minireview: The melanocortin 2 receptor accessory proteins. Mol Endocrinol 24:475-484.

Weber A, Clark AJ. 1994. Mutations of the ACTH receptor gene are only one cause of familial glucocorticoid deficiency. Hum Mol Genet 3:585-588.

Wendler A, Wehling M. 2013. PGRMC2, a yet uncharacterized protein with potential as tumor suppressor, migration inhibitor, and regulator of cytochrome P450 enzyme activity. Steroids 78:555-558.

Wiedemann N, van der Laan M, Pfanner N. 2009. SnapShot: Import and sorting of mitochondrial proteins. Cell 138:808-808.e1.

Winkler H, Apps DK, Fischer-Colbrie R. 1986. The molecular function of adrenal chromaffin granules: Established facts and unresolved topics. Neuroscience 18:261-290.

Wittwer CT, Herrmann MG, Moss AA, Rasmussen RP. 2013. Continuous fluorescence monitoring of rapid cycle DNA amplification. 1997. Biotechniques 54:314-320.

Yamazumi Y, Kamiya A, Nishida A, Nishihara A, Iemura S, Natsume T, Akiyama T. 2009. The transmembrane nucleoporin NDC1 is required for targeting of ALADIN to nuclear pore complexes. Biochem Biophys Res Commun 389:100-104.

Acknowledgement

This work was carried out at the Children's Hospital at the Technische Universität Dresden. I want to thank Prof. Dr. med. Reinhard Berner and Prof. Dr. med. Angela Rösen-Wolff for making it possible to carry out this work at the research facility of the Department.

I owe my deepest gratitude to my supervisor Prof. Dr. med. Angela Hübner. I thank her for her advice, help and continous optimism. In addition, I received insightful suggestions from the other members of my Thesis Advisory Committee: PD Andreas Androutsellis-Theotokis and Prof. rer. nat. Henning Morawietz. I have greatly benefited from their enthusiasm.

I would particularly like to thank Dr. rer. nat. Katrin Köhler for giving comments and suggestions. Her guidance and supervision in the laboratory were invaluable.

I have had the excellent technical assistance of Dana Landgraf. I am deeply grateful for her advice and warm encouragement.

It is a pleasure to thank all colleagues at the Children's Hospital at the Technische Universität Dresden and at the Centre for Endocrinology, Diabetes and Metabolism at the University of Birmingham.